Pacheco-Labrador, J., Migliavacca, M., Ma, X., **Mahecha, M.**, Carvalhais, N., Weber, U., Benavides, R., Bouriaud, O., Barnoaiea, I., Coomes, D.A., **Bohn, F.J.**, **Kraemer, G.**, Heiden, U., **Huth, A.**, Wirth, C. (2022):
Challenging the link between functional and spectral diversity with radiative transfer modeling and data
Remote Sens. Environ. **280** , art. 113170

http://dx.doi.org/10.1016/j.rse.2022.113170

Challenging the link between functional and spectral diversity with radiative transfer modeling and data

Javier Pacheco-Labrador[1], Mirco Migliavacca[2,1], Xuanlong Ma[3,4,5], Miguel Mahecha[6,7], Nuno Carvalhais[1,8], Ulrich Weber[1], Raquel Benavides[9], Olivier Bouriaud[10,11], Ionut Barnoaiea[10,12], David A. Coomes[13], Friedrich J. Bohn[14,15], Guido Kraemer[6], Uta Heiden[16], Andreas Huth[15,7,17], Christian Wirth[18,7,1]

[1] Max Planck Institute for Biogeochemistry, Hans Knöll Straße 10, Jena, D-07745, Germany
[2] current address: European Commission, Joint Research Centre (JRC), Ispra, Italy
[3] College of Earth and Environmental Science, Lanzhou University, Lanzhou, Gansu, China 730000
[4] International Research Center of Big Data for Sustainable Development Goals, Beijing, China, 100094
[5] State Key Laboratory of Remote Sensing Science, Beijing Normal University, Beijing, China, 100875
[6] Remote Sensing Center for Earth System Research, Leipzig University, Leipzig, Germany
[7] German Centre for Integrative Biodiversity Research (iDiv), Halle-Jena-Leipzig, Germany
[8] Departamento de Ciências e Engenharia do Ambiente, DCEA, Faculdade de Ciências e Tecnologia, FCT, Universidade Nova de Lisboa, 2829-516 Caparica, Portugal
[9] Departamento de Sistemas y Recursos Naturales. E.T.S. Ingeniería de Montes, Forestales y del Medio Natural, Universidad Politécnica de Madrid, C/ José Antonio Novais 10, 28040, Madrid, Spain
[10] University 'Ștefan cel Mare' of Suceava, Universității 13, Suceava 720229, Romania
[11] Laboratoire d'Inventaire Forestier, IGN, Nancy, France
[12] Geomatics Laboratory, Faculty of Forestry, University 'Ștefan cel Mare' Suceava, Romania
[13] Department of Plant Sciences and the Conservation Research Institute, Downing Street, Cambridge, CB2 3EA, United Kingdom.
[14] Department of Computational Hydrosystems, Helmholtz Centre for Environmental Research – UFZ, Leipzig, Germany
[15] Department of Ecological Modelling, Helmholtz Centre for Environmental Research – UFZ, Leipzig, Germany
[16] German Aerospace Center (DLR), Remote Sensing Technology Institute (IMF), Oberpfaffenhofen, 82234 Wessling, Germany
[17] Institute of Environmental Systems Research, University of Osnabrück, Osnabrück, Lower Saxony, Germany
[18] Systematic Botany and Functional Biodiversity, Leipzig University, Leipzig, Germany.

Keywords: Spectral diversity, functional diversity, radiative transfer model, biodiversity, Sentinel-2, DESIS

ABSTRACT

In a context of accelerated human-induced biodiversity loss, remote sensing (RS) is emerging as a promising tool to map plant biodiversity from space. Proposed approaches often rely on the Spectral Variation Hypothesis (SVH), linking the heterogeneity of terrestrial vegetation to the variability of the spectroradiometric signals. Yet, due to observational limitations, the SVH has been insufficiently tested, remaining unclear which metrics, methods, and sensors could provide the most reliable estimates of plant biodiversity. Here we assessed the potential of RS to infer plant biodiversity using radiative transfer simulations and inversion. We focused specifically on "functional diversity," which represents the spatial variability in plant functional traits. First, we simulated vegetation communities and evaluated the information content of different functional diversity metrics (FDMs) derived from their optical reflectance factors (R) or the corresponding vegetation "optical traits," estimated via radiative transfer model inversion. Second, we assessed the effect of the spatial resolution, the spectral characteristics of the sensor, and signal noise on the relationships between FDMs derived from field and remote sensing datasets. Finally, we evaluated the plausibility of the simulations using Sentinel-2 (multispectral, 10 m pixel) and DESIS (hyperspectral, 30 m pixel) imagery acquired over sites of the Functional Significance of Forest Biodiversity in Europe (FunDivEUROPE) network. We demonstrate that functional diversity can be inferred both by reflectance and optical traits. However, not all the FDMs tested were suited for assessing plant functional diversity from RS. Rao's Q index, functional dispersion, and functional richness were the best-performing metrics. Furthermore, we demonstrated that spatial resolution is the most limiting RS feature. In agreement with simulations, Sentinel-2 imagery provided better estimates of plant diversity than DESIS, despite the coarser spectral resolution. However, Sentinel-2 offered inaccurate results at DESIS

spatial resolution. Overall, our results identify the strengths and weaknesses of optical RS to monitor plant functional diversity. Future missions and biodiversity products should consider and benefit from the identified potentials and limitations of the SVH.

1. INTRODUCTION

Human activities are leading to a massive and accelerated loss of Earth's life forms (Barnosky et al. 2011; Ceballos et al. 2015); at the same time, the efforts to understand and prevent this loss still lack global, continuous, and systematic information connecting biodiversity and its decline drivers (Hardisty et al. 2019; Pereira et al. 2012). While remote sensing (RS) provides operational monitoring of some of the major drivers of biodiversity variation at a global scale (e.g., land cover, land use, and climatic variables) (Small and Sousa 2016; Sohl and Sleeter 2012; Yang et al. 2013), there are no comparable capabilities for mapping plant biodiversity and its changes. A first step towards developing such a capability was the definition of the Essential Biodiversity Variables, a set of "measurements required to study, report, and manage biodiversity change" (c.f., (Pereira et al. 2013)). The Essential Biodiversity Variables are analogous to the Essential Climate Variables (GCOS 2003), designed to understand and monitor climate change (Scholes et al. 2012). The majority of Essential Climate Variables rely on RS to provide continuous and systematic information over the whole Earth's surface (Yang et al. 2013). Similarly, RS is expected to provide a significant fraction of the Essential Biodiversity Variables (Hardisty et al. 2019; Jetz et al. 2019).

The interest of the RS community in biodiversity has grown over the last decade in parallel with advances in computer science and RS technology (Rocchini et al. 2010; Turner et al. 2003; Wang and Gamon 2019). Biodiversity is a complex concept involving multiple facets: taxonomic as the diversity of taxonomic groups (often species), phylogenetic as the branch length of the evolutionary tree of a community, and functional as the diversity of functional traits; consequently, many RS-based Essential Biodiversity Variables have been proposed (Skidmore et al. 2021). However, there is no clear community consensus, as is the case for the meteorological and biophysical variables considered Essential Climate

Variables, about which EBVs should be taken forward. One of the most promising methods to assess biodiversity from optical RS relies on the Spectral Variation Hypothesis (SVH), which states that the variability of the spectral signals of a remote sensing image, termed “spectral diversity.”, should reflect the spatial variation of the environment. The environmental heterogeneity would relate to the variability of plant species, traits, and/or canopy structure (Palmer et al. 2002; Ustin and Gamon 2010), among other factors (Rocchini et al. 2010; Wang and Gamon 2019). At the same time, plant diversity could relate to the diversity of species of other *taxa* dependent on particular plant species (Jetz et al. 2019). According to Wang and Gamon (2019), the main approaches proposed to quantify plant diversity from RS rely on a) classification and mapping of individual species or broad functional types (Ibarrola-Ulzurrun et al. 2019; Stagakis et al. 2016; Sun et al. 2019), b) classification and mapping of habitats (Kerr and Ostrovsky 2003; Stein et al. 2014), c) estimation of vegetation traits (optical traits) and the analysis of their variability, mimicking trait sampling in field surveys (Hauser et al. 2021a; Schneider et al. 2017; Torresani et al. 2021), and d) direct analysis of the spectral diversity (Hauser et al. 2021b; Rocchini et al. 2021; Wang et al. 2018a; Warren et al. 2014). The first two approaches, while valuable, strongly depend on the spatial scale and the classification method. Limitations for classifying individual species are sometimes overcome by targeting instead functional types, which might be too rigid to describe the ecosystem’s functionality (Van Cleemput et al. 2021; Wang and Gamon 2019). Alternatively, the characterization of functional diversity might provide a deeper insight into the biodiversity-ecosystem function relationships than taxonomic estimates (Jetz et al. 2016). The last two approaches seek to characterize vegetation’s taxonomical, functional, and even phylogenetic diversity through its spectral diversity or the diversity of optical traits derived from spectral information (Cavender-Bares et al. 2020). Still, recent literature suggests that spectral and taxonomic diversities might not be robustly correlated (Fassnacht et al. 2022). Nonetheless, most of these methods have only been evaluated over relatively small extents (Féret and Asner 2014; Gholizadeh et al. 2018; Schneider et al. 2017; Schweiger et al. 2018; Torresani et al. 2019; Wang et al. 2018a), and as of now, there are no comprehensive databases to assess their robustness and applicability in a global context.

RS missions must consider the trade-offs between spatial, spectral, and temporal resolutions (Gamon et al. 2020). For biodiversity studies, pixel size should ideally allow the identification of individual plants without being confounded by variability within the plant signal (e.g., shading and the presence of different plant elements such as branches, soil, or understory vegetation) (Nagendra 2001; Nagendra and Rocchini 2008). However, individual plants are typically smaller than pixels, which hampers the characterization of biodiversity. For example, Wang et al. (2018a) explored how increasing pixel size reduced spectral sensitivity to taxonomic diversity in a grassland. Alternatives to reduce the need for accurate plant discrimination include fuzzy classification (Feilhauer et al. 2021), estimation of optical traits at the resolution of the RS sensor (Torresani et al. 2021), or direct estimation of plant functional diversity from spectral diversity (Ma et al. 2019). However, these approaches are still sensitive to sensor spatial resolution since larger pixels integrate more species and traits and, therefore, more and more variability. At the same time, mixing species can reduce the capability of retrieving vegetation optical traits (Darvishzadeh et al. 2008). In addition, the sensor spectral configuration (resolution, sampling, and range) must provide sufficient information to discriminate between different species or quantify optical traits. Hyperspectral data continuously and finely resolve the spectral properties of Earth surfaces (Goetz 2009) and therefore offer the best chances for successful classification (Dalponte et al. 2009; Sluiter and Pebesma 2010) or trait retrieval (Lee et al. 2004; Lu et al. 2019). Nonetheless, spaceborne sensors must sacrifice either the spectral or the spatial resolution, and it remains unresolved whether high-resolution multispectral or mid-resolution hyperspectral missions are more useful for biodiversity assessment.

Spectral and functional diversities can involve multiple variables (i.e., plant traits or spectral bands). Different authors have compared the variability of spectral signals in individual wavebands, combinations of these, or averaged statistics in certain spectral regions (Féret and Asner 2014; Ma et al. 2019; Wang et al. 2018a), as well as the variability of individual optical traits estimated from RS (Rossi et al. 2020; Torresani et al. 2021) with field biodiversity data. Alternatively, ecologists have proposed several functional diversity metrics (FDMs) to summarize the information in multidimensional datasets of species traits. These metrics quantify different aspects of functional diversity (i.e., richness, evenness, and divergence) with single scalars (Laliberté and Legendre 2010; Mason et al. 2005; Villéger et al. 2008). The computation of FDMs often requires removing the covariance between variables (Anderson 2006); however, despite the abstraction, FDMs are informative and sensitive to underlying assembly processes (Mouchet et al. 2010). Typically, FDMs are constructed from plant functional trait data collected in the field (e.g., measurements of pigment and mineral nutrient concentrations taken on leaf samples). These metrics can also be computed from RS variables such as spectral reflectance factors and optical traits (Schneider et al. 2017; Torresani et al. 2019), being possible to replace taxonomic species with the "spectral species" concept (Féret and Asner 2014). What remains unclear is to what extent FDMs computed from spectral data or optical traits can be translated to FDMs computed from vegetation functional traits collected in the field, and the role of the spectral configuration (resolution, sampling, and range), spatial resolution, and signal noise.

So far, the SVH has been inconsistently tested. The works mentioned above evaluated the potential of different metrics, methods, and sensors with little overlap, preventing a solid comparison of their performance. Moreover, the lack of accurate validation data covering broad ranges of traits and communities consistently imaged by multiple sensors of well-known uncertainties has limited the generalization of the results. To overcome these issues, we evaluate the potential of different FDMs to relate spectral and functional diversity using both synthetic and observational datasets. Our study aims to answer the following questions: a) Which remote sensing-based FDMs are able to capture functional diversity from field plant traits? b) What are the advantages and disadvantages of computing FDMs directly on the spectral reflectance factors (R) or optical traits (T_{optical}) estimated via radiative transfer model (RTM) inversion? c) Are the relationships between field and remote sensing-based FDMs consistent when compared at local and global scales? d) How do RS features such as spectral configuration, spatial resolution, and signal noise affect the relationships between vegetation and remote sensing-based FDMs? To answer these questions, we first developed an RTM simulation framework that allowed us to produce synthetic vegetation communities and the related spectral signals featuring different spectral and spatial configurations and noise. Then, using these simulations, we evaluated and compared two common RS methods to map functional diversity: spectral signals (i.e., reflectance factors) or optical traits estimated from inverse modeling. Finally, we evaluated the coherence of the simulation results using DLR Earth Sensing Imaging Spectrometer (DESIS) and Sentinel-2 imagery and field taxonomic and functional diversity estimates from forest plots of the Functional Significance of Forest Biodiversity in Europe (FunDivEUROPE) network (Baeten et al. 2013).

2. METHODS

Fig. 1 summarizes the simulation and data analysis workflows. First, we simulated artificial communities of plant species, each defined by a unique set of traits (i.e., RTM parameters) and the individual species' reflectance factors using an RTM. Then, we applied different RS features (spatial resolution, spectral configuration, and noise) to the reflectance factors to represent how different remote sensors perceived the plant communities. Using this simulation framework, we evaluated the relationships between quantitative FDMs computed from the plant traits (as could be measured in the field) and RS variables (either reflectance factors or optical traits estimates) and how these were affected by the RS features (Fig. 1a, section 2.3). Finally, we analyzed different sets of satellite imagery acquired over FunDivEUROPE biodiversity monitoring plots and assessed if the relationships between field and remote sensing FDMs were coherent with the former simulations (Fig. 1b, section 2.4).

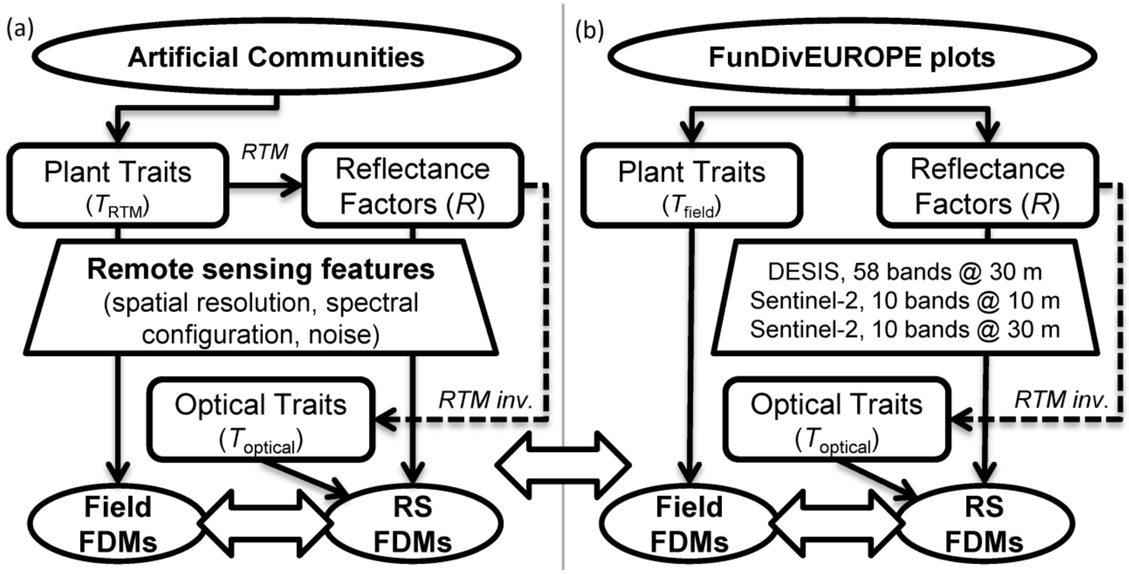

Figure 1. Flowchart outlining analyses of simulated (a) and observational data (b) to assess the capability of different functional diversity metrics (FDMs) to link spectral and vegetation functional diversity and the effect of different remote sensing features. Solid lines indicate the direct use of the data or models; dashed lines indicate the inverse use of a radiative transfer model (RTM). In the simulations (a), some analyses include the effects on plant traits of added noise and different spatial resolutions.

2.1 Functional diversity metrics

We evaluated the capability of Functional richness (*FRic*), evenness (*FEve*), diversity (*FDiv*), dispersion (*FDis*), and Rao's quadratic entropy *Q* (*RaoQ*) metrics (Botta-Dukát 2005; Laliberté and Legendre 2010; Villéger et al. 2008) to connect field and RS-based functional diversity. These metrics were computed with the *dbFD* R-package (Laliberté and Legendre 2010) using traits Euclidean distance as the dissimilarity measure. The package applies standardization of the variables and Principal Coordinates Analysis (Anderson 2006) on the distance matrix to remove the influence of variables' magnitude and redundant information, respectively. Moreover, we used a parametric formulation of Rao's *Q* (Eq. 1) as proposed by Rocchini et al. (2021) with values of the parameter α, ranging from 0 to infinity. In this case, we first applied standardization and principal component analysis (PCA) (Pearson 1901) to the traits before computing the Euclidean distance, keeping only the components that explained 98 % of the variance in total. This approach allowed us to reduce the number of variables and evaluate the effect of noise (section 2.3.4).

$$\mathrm{Rao}Q_{\alpha} = \left(\sum_{i,j}^{N} p_i p_j {d_{ji}}^{\alpha} \right)^{\frac{1}{\alpha}} \tag{1}$$

where i and j are indices for each species in the community, p their respective probabilities, and d is a symmetric measure of multidimensional distance between the species traits or, in this case, a set of their principal components.

We computed these FDMs from remote sensing variables that were either reflectance factors or optical traits estimated by inverting an RTM against the reflectance factors (T_{optical}, section 2.3.4 and 2.4.3). We also used plant traits at the field level ("field plant traits"), either inputs of the RTM used to simulate reflectance factors (T_{RTM}, section 2.2) or sampled in the FunDivEUROPE plots (T_{field}, section 2.4.1). Notice that not all of these traits are "functional traits" *sensu* Díaz and Cabido (2001), but vegetation characteristics or structural state variables as they are not species-specific and change with ontogeny, environment, and forest management (e.g., canopy height or leaf area index). Still, we used these traits since ecologists have selected them to characterize functional diversity in mature forests (i.e., T_{field}) (Baeten et al. 2013; Benavides et al. 2019a; Benavides et al. 2019b), or since modelers use them to describe light-vegetation interaction (i.e., T_{RTM}) (North 1996; Verhoef 1985). The implications of this choice are discussed in section 4.4.

2.2 Radiative transfer model and emulation

RTMs describe light-matter interaction. They mechanistically link vegetation parameters (here referred to as traits), describing plant structure and biochemistry with the spectral signals perceived by remote sensors. Therefore, RTMs allow simulating canopy reflectance factors from a set of model parameters and retrieving plant traits from spectral observations through inverse modeling (Jacquemoud et al. 2009). In this work, we used the Soil Canopy Observation, Photochemistry and Energy fluxes (SCOPE) model (van der Tol et al. 2009) to simulate vegetation's optical properties as a function of plant traits (i.e., T_{RTM}). SCOPE includes the leaf RTM Fluspect-CX (Vilfan et al. 2018), which incorporates anthocyanins specific absorption coefficients from PROSPECT-D (Féret et al. 2017). SCOPE T_{RTM} includes 1) leaf traits such as the number of internal leaf layers (N, layers), and chlorophyll a and b (C_{ab}, µg cm^{-2}), carotenoids (C_{ca}, µg cm^{-2}), anthocyanins (C_{ant}, µg cm^{-2}), senescent pigments (C_{s}, a.u.), dry matter (C_{dm}, g cm^{-2}) and water (C_{w}, g cm^{-2}) contents; and 2) traits describing vegetation structure as the mean and bimodality of the leaf inclination distribution function ($LIDF_a$ and $LIDF_b$, respectively), leaf area index (LAI, m^2 m^{-2}), canopy height (h_{c}, m), and the leaf width (l_{w}, m). Additional model parameters describing soil optical properties and illumination-observation conditions are described in Table S1.

In addition, we used statistical models or emulators (Gómez-Dans et al. 2016) to enable fast computation of large datasets of reflectance factors with SCOPE. We trained and validated two shallow neural networks predicting specie's reflectance factors from their traits, each with a different set of look-up tables. We used the first for simulation (section 2.3.3) and the second to retrieve optical traits via RTM inversion (section 2.3.4). Using two different emulators allowed us to force a model error in the retrieval, making it more realistic (Supplementary SM1 and Table S2 describe the emulators' training and comparison and present their statistics, respectively).

2.3 Simulation of traits and spectral diversity

Fig. 2 represents a schematic with the details of the simulation of synthetic vegetation communities and their spectral signals, the simulation of different remote sensing features on these signals, and the various comparisons of the FDMs computed from field plant or remote sensing data.

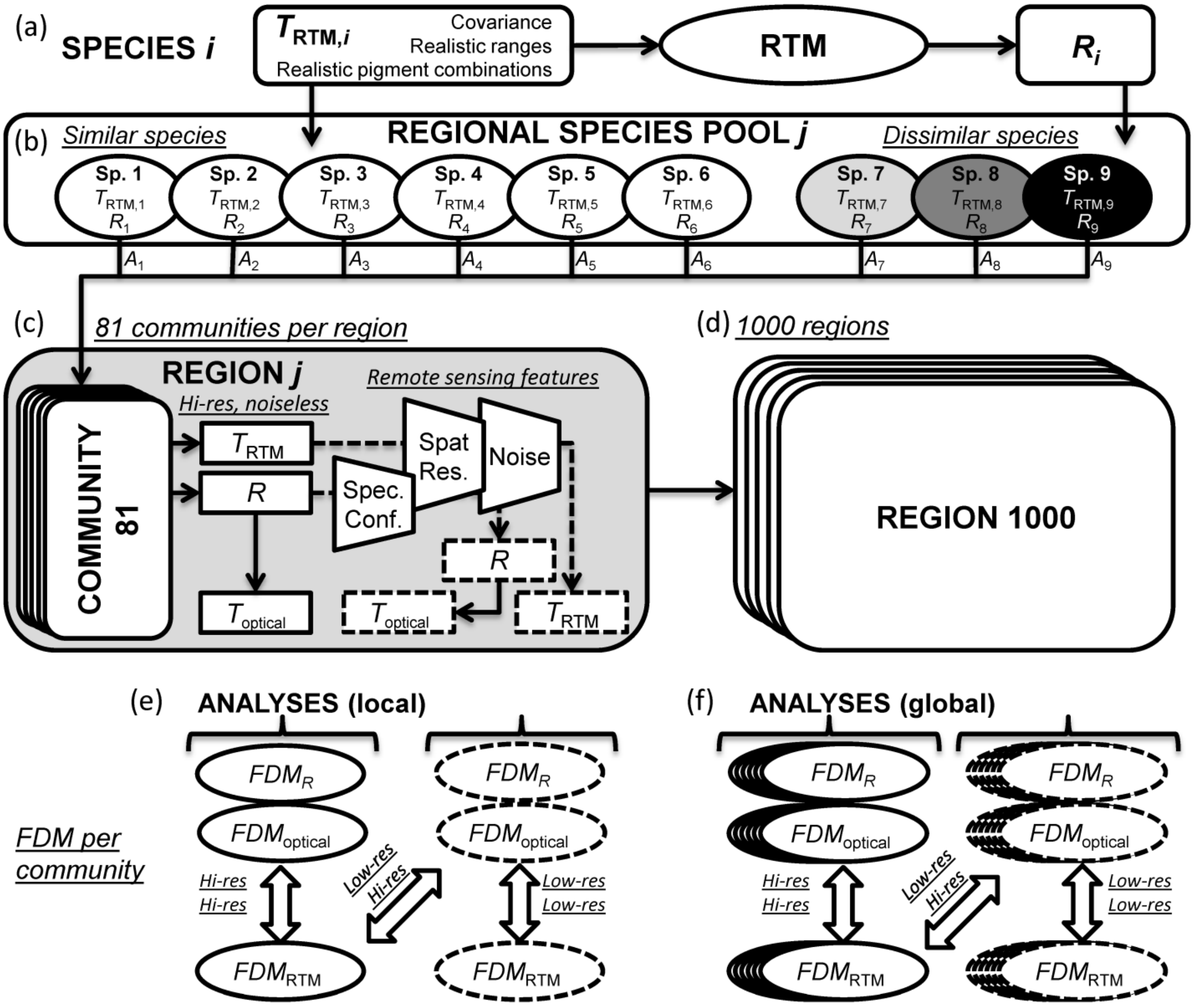

Figure 2. Detailed simulation and analysis workflow. Each species (i) is defined by a plausible set of field plant traits (T_{RTM}), the input of a radiative transfer model (RTM) that predicts the associated reflectance factor (R) (a). Several species (9 in this example) are gathered within a regional species pool (b). Some species feature traits with close or similar values (similar species), whereas others feature dissimilar trait values (dissimilar species). Then, the species from the pool are sampled with different abundances (A) to produce 81 communities per region (c); the original

traits and reflectance factors (solid lines) are transformed by different remote sensing features (dashed lines). In both cases, the plant traits are also estimated from the optical signals via radiative transfer model inversion (optical traits, T_{optical}). In total, 1000 regions are produced from a corresponding number of species pools (d). Functional diversity metrics (FDM) are computed from the abundances and either the field vegetation traits (FDM_{RTM}), the optical traits (FDM_{optical}), or the spectral reflectance factors (FDM_R) of each community. The relationships between the FDMs at different spatial resolutions are compared for each region (e) and all the regions at the same time (f)

2.3.1 Species, communities, and regions

We defined each synthetic plant species with 1) a unique set of plausible biochemical and structural traits (i.e., T_{RTM}) and 2) the corresponding reflectance factors predicted by the emulator (Fig. 2a). Field plant traits were randomly sampled; however, we ensured plausible combinations of traits by accounting for known ranges in different types of vegetation (e.g., forests, crops, grasslands, etc., reported in Table S1) and traits covariance identified in spectral libraries (Appendix A). Since we emulated a unidimensional RTM, we did not further describe these species (e.g., stem type or crown shape) nor attempted to focus on any specific vegetation type or ecosystem. The limitations of the modeling framework are discussed in section 4.3.

Between 5 and 30 synthetic species were gathered to produce regional species pools (Fig. 2b). The pools contain all the species present in a region (or remote sensing image) that mix later in different communities (or moving windows used for image analysis). In practice, the pools are a species-by-traits matrix containing the traits (i.e., T_{RTM}) of the species present in a region. In nature, biotic and abiotic filtering and interactions determine species assemblages according to their traits (Jucker et al. 2018). These processes can prevent or enable the combination of traits with very similar or very different values in the same community. Therefore, we ensured assemblage variability by different fractions of similar and dissimilar species in the pools. We forced part of the pool species to be similar by sampling their traits within narrow ranges. For example, chlorophyll content (C_{ab}) could be limited between 20 and 30 μg cm^{-2}.

In contrast, we also produced dissimilar species by sampling their traits within wide plausible bounds (0-100 µg cm^{-2} for C_{ab} in Table S1). The fraction of similar and dissimilar species and the width of the sampling range for the similar species were randomly set. We set the same soil properties for all the species for each pool, but these varied between pools. Contrarily, we fixed a constant diffuse-to-global radiation ratio (δ_{DG} = 0.20) and sun zenith angle (θ_{sun} = 30°) for all the simulations.

Finally, we simulated 81 communities per region by combining the regional pool species with different relative abundances (*A*) (Fig. 2c). First, we numbered the species, clustering similar and dissimilar species separately (e.g., in Fig. 2b, similar species range from 1 to 6, and dissimilar species from 7 to 9). Then we assigned the abundances using the probability predicted by a Gaussian distribution for these numbers maximizing the range of possible combinations of the species pool (Appendix B). To do so, we gradually modified the dominant species (the mean) and the degree of dominance (the standard deviation) of each community. Fig. 3 exemplifies the relative abundances of the 81 communities produced for the species pool in Fig. 2b and highlights the most extreme cases.

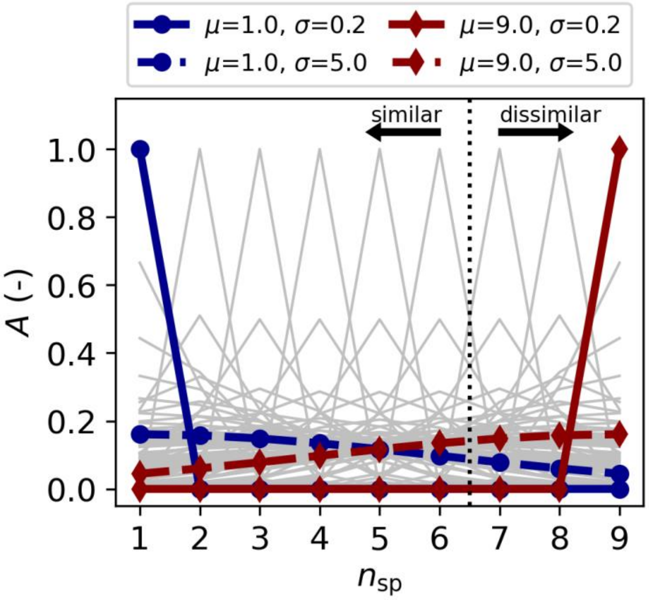

Figure 3. Example of the relative abundances (*A*) simulated for the regional species pool in Fig. 2b (9 species). The species are indexed with integer values (n_{sp}), separating similar from dissimilar species. The relative abundances are

generated by gridding the mean (μ) and standard deviation (σ) of the Gaussian distribution assigning species abundances. The figure highlights the most extreme cases where species 1 (similar) or 9 (dissimilar) are dominant (determined by μ), with maximum and minimum degrees of dominance (with $\sigma = 0.2$ and $\sigma = 5.0$, respectively).

2.3.2 Remote sensing features

We evaluated the effects of three features of the RS data on the relationships between FDMs (Fig. 2c): 1) spectral resolution and configuration (i.e., bands width, range, location), 2) spatial resolution, and 3) signal noise. Since field data are also uncertain, we applied the same noise level to reflectance factors and field plant traits (Fig. 2c). We simulated three levels for each RS feature and tested all the possible (27) combinations (Table 1). This analysis envisaged evaluating the trade-offs between different mission concepts to study functional diversity from space.

Table 1. Remote sensing features tested in the simulation analysis. The noise level reported was applied to the simulated reflectance factors and the field plant traits. Regarding the spectral configuration, DESIS and Sentinel-2 Multi-Spectral Instrument (MSI) spectral response functions were obtained from imagery metadata (section 2.4.1) and the European Space Agency (ESA 2017), respectively. The first row presents the ideal combination of features (maximum resolution, noiseless) on which the rest of the simulations are based.

Spectral configuration	**Spatial Resolution**	**Noise**
Full-hyperspectral 2001 bands between 400-2400 nm, 1 nm step	High: $S_{res,100}$ All the species of the community are individually discriminated	Low: $\sigma_{noise} = 0$ % Noiseless signal
DESIS 58 bands (4x binned) between 410-986 nm	Medium: $S_{res,50}$	Medium: $\sigma_{noise} = 5$ % 5 % of Gaussian noise

	Half of the species of the community are observed as a mixture	
Sentinel-2 10 bands between 490-2190 nm	Low: $S_{res,0}$ None of the species of the community can be individually identified; they are all mixed by the sensor	High: σ_{noise} = 10 % 10 % of Gaussian noise

Species' reflectance factors were initially simulated at 1 nm step between 400 and 2400 nm ("full-hyperspectral") and then convolved to the spectral bands of two different sensors: DESIS and Sentinel-2. DESIS is a visible and near-infrared hyperspectral imager onboard the International Space Station (Kerr et al. 2016). Sentinel-2 is one of the Copernicus missions managed by the European Space Agency (ESA). It carries the Multi-Spectral Instrument (MSI), a visible, near, and short-wave infrared multispectral imager that maps Earth's surface properties with ten wavebands (Drusch et al. 2012).

Since our simulation did not describe the spatial distribution of the species within each community, we defined the spatial resolution as the sensor's capability to discriminate between individual species and their spectral signatures. Initially, the simulations represented highly resolved imagery, providing an accurate characterization of each species and their abundances in the community ($S_{res,100}$). Then we ran two additional simulations where the sensor could only discriminate half ($S_{res,50}$) or none of the community species ($S_{res,0}$). In these cases, new species were perceived as a linear combination of the reflectance factors and the abundances of the species that could not be distinguished (Appendix C). In addition, we applied the same transformation to the field plant traits (T_{RTM}) to compare field and RS data at the same spatial resolution (section 2.3.5).

2.3.3 Simulations

In total, we produced 27 simulations (all the column combinations in Table 1), each consisting of 1,000 species pools and 81 communities (thus 81,000 communities), integrating a total of 16,153 species (Fig. 2d). For comparison, we initialized all the simulations with the same noiseless and full spectral and spatial resolution abundances, reflectance factors, and field plant traits (Table 1, first row). Then, these were modified by combinations of the different levels of the RS features to assess their effect on the relationships between field and remote sensing FDMs. Fig. 4a-c exemplifies the simulation of a synthetic community (similar and dissimilar specie's abundances, spectra, and traits, respectively) and the role of the RS features (Fig. d-i). The degradation of the spatial resolution modifies the sensor's perception of the abundances (Fig. 4a,d,g) and spectral properties (Fig. 4b,e,h). When pixels become larger, they can include new species from outside the area occupied by the community (or a reference field plot (Gholizadeh et al. 2018)). From a remote sensing perspective, these communities could just be moving windows where pixels are selected to compute FDMs (e.g., Rocchini et al. (2021)). Moreover, the mixture of spectral signals can hide the signature of the rarest species, reduce the representativeness of locally dominant species, and, overall, reduce spectral diversity in the region. At the same time, the convolution to spectral bands of different sensors reduces the detail and extent of the spectral data. In contrast, noise increases variability (Fig. 4e,h vs. Fig. 4f,i).

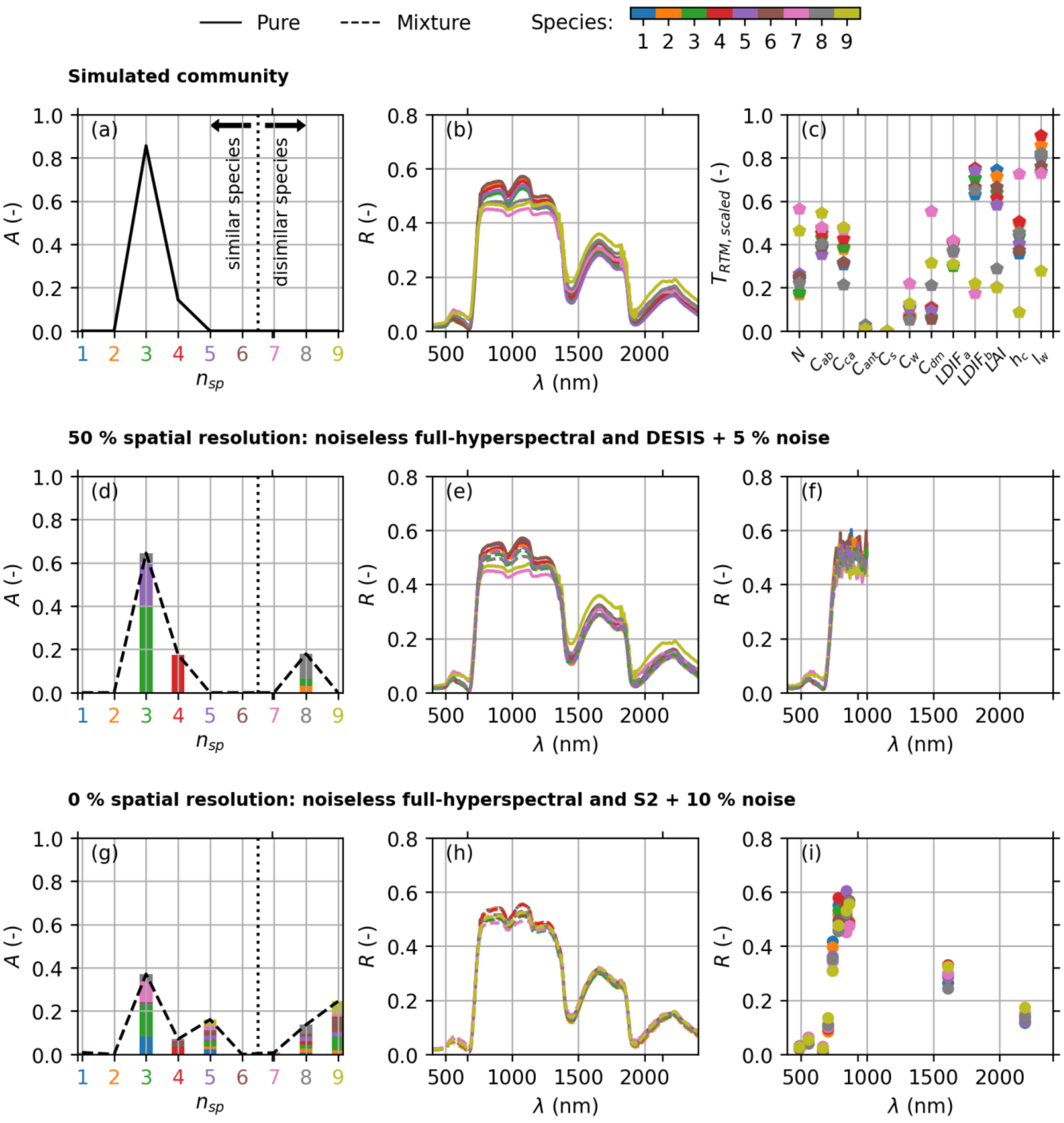

Figure 4. Example of the simulation of a synthetic community and effect of different remote sensing features on the perception of specie's reflectance factors and abundances. The first row presents the original abundances (*A*) (a), species reflectance factors (*R*) (b), and field plant traits (T_{RTM}) scaled within the bounds set for the simulation (c). In the abundance subplots (first column), the black-pointed line separates similar (on the left) from dissimilar species (on the right). The color assigned to each species' number (n_{sp}) identifies the corresponding reflectance factors and traits in the remaining subplots. Solid lines represent pure species, whereas dashed lines represent spectral mixtures

due to spatial resolution degradation. The second row degrades spatial resolution so that only 50 % of the species in the pool can be discriminated, leading to new estimates of species abundances (d); the color bars represent the contribution of each species to the new species abundance, as observed by the remote sensor. Sensed reflectance factors, full-hyperspectral and noiseless (e), or convolved to DESIS spectral bands with a 5% random noise (f). The third row degrades spatial resolution so that none of the species can be identified, leading to new estimates of species abundances (g); the color bars represent the contribution of each species to the new species abundance, as observed by the remote sensor. Sensed reflectance factors, full-hyperspectral and noiseless (e), or convolved to Sentinel-2 MSI spectral bands with a 10% random noise (i).

2.3.4 Retrieval of optical traits

We estimated optical traits from the species' reflectance factors via inversion of the emulated RTM (T_{optical}) for each of the 27 simulations (Fig. 2c). This way, we accounted for the effect of the different remote sensing features on the retrieval. Additionally, using a second emulator for the inversion, we accounted for model error (models' inaccuracy or limitation to represent the observation) since both emulators predict slightly different reflectance factors for the same input. This approach does not aim to analyze or quantify the effect of different model structures and vegetation features in the inversion of RTMs, but to include a plausible source of uncertainty inherent to RTM inversion. We estimated the optical traits using a numerical optimization approach (Jacquemoud et al. 2009) in two steps. First, we calculated an initial solution using a look-up table approach. Then, the most relevant vegetation parameters were further optimized using the L-BFGS-B algorithm (Zhu et al. 1997) (Supplementary SM2 provides a complete description).

2.3.5 Functional diversity metrics computation and comparison

For each simulation (27), we computed the FDMs from field plant traits (T_{RTM}, as if measured in the field) and remote sensing data (reflectance factors or optical traits estimated via model inversion). FDMs were independently computed for the 81 communities of each region as described in section 2.1 (Fig. 2e).

We analyzed the relationships between field-based (T_{RTM}) and RS-based (R or T_{optical}) metrics to understand their ability to capture vegetation functional diversity from space. Linear models were evaluated using the coefficient of determination (R^2) and the normalized root mean squared error (*NRMSE*, normalized by the 95 % confidence interval of the dependent variable to reduce the effect of outliers).

Also, we evaluated FDM relationships at global and local scales to understand their consistency and applicability in both contexts. First, we compared at once all the species pools of each simulation (global, 81 communities by 1,000 species pools) to assess their capability to provide information comparable between different ecosystems, regions, or RS images (Fig. 2f). Then we compared the FDMs of the communities of each species pool separately (local, 1,000 species pools) and extracted the median and the 95 % confidence interval of the statistics (Fig. 2e). This second comparison studied the capability of each FDM to infer functional diversity within a single ecosystem, region, or image.

In addition, we evaluated the effect of the resolution at which field traits are sampled and compared with RS metrics (Fig. 2e,f). On the one hand, we compared field FDMs at maximum spatial resolution (hi-res) to simulate the mismatch between imagery and field surveys characterizing individual species (this means field $S_{\mathrm{res},100}$ vs. remote sensing $S_{\mathrm{res},50}$ or $S_{\mathrm{res},0}$). This analysis simulates the case where ecology studies characterizing individual species are combined with remote sensing data, as in section 2.4. On the other hand, we compared vegetation FDMs at the spatial resolution of the sensor (RS-res, comparing $S_{\mathrm{res},50}$ vs. $S_{\mathrm{res},50}$ or $S_{\mathrm{res},0}$ vs. $S_{\mathrm{res},0}$, respectively). Here, we simulated field surveys characterizing vegetation within plots specifically designed to match satellite pixels (e.g., Hauser et al. (2021a; 2021b)) but not identifying individual species. This second analysis represents the case of typical remote-sensing oriented surveys where field datasets are integrated, mimicking the remote sensor's spatial resolution.

For all these cases, we compared the FDMs' performance of the 27 simulations to understand the effect of the remote sensing features and signal noises under evaluation.

2.4 Estimation of functional diversity with DESIS and Sentinel-2 at FunDivEUROPE sites

2.4.1 Study sites and field-based biodiversity metrics

We combined field and RS data collected in plots of the FunDivEUROPE network (http://www.fundiveurope.eu) (Baeten et al. 2013; Benavides et al. 2019a; Benavides et al. 2019b). The 30 x 30 m plots covered matured forests in Spain (Mediterranean oak and pine woodland) and Romania (mountainous mixed conifer and beech). The other network regions were discarded from the analysis since they were not covered by DESIS (i.e., Finland) or because foliar traits had not been measured (Ma et al. 2019). In each country, the plots were located to cover the local diversity gradients of the pool of (up to four) dominant tree species, covering 5 x 5 km and 50 x 50 km regions in Romania and Spain, respectively. FunDivEUROPE design ensured the inclusion of different levels of taxonomic richness, each comprehending different mixtures of species and sufficient representativeness of each species featuring similar frequencies (Baeten et al. 2013). Plant traits were measured in the dominant tree species, and field-based FDMs were computed in plots where dominant species covered more than 95 % of the abundance (Ma et al. 2019).

In each plot, ten trees per species with a diameter at breast height (*DBH*, m) larger than 7.5 cm were selected to measure *DBH*, h_c (tree height), and crown cross-sectional area (*CCSA*, cm^2). *LAI* was determined for the whole plot with an LAI-2000 Plant Canopy Analyzer (LI-COR, Lincoln, NE, USA), as described in Grossiord et al. (2014), and therefore it was not used to compute field FDMs. Moreover, a top south-facing branch was cut per tree, and around ten leaves per branch were sampled. Half of them were used to determine leaf nitrogen concentration (N_{mass}, %) and leaf carbon concentration (C_{mass}, %). The other half was used to determine leaf area (l_a, mm^2), specific leaf area (*SLA*, mm^2 mg^{-1}), and leaf dry matter concentration (*LDMC*, mg g^{-1}) (Benavides et al. 2019a; Benavides et al. 2019b). In total, 1763 trees were sampled. The field campaigns took place in July in Romania 2013 and June 2013 in Spain.

We did not compute the FDMs in the *dbFD* package on these field-measured traits since *FRic* and *FDiv* require more species than traits, and the maximum plot richness is four. Instead, we applied standardization, PCA, and computed parametric Rao's *Q*. As before, we kept the components explaining 98 % of the variance. We also calculated two taxonomic diversity metrics: the Shannon index (*H*) and species richness (*S*). Where *S* equals the number of species in the plot (up to 4), and *H* predicts the uncertainty of guessing the species of individuals randomly sampled from the community (Shannon 1948). *H* (Eq. 2) increases as the community's richness and evenness do.

$$H = -\sum_{i=1}^{S} A_i \log(A_i) \tag{2}$$

2.4.2 Imagery and reflectance-based biodiversity metrics

We analyzed DESIS and Sentinel-2 imagery acquired over the FunDivEUROPE plots described in section 2.4.1. Following Ma et al. (2019), we used for all the analyses Sentinel-2 imagery acquired in the summer of 2015 since it was the closest to field sampling. However, DESIS imagery corresponds to the summer of 2020. Therefore, to improve DESIS and field data comparability, we also processed Sentinel-2 imagery acquired in the summer of 2020 and used these images to discard field plots that substantially changed after 2015 (Supplementary SM3) and assess the effect of the temporal gap on the evaluation of DESIS in FunDivEUROPE. Table 2 summarizes the imagery used and the number of plots selected according to their temporal stability, absence of clouds, and field data availability.

Table 2. DESIS and Sentinel-2 imagery selected over FunDivEUROPE plots. Mean atmospheric optical thickness (*AOT*), sun zenith (θ_{sun}), view zenith (θ_{sun}), and azimuth phase ($\Delta\phi$) angles of the plots selected are also presented.

Country	Date	Plots	Mean θ_{sun}	Mean θ_{view}	Mean $\Delta\phi$	Mean *AOT*

		selected				
DESIS						
Spain	2020-Jun-29 10:11	14	30.8	23.9	6.6	0.264
Romania	2020-Jun-29 07:02	8	45.9	2.1	3.7	0.283
Sentinel-2						
Spain	2015-Jul-29 11:00	25	2.6	26.1	121.0	0.015
Romania	2015-Jul-29 09:20	19	5.8	30.7	121.5	0.014
Spain	2020-Jun-22 10:56	23	2.7	21.5	127.5	0.082
Romania	2020-Jul-09 09:06	11	9.2	28.1	51.6	0.081

We downloaded DESIS L2A products from the EOWEB® GeoPortal (https://eoweb.dlr.de/egp/); standard radiometric, atmospheric, and terrain corrections were automatically applied by DLR (Alonso et al. 2019). During download, we applied nearest-neighbor resampling and a default ozone column value of 330 Dobson units. Metadata files provided the average atmospheric optical thickness (*AOT*) sensor height and sun and view angles at the scene's center, from which we calculated the corresponding angles on each plot. Sentinel-2 images were processed using the ESA's Sen2Cor processor (v2.2.0, https://step.esa.int/main/third-party-plugins-2/sen2cor/) to produce L2A bottom of the atmosphere reflectance factors. Then we pan-sharpened the 20-m bands (B05-B07, B8A, B11, and B12) to 10 m spatial resolution using the unmixing method developed by Brodu (2017) and implemented in the ESA's Sen2Res toolbox (http://step.esa.int/main/snap-supported-plugins/sen2res/). Further details of Sentinel-2 imagery processing can be found in Ma et al. (2019). Next, we obtained the corresponding *AOT* from the products of the atmospheric correction and estimated all the sun and view angles using the python package *sentinel2_angle_bands* (https://github.com/brazil-data-cube/sentinel2_angle_bands). Then, we resampled

Sentinel-2 to DESIS spatial resolution to understand to what extent the differences between the functional diversity estimates of each mission could be related to their spatial or spectral features.

We extracted the 3 x 3 pixels windows centered on each FunDivEUROPE plot with spatial resolutions of 10 ($S2_{10}$) and 30 m ($S2_{30}$ and DESIS). We gathered these data to get single standardization and PCA models for each sensor, keeping the components that explained 98 % of the variance to reduce signal noise. Then we computed the FDMs described in section 2.1; in this case, each pixel of the 3 x 3 window was considered a unique species whose abundance was the inverse of the number of pixels in the window, as described in Rocchini et al. (2021). Fig. 5 shows an example of the spectral data available in one of the FunDivEUROPE sites in Spain for $S2_{10}$ (Fig. 5a,d), $S2_{30}$ (Fig. 5b,e), and DESIS (Fig. 5c,f). $S2_{10}$'s high spatial resolution allows sampling the internal variability of the field plot with a 3 x 3 window; DESIS resolution equals the plot size (30 m) and instead samples the variability of the surroundings of the plot. Also, DESIS more finely captures the visible and near-infrared region’s variability, whereas Sentinel-2 captures a larger spectral diversity in the short-wave infrared. These differences can be observed both in the imagery and the spectra.

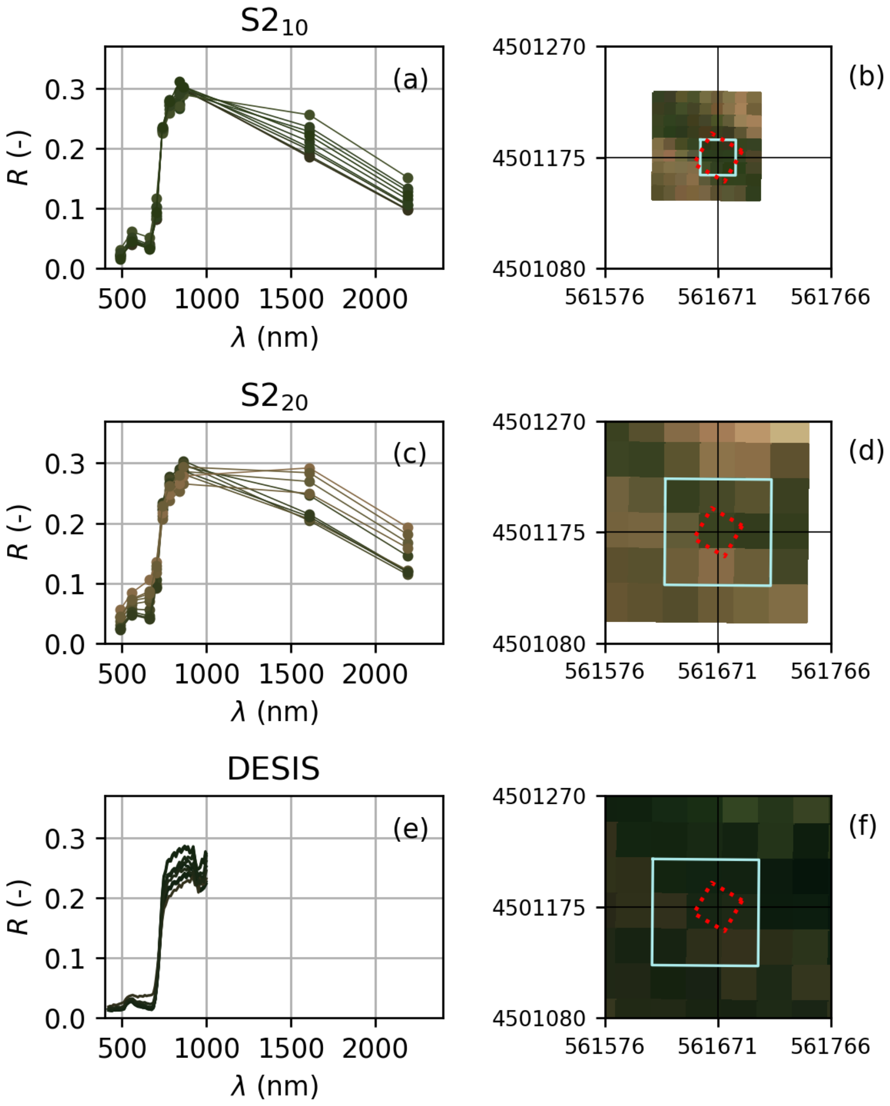

Figure 5. Example of the remote sensing data used in one of the FunDivEUROPE sites in Spain (SPA01). Spectra of the 3 x 3 pixels window used to compute the functional diversity metrics (first column) and red-green-blue composition of the clips around the site (second column) together with the plot (red dashed line) and the 3 x 3 pixels window (pale blue) used to compute functional diversity metrics. Sentinel-2 MSI @ 10 m pixel in 2015 ($S2_{10}$, first row), Sentinel-2 MSI @ 30 m pixel in 2015 ($S2_{30}$, second row) and DESIS @ 30 m pixel in 2020 (third row). Spectra and imagery pixel colors are matched.

2.4.3 Optical traits retrieval and biodiversity metrics

FDMs were also computed from optical traits (T_{optical}) estimated from DESIS, S2$_{10}$, and S2$_{30}$ reflectance factors for all the pixels within the 3 x 3 window surrounding each plot. We used an approach similar to the one described in section 2.3.4; however, in this case, we inverted the model (not the emulator) in the second step to account for the off-nadir view angles and regularized the cost function (Supplementary SM4). Next, we assessed the retrieval quality by comparing *LAI*, chlorophyll concentration (µg g^{-1}) (computed from C_{ab}, and dry matter content (C_{dm}) estimates), and C_{dm} with field *LAI*, leaf N_{mass}, and C_{dm}, respectively. After the inversion, we computed the FDMs described in section 2.1 on the estimated optical traits. As with the imagery, we gathered all the optical traits to provide a common standardization and PCA models for dimensionality reduction and kept the components explaining at least 98% of the variance.

3. RESULTS

3.1 Links between functional diversity metrics

The comparison of FDMs computed from field plant traits (T_{RTM}) and reflectance factors (*R*) under ideal conditions (noiseless, full-hyperspectral, and maximum spatial resolution) at the global scale (all data simultaneously) showed that $RaoQ_{\alpha=1}$ (Fig. 6g) presents the highest R^2, followed by *FDis* (Fig. 6d) and $RaoQ_{\alpha=2}$ (Fig. 6h), and then *RaoQ* (Fig. 6e), *FRic* (Fig. 6a) and $RaoQ_{\alpha=\infty}$ (Fig. 6i). The strength of the relationships of the parametric *RaoQ* (Rocchini et al. 2021) decreased with the value of α (not shown). For $\alpha = 0$, extreme values strongly reduced the coherence of the relationship. *FDiv* (Fig. 6c) and especially *FEve* (Fig. 6b) showed weak relationships. Results at the global scale were coherent with those found at the local scale (1000 comparisons, one per species' pool); median values of R^2 (and *NRMSE*) were always larger than those found at the global scale (e.g., 0.75 vs. 0.89 R^2 for $RaoQ_{\alpha=1}$). However, the performance at the local scale featured large variability. The 2.5 % percentile of the R^2 distribution was below 0.35 in most of the metrics, except for $RaoQ_{\alpha=1}$ and *FRic*. Most FDMs reached very high R^2 (~ 0.98) locally, except

FDiv and *FEve*, whose maximum (97.5 % percentile) values are 0.64 and 0.62, respectively. Still, median values were low for these FDMs, suggesting that vegetation evenness and divergence could not be reliably inferred from imagery using these metrics at local scales.

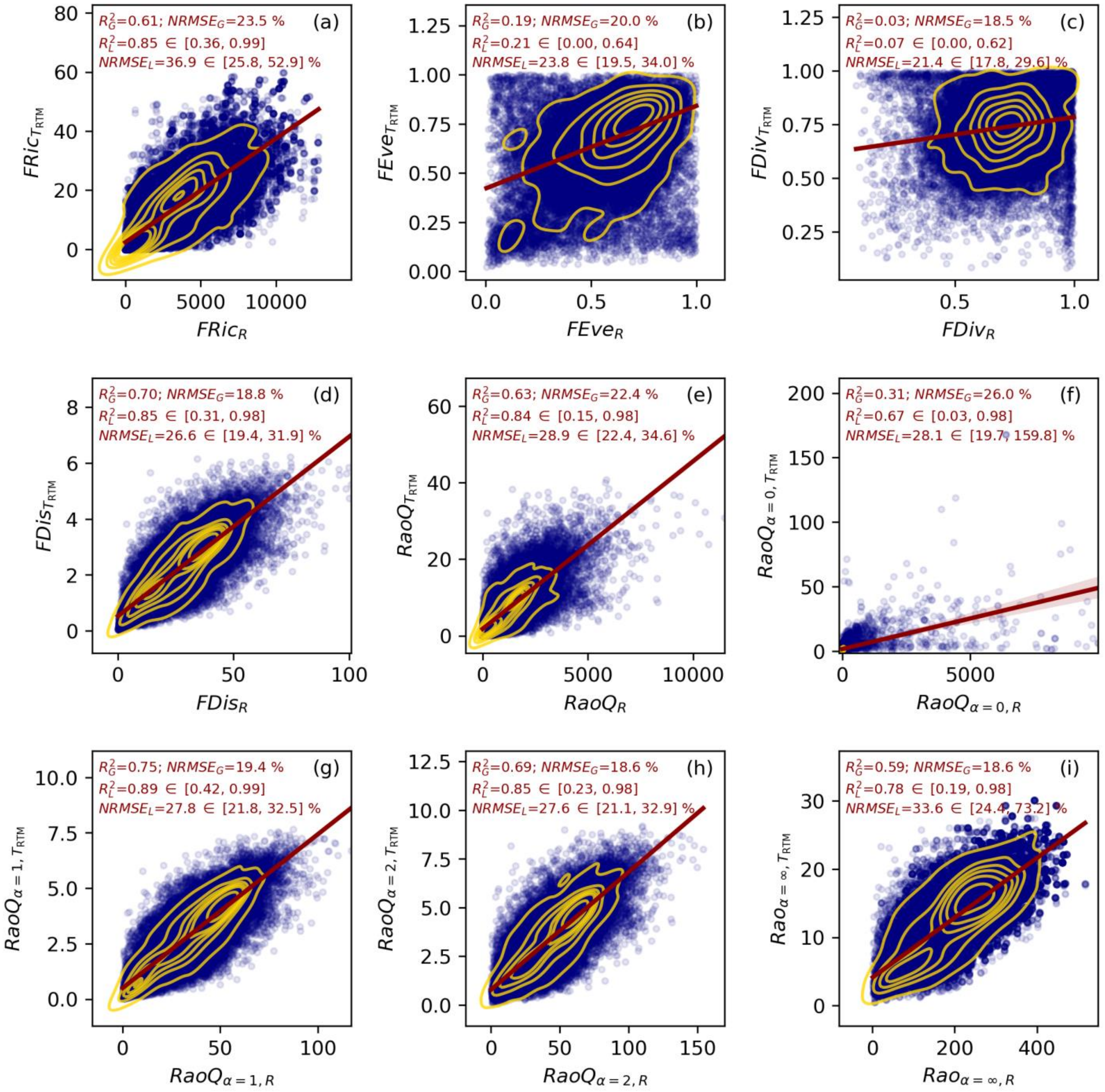

Figure 6. Relationship between the functional diversity metrics computed from the reflectance (subscript "*R*") factors and field plant traits (subscript "T_{RTM}") using the *dbFD* package (a-e) or the parametric Rao's *Q* formulation with different values of the parameter *α* (f-i). Regression lines summarize the comparison at the global scale; the

shaded areas around the regression lines represent the 95 % confidence interval of the line. Each subplot includes the statistics of the relationship at the global scale (on top, subscript “G”) and the median and 95 % confidence interval of the statistics at the local scale (below, subscript “L”).

The comparison of FDMs computed from field plant traits (T_{RTM}) and estimated optical traits (T_{optical}) under ideal conditions (Fig. 7) led to results similar to those obtained with the reflectance factors (Fig. 6). However, this time FDMs’ performance was higher in almost all the cases, both at the global and the local scales (median values). Higher correlations occurred despite the uncertainties in the retrieval (Fig. S1) and the fact that FDMs were computed from a subset of the optical traits controlling R (Supplementary SM2). T_{optical} were retrieved with different degrees of success. Evaluated against the field plant traits, the estimates of LAI and $LIDF_{\mathrm{a}}$ (Fig. S1j,h, respectively) showed biases but high R^2 values. C_{ab}, C_{dm}, and C_{w} (Fig. S1b,f,g, respectively) were acceptably retrieved with frequent overestimation for low values. The leaf parameter N (Fig. S1a) was often underestimated, $LIDF_{\mathrm{b}}$ (Fig. S1i) was weakly constrained, whereas C_{s} and C_{ant} (Fig. S1d,e) were consistently underestimated. The retrieval performance was slightly better when evaluated at local scales (median of the statistics); however, there was a large dispersion of R^2, whose lowest values were close to 0.0 in all the cases. The retrievals worsened as the remote sensing resolutions decreased and the noise increased (Table S3). Results were slightly better when the model error was minimized using the same emulator for simulation and inversion, both in the retrieval (Fig. S2) and the relationships between FDMs (Fig. S3). This analysis proved that model error (Table S2) influences the estimation of plant functional diversity with the optical trait estimation approach.

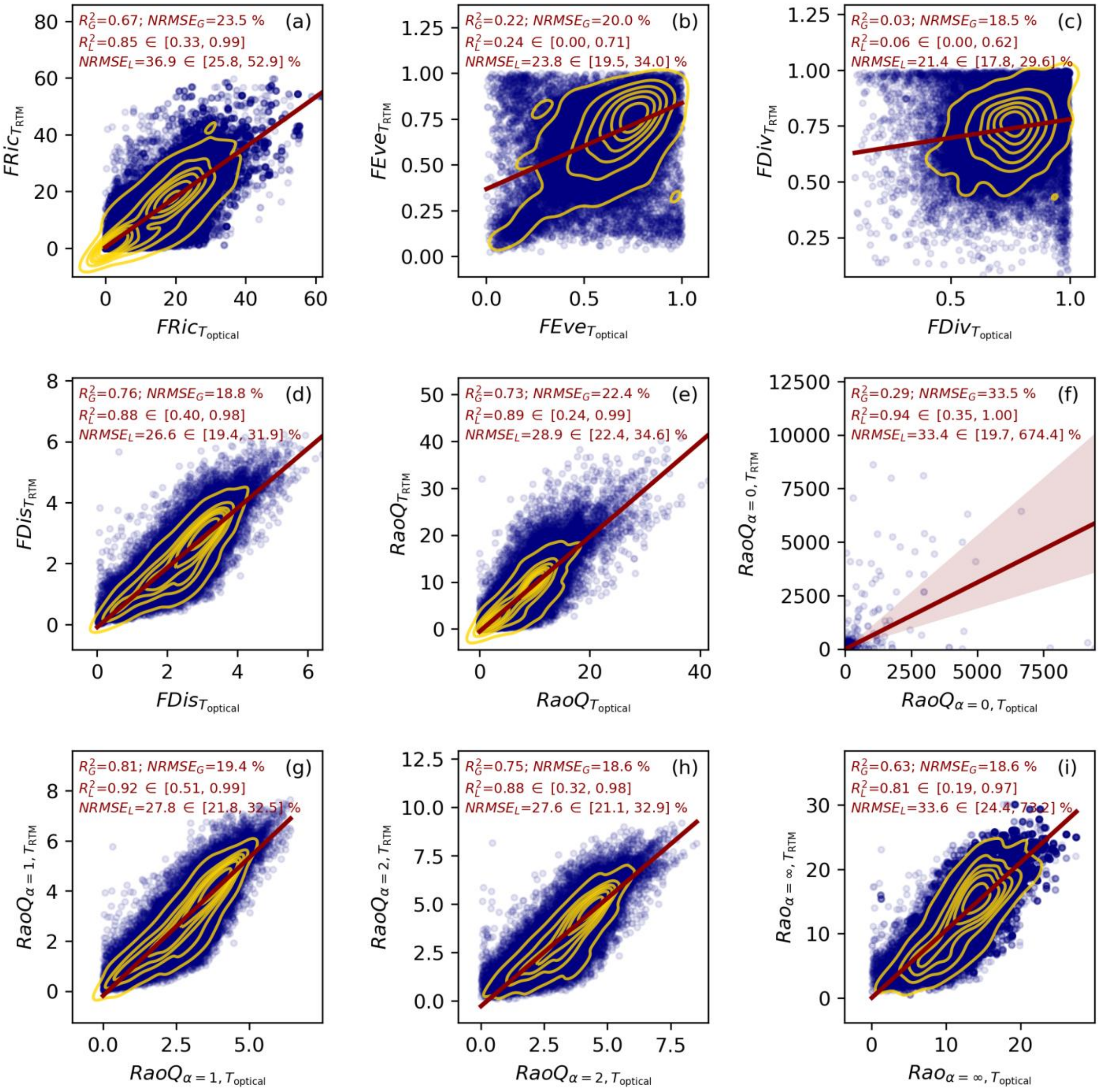

Figure 7. Relationship between the functional diversity metrics computed from optical traits estimated via radiative transfer model inversion (subscript "T_{optical}") and field plant traits (subscript "T_{RTM}") using the *dbFD* package (a-e), or the parametric Rao's Q formulation with different values of the parameter α (f-i). Two different emulators simulated the reflectance factors and estimated the optical traits to induce model error. Regression lines summarize the comparison at the global scale; the shaded areas around the regression lines represent the 95 % confidence interval of the line. Each subplot includes the statistics of the relationship at the global scale (on top, subscript "G") and the median and 95 % confidence interval of the statistics at the local scale (below, subscript "L").

The relationships between field (T_{RTM}) and remote sensing-based (R or T_{optical}) FDMs depended on the remote sensing features (spatial, spectral, and signal noise) and the way the metrics were compared (scale and spatial mismatch). The joint analysis of all these factors (Fig. 8) confirmed that 1) *RaoQ*, *FDis*, and to a lesser extent *FRic*, allow the estimation of plant functional diversity from remote sensing. 2) Local-scale relationships (Fig. 8e-h) were stronger on average than global relationships (Fig. 8a-d) ($\tilde{R}_{\mathrm{L}}^2 > R_{\mathrm{G}}^2$). The analysis also led to three additional discoveries: 1) Spatial resolution loss is the most relevant factor reducing the correlation between remote sensing metrics and field metrics in all the cases (differences in marker colors); whereas the effect of spectral configuration and noise depends on the approach used to compute FDMs (reflectance or optical traits). Noise and spectral configuration had little effect when field FDMs at maximum spatial resolution were compared with R-based metrics at sensor resolution (hi-res, Fig. 8a,e, and Table S4). However, these became more important when the metrics were computed from optical traits (hi-res, Fig. 8c,g and Table S5). Then, in the absence of noise (brightest tones, smallest markers), R^2 was larger than for the reflectance-based approach (Fig. 8a,e), and differences between sensors (marker shape) were small at all the spatial resolutions. However, except for the Full-hyperspectral configuration, R^2 decreased as noise increased (larger and darker markers), making the correlations weaker than for the reflectance-based FDMs. Still, when no species could be discriminated ($\mathrm{S}_{\mathrm{res,0}}$) noise and spectral features lost most influence, and R^2 was low in all cases. 2) When remote sensing estimates were compared with field data integrated at the sensor spatial resolution (RS-res, mimicking the image pixels), the relationships were more robust to the spatial resolution loss. Moreover, metrics computed from reflectance factors (Fig. 8b,f and Table S6) were more robust than those computed from retrieved optical traits (RS-res, Fig. 8d,h, and Table S7 vs. Fig. 8c,g). 3) For both approaches (reflectance or optical trait-based metrics), matching field and remote sensing resolutions (RS-res, Fig. 8b,d,f,h) led to spurious R^2 increases for *FRic*, *FEve*, and *FDiv*; induced by noise or spatial resolution loss.

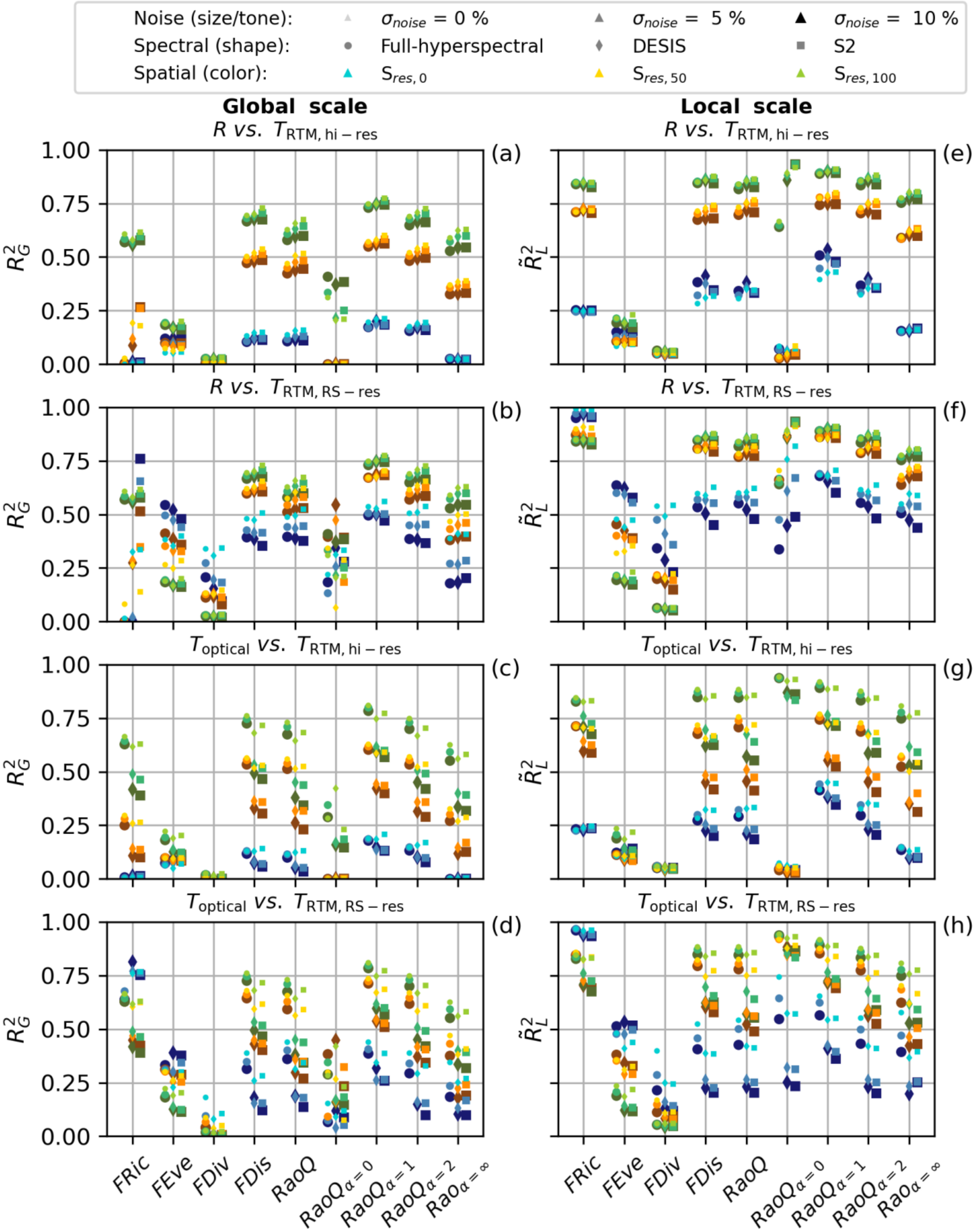

Figure 8. Evaluation of remote sensing features on the relationships between functional diversity metrics. Metrics computed from field plant traits (T_{RTM}) are compared with remote sensing metrics computed either from reflectance factors (R) or estimated optical traits (T_{optical}). The left column presents R^2 of the relationships between metrics

compared at the global scale (R_G^2), the right column shows the median R^2 of the evaluation at the local scale ($\tilde{R}_L^2$). Functional diversity metrics computed from reflectance factors at sensor resolution are compared with field metrics at maximum spatial resolution (hi-res), representing the mismatch between remote sensors and field surveys (a, e) and remote sensing resolution (RS-res) mimicking remote sensing-oriented field surveys (b, f). Functional diversity metrics computed from estimated optical traits at senor resolution are compared with field metrics at maximum spatial resolution (hi-res) (c, g) and remote sensing resolution (RS-res) (d, h). Markers show different spectral configurations; color ranges indicate spatial resolution, whereas marker size and tone represent noise level.

3.2 DESIS and Sentinel-2 imagery over FunDivEUROPE sites

As in the simulations, optical traits retrieval from RS was not exempt from uncertainty. Still, the evaluation against field traits (Fig. S4, subscript "F") suggests that, at least for key traits, such as *LAI*, C_{ab}, and $C_{dm,}$ the retrieval results were reasonable and within the expected performances (Table S3), or at least similar for all the RS datasets. *NRMSE* ranged between 21 and 37 % for the three variables, whereas R^2 showed larger variability (from 0.00 to 0.93). The retrieval of *LAI* (Fig. S4a,d,g) was most problematic in Romania, still taking both countries together (All), R^2 was high ($R^2 \geq 0.92$ for Sentinel-2, $R^2 = 0.65$ for DESIS). Chlorophyll concentration (per unit mass) showed positive relationships with field N_{mass} (Fig. S4b,e,h). Coherently with the simulations (Table S3), the retrievals' performance generally increased with spatial resolution. In the case of DESIS, the lower R^2 might relate to larger uncertainties in *LAI* and C_{dm} retrieval. C_{dm} was overestimated, especially for DESIS in Spain (Fig. S4c,f,i), but the correlations were moderately strong for the whole dataset (R^2 between 0.47 and 0.54). The fact that DESIS does not cover the short wave infrared might explain this bias, which agrees with the performances found in the simulations (Table S3). Retrieval performances were similar or even higher for Sentinel-2 in 2020 (Fig. S5).

The comparison of FDMs computed from satellite imagery and field plant traits sampled in the FunDivEUROPE plots led to metric and sensor-dependent results (Fig. 9). These were evaluated with the Pearson correlation coefficient ($r_{Pearson}$) to identify negative correlations. *FEve* and *FDiv* were never significantly correlated, and *FRic* only weakly once. $S2_{10}$ showed significant positive correlations between field taxonomic and functional diversity metrics for most of the remaining FDMs. *R*-based metrics (Fig. 9a,d) were more significantly and more often correlated than those calculated from optical traits (Fig. 9g,j) except with the taxonomical field metrics (species richness *S* and Shannon index *H*). DESIS only achieved a significant correlation between *FDis* computed from reflectance factors and field species richness (Fig. 9c). Also, weak significant correlations were found between field and optical trait metrics with field $RaoQ_{\alpha=0}$ when Sentinel-2 was resampled to DESIS spatial resolution ($S2_{30}$) (Fig. 9k). Nonetheless, simulations showed that $RaoQ_{\alpha=0}$ was prone to extreme values that might inflate correlations in small datasets. The fact that only $RaoQ_{\alpha=0}$ correlates and no others such as $RaoQ_{\alpha=1}$ or *FDis* suggest these results could be spurious. Despite the significance, the relationships found for $S2_{10}$ were relatively weak. The maximum R^2 found in significant correlations for each group of FDMs evaluated were 0.27 (Fig. 9a), 0.30 (Fig. 9d), 0.18 (Fig. 9g), and 0.18 (Fig. 9j). For DESIS and $S2_{30}$, the maximum significant R^2 were 0.20 (Fig. 9c) and 0.09 (Fig. 9k), respectively. Overall results were similar but weaker for Sentinel-2 imagery in 2020 (Fig. S6). FDMs computed from optical traits did not achieve significant correlations in this case.

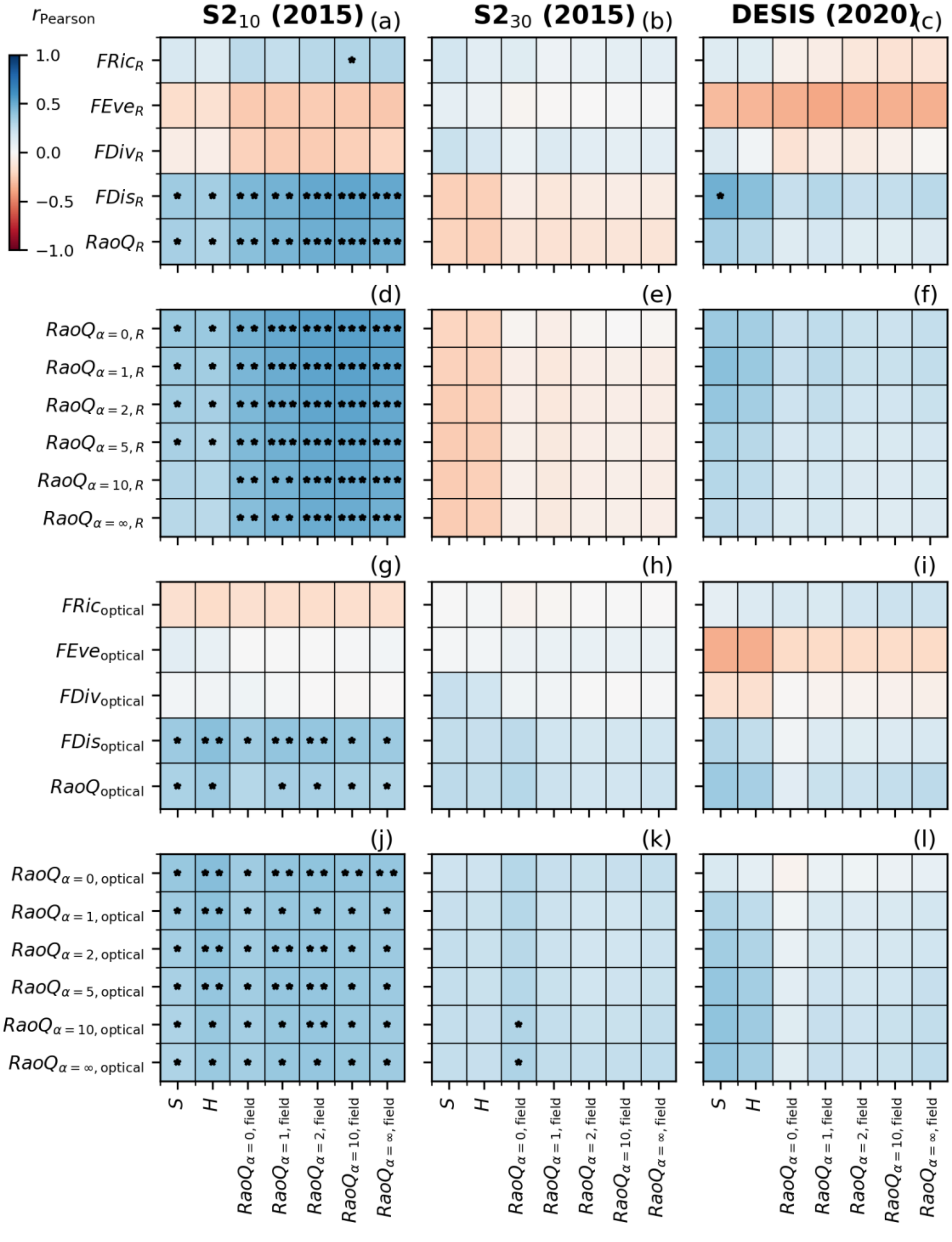

Figure 9. Pearson correlation coefficient between taxonomical and functional diversity metrics computed from field plant traits (subscript "field", *x*-axis) and functional diversity metrics computed from remote sensing information (*y*-axis): the reflectance factors (subscript "*R*", first two rows) or the optical traits (subscript "optical", last two rows).

In each case, the *dbFD* package metrics are presented first, and the parametric Rao's *Q* afterward. The statistics correspond to Sentinel-2 MSI @ 10 m spatial resolution ($S2_{10}$, first column), Sentinel-2 MSI @ 30 m spatial resolution ($S2_{30}$, second column), and DESIS at 30 m spatial resolution (DESIS, third column). Sentinel-2 imagery was acquired in 2015. Asterisks indicate the significance of the correlation (two-tailed) according to its p-value (*p*): *** → $p < 0.001$, ** → $0.001 \leqslant p < 0.01$, and ** → $0.01 \leqslant p < 0.05$.

4. DISCUSSION

4.1 Can we infer functional diversity from space?

Our simulations demonstrate that the SVH is valid for some aspects of functional diversity, but not all of them. Metrics based on the dispersion (Rao's *Q* formulations, *FDis*) and, to a lesser extent, range (*FRic*) can provide robust insight into plant functional diversity from RS data. However, the metrics related to evenness and divergence failed to connect spectral and plant functional diversities. To our knowledge, this is the first study that evaluates these links mechanistically and in a generalizable way. Previous studies also addressed specific questions supporting modeling with local data only, covering a limited range of traits, combinations of species, and sensors (Fassnacht et al. 2022; Hauser et al. 2021b; Heumann et al. 2015; Laliberté et al. 2020; Wang et al. 2018b). Our simulations also demonstrate that plant functional diversity can be inferred from optical traits with even higher precision despite the inherent uncertainties of the retrieval. This fact might be explained by the RTM removing the non-linearity between field plant traits and canopy reflectance and the contribution of other elements such as soil.

The potential of Rao's *Q* and *FDis* metrics to connect plant functional and spectral diversity might rely on the fact that they account both for relative abundances and the ranges of the traits in the multidimensional space. We hypothesize that these metrics would be little affected by equifinal estimates of optical traits as long as these exchange their variability while keeping the diversity information in the overall set of traits evaluated. Hauser et al. (2021a) also found good correlations with field FDMs using this approach. *FRic* showed lower performance and robustness than the dispersion metrics, likely since it does not account for the relative abundance of species. Moreover, since *FRic* is the trait's convex hull volume, it is potentially sensitive to extreme values. *FRic* presents a strong sensitivity to the degradation of spatial resolution (Fig. 8a,c,e,g) but shows much stronger correlations (even spuriously increased) when field data are compared at the spatial resolution of the sensor at local scales (Fig. 8f,h). These results are consistent with the convex-hull-based metric's better performance than Rao's *Q* reported by Hauser et al. (2021b). In all cases, dimensionality reduction might contribute to the robustness against noise and other uncertainties. However, noise might as well compensate for the loss of variability induced by degraded spatial resolution (Fig. 4b,e,h), spuriously increasing the strength of the relationships between some of the FDMs (Fig. 8).

The large scattering observed in the relationships between the indices of evenness and divergence computed from remote sensing and field plant variables might be related to the fact that these metrics look at the dispersion of species within the convex-hull formed by their traits but ignore its volume (Laliberté and Legendre 2010). Combined with the non-linear nature of the relationships between reflectance and field plant traits, this fact might allow for situations where intermediate values of field *FEve* or *FDiv* lead to extreme values of the RS-based metrics and *vice versa*. *FEve* is the metric the least correlated with *FDis* and Rao's *Q* (Laliberté and Legendre 2010), and when compared, RS and field values are widely scattered (Fig 5b and 6b). *FDiv* is more related by construction to *FDis* but presents numerous cases where one of the metrics (from RS or field) takes an extreme value (close to 0 or 1), independently of the other (Fig. 6c and 7c). Ignoring the convex-hull volume might make these metrics less robust to uncertainty and equifinality of the optical traits, leading to spurious correlation increases when metrics are compared at sensor resolution (Fig. 8b,d,f,h).

4.2 Are plant diversity indices comparable beyond a single image or ecosystem?

Especially for Rao's *Q*, *FDis*, and *FRic*, the relationships between RS and vegetation functional diversity are robust at global (e.g., between ecosystems or images) and local (a smaller region or a single image) scales. However, even if median R^2 is larger at the local scale, the large variability of performances registered (Table S4-S7) recommends caution when interpreting RS estimates locally or within a limited number of ecosystems. This performance's variability implies that moderate correlations might be found for *FEve* and *FDiv* in local studies allowing for plausible interpretation of their patterns with the known ecological features of the study site (e.g., Schneider et al. (2017)). However, our results suggest that these metrics should not be trusted since R^2 is prone to be inflated by noise and spatial resolution degradation (Fig. 8). More research is needed to understand the control of specific plant traits on the relationships between functional and spectral diversity and the situations where the metrics are most prone to fail or succeed. For example, Rocchini et al. (2021) suggested that the mixture of crops and urban areas spuriously inflated spectral variability. In our simulations, 11.89 % of the species featured $LAI < 1.0$, which might have produced similar effects. When possible, misleading information should be removed from the spectral datasets to ensure that the spectral variability is only driven by plant diversity. For example, Gholizadeh et al. (2018) and Laliberté et al. (2020) proposed to classify and mask non-vegetated pixels (soil and shades, respectively) before remote characterization of taxonomic and functional plant diversity. In this regard, the inversion of RTMs might contribute to separating background effects from vegetation properties since both are represented.

Interestingly, Rao's *Q*, *FDis*, and *FRic* are comparable between different ecosystems/images despite not sharing a common standardization (and dimensionality reduction). Botta-Dukát (2005) indicated that the same standardization should be applied to the whole dataset when comparing different communities. However, this approach is unsuitable for operational remote sensing since RS products cannot be reprocessed every time a new image is added to the dataset. Botta-Dukát (2005) proposed scaling within plausible trait ranges as an alternative to this standardization. However, his study did not consider a posterior dimensionality reduction, where standardization could be advantageous (van den Berg et al. 2006).

Whether or not global RS products of plant functional diversity require a common standardization/dimensionality reduction model needs to be solved before these can be implemented. We tried to apply a common standardization and PCA model to all the data simulations to explore the possibility of using default models to all RS imagery of a mission. These models were not produced from the simulation used to compute FDMs but from an independent simulation of 10,000 species. The approach failed to improve the performance of the parametric Rao's *Q* metrics, with the R^2 falling below 0.25 at the global scale (not shown). Our simulations show that applying image-based standardization and PCA still allows the comparison of FDMs between different regions or images. Therefore, this approach should also be suitable for analyzing time series and the development of global RS products. Nonetheless, the correlations are weaker than at the local scale (in average). Therefore, alternative methods improving the precision and spatio-temporal consistency of future global plant diversity maps should be explored.

4.3 What are the limitations and ways forward?

Our simulations reveal that spatial resolution, defined as the capability to resolve or identify the spectral properties of individual species, plays the most relevant role in the ability of RS to infer plant functional diversity. In an RS validation framework, the decrease of spatial resolution produces specie's spectra and abundances that do not correspond with those measured in the field and, therefore, a discrepancy between the FDMs compared. Moreover, as the pixel size increases, it includes new species and trait values not present in the field plots used as a reference for RS (e.g., results in section 3.2). New species could also be introduced by the spatial mismatch between RS pixels and field plots. We compared field FDMs with the RS estimates simulating this mismatch and found that the degradation of spatial resolution strongly reduced the performance of RS to infer functional diversity (Fig. 8a,c,e,g). We also compared both data at the RS scale, trying to reproduce what is observed by the sensor from field data. Spatial matching reduced performance loss, but it was still considerable when none of the species could be identified (Fig. 8b,f,d,h).

In addition, we proved that model error influences optical traits retrieval (Fig. S1 vs. Fig. S2) and the subsequent estimation of functional diversity (Fig. 7 vs. Fig. S3). Therefore, a careful selection of the RTM to best represent the canopy monitored could benefit this approach.

Surprisingly, sensor spectral configuration plays a minor role when FDMs are directly computed from *R*. Likely, dimensionality reduction lessens the differences between the information present in datasets of different spectral features. However, this can also be understood as a need for metrics capable of optimally extracting functional diversity information from hyperspectral data. Still, notice that standardization and removal of variables covariance is necessary; simulations avoiding these steps led to weak correlations between FDMs (not shown). Nonetheless, sensor spectral features were more influential when FDMs were computed from optical traits; which suggests that hyperspectral missions (e.g., Environmental Mapping and Analysis Program (EnMAP), DESIS, PRecursore IperSpettrale della Missione Applicativa (PRISMA), Copernicus Hyperspectral Imaging Mission (CHIME), Surface Biology and Geology (SBG)) should be preferred for this approach. Furthermore, simulations show that reducing sensor spectral range or resolution makes this approach more sensitive to noise and spatial resolution decrease (Fig. 8c,d,g,h).

Analyzing the impact of different remote sensing features clarified the limits and possibilities of different mission concepts to infer plant functional diversity from space. When the spatial resolution is prioritized, FDMs based on *R* directly are most likely to succeed. When the spectral resolution is higher (e.g., hyperspectral imagers), the approaches based on optical traits would be advantageous under two conditions: low noise and accepting that trait variability is assessed between small communities of vegetation (pixels), not individual species. In all the cases, both approaches might be used together to evaluate the robustness/reliability of the estimates. Ideally, a biodiversity monitoring system would benefit from combining mid-spatial-resolution hyperspectral imagers (e.g., EnMAP, DESIS, PRISMA, CHIME, SBG, etc.) with high-spatial-resolution multispectral sensors (e.g., Sentinel-2); potentially also sharpening or down-scaling the hyperspectral data. This combination could provide redundant (and thus more robust) estimates of plant functional diversity, exploiting each mission concept’s best features.

Our results are robust to simulation design. For example, simulations not constraining the plausibility of the relationships between leaf traits led to similar results and the same conclusions (not shown). Additional challenges not addressed in this work could increase the uncertainty of the relationships explored. Still, they could be analyzed in the future using a modeling framework like the one described here. For example, our simulations ignored intra-specific functional variability. It could complicate species classification from remote sensing and lead to divergences between taxonomic and functional diversities. However, from a remote sensing perspective, two pixels can be considered different species, being the degree of functional diversity determined by their dissimilarity and not their taxonomic classification. We hypothesize that intra-specific variability might be the least problematic when RS and field data are compared at the same spatial resolution. An additional challenge would be assessing nearby species functionally different with similar spectral properties. Also, using a unidimensional RTM might not be representative of canopies with a strong geometrical scattering component. The effects of canopy geometry could be further analyzed with three-dimensional RTMs. We did not consider either the vertical overlap of species, which reduces the contribution of the shortest plants to the RS signal. However, these plants might be sampled in field surveys, leading to mismatches between ground and remote estimates of plant functional diversity. In this regard, active RS using radar or lidar could offer additional information on the vertical distribution of vegetation and the variability of plants in the understory and characterize vegetation (structural) properties (Asner et al. 2017; Bae et al. 2019; Ma et al. 2020; Simonson et al. 2014; Valbuena et al. 2020). However, active RS would also be the subject of the issues related to spatial resolution and noise. Spaceborne radar missions such as Sentinel-1 (Torres et al. 2012) can today provide global coverage with pixel sizes close to the size of tree crowns. However, the complexity of the SAR backscatter, the enlarged footprint from oblique observation, and signal noise might limit the discrimination of individual trees (Bae et al. 2019). Still, radar information could be valuable, providing information regarding the understory and soil water content, which could relate to the distribution of species governing the top of the canopy (Fauvel et al. 2020). Spaceborne lidar does not yet offer comparable coverage and resolutions. Still, with a footprint of 25 m, Global Ecosystem Dynamics Investigation (GEDI) mission (Coyle et al. 2015) could provide valuable information on the vertical distribution of vegetation that could be enhanced when combined with optical or radar data (Valbuena et al. 2020). Beyond global coverage products, our simulations suggest that the airborne and drone-borne platforms would offer the best possibilities to infer functional diversity remotely. Especially the airborne systems allow the combination of active and passive sensors featuring high spatial resolutions (Adhikari et al. 2020; Almeida et al. 2021; Asner et al. 2017; Schneider et al. 2017; Zhao et al. 2018), and including visible and near-infrared (Gholizadeh et al. 2019; Melville et al. 2019) and short-wave infrared hyperspectral configurations (Asner et al. 2015; Jetz et al. 2016). Furthermore, they can carry sensors to map other signals intimately linked to plant function, such as chlorophyll sun-induced fluorescence (Tagliabue et al. 2020). Nowadays, these sensors are the most suitable for detailed surveillance of valuable and endangered areas or the generation of high-quality datasets that enable the development or evaluation of methods to be later applied to satellite imagery.

4.4 Applied optical remote sensing of plant functional diversity: a case study on the forests of the FunDivEUROPE Network

The comparison between field estimates of functional diversity in forests and RS imagery from Sentinel-2 and DESIS sensors was consistent with the conclusions drawn from the simulations. The best-performing metrics in the simulations Rao's *Q* and *FDis* provided significant correlations in the study case most of the time. However, Sentinel-2 and DESIS performances were very different. Only $S2_{10}$ provided several significant correlations with field FDMs (weak, $R^2 \leqslant 0.30$, but coherent with simulations, e.g., Fig. 8). This analysis does not seek to assess the missions' potential to estimate plant functional diversity since none of them can, for example, identify the species of the field plots and are therefore suboptimal for such evaluation. The value of this exercise is the coherence found between our simulation framework and observations. A potential reason for DESIS lower performance might be the larger mismatch between the acquisition of DESIS and field data (7 years). We minimized the effect of this temporal gap by limiting the analysis of DESIS to plots stable between 2015 and 2020. Sentinel-2 imagery acquired in 2015 and 2020 provided similar results. Still, the strength of the correlations decreased in 2020, and these were not significant for the metrics computed from the optical traits (Fig. S9 vs. S6) despite some being closer to field data in 2020 (Fig. S4 vs. S5). Thus, the temporal gap might account for part of the differences between DESIS and Sentinel-2. However, the lack of significant correlations of Sentinel-2 resampled at 30 m suggests that the coarser spatial resolution of DESIS (equal to field plot size) and not the temporal mismatch was the main limitation for comparing field and RS estimates of plant diversity. Still, unlike in the simulations, we could not disentangle the contribution of the different sources of uncertainty and mismatches when comparing this imagery.

Our results agree with the fact that 10 m spatial resolution is enough to characterize the internal variability of the plots. However, it was insufficient to discriminate the individual species and thus suboptimal for estimating functional diversity. The correlations between FDMs were stronger for reflectance (Fig. 9a,d) than for optical trait-based metrics (Fig. 9g,j), which agrees with the stronger sensitivity of this method to noise and spectral configuration found in the simulations (Fig. 8c,d). The spatial mismatch between plots and RS pixels might have added additional uncertainty. However, the 10 m buffer of similar forest type, structure, and composition kept around the plots to minimize border effects should minimize this uncertainty for $S2_{10}$. Looking at the taxonomical metrics, $S2_{10}$ found significant correlations with species richness *S* and more strongly with the Shannon index *H*. DESIS found a weak but significant relationship between *FDis* and *S*; whereas $S2_{30}$ still found weak significant correlations for $RaoQ_{\alpha=0}$, which simulations suggest might be spurious. Within the field metrics, *H* positively correlated with *S* ($R^2 = 0.47$), and $RaoQ_{\alpha=1}$ with *H* ($R^2 = 0.96$) and *S* ($R^2 = 0.64$). The correlation between functional and taxonomic diversity seems to be also captured by $S2_{10}$ but not by $S2_{30}$. In the case of DESIS, *FDis* correlation with field *S* might result from the richer spectral resolution capturing distinctive features of individual species, even if these could be individually recognized. Nonetheless, as shown in the simulations, these results are in part dependent on the spatial mismatch between field and RS data; in the case of DESIS and $S2_{30}$, stronger correlations could be found if evaluated at their spatial resolution. The development of RS of biodiversity products will benefit from establishing dedicated field plots, such as those proposed by Hauser et al. (2021a), where vegetation is characterized in gridded plots that can be matched with pixels of RS imagers.

An additional challenge for RS of plant functional diversity is the conceptual gap between ecology and RS regarding traits (Ustin and Gamon 2010). While the ecologists are interested in traits with ecological, functional, and adaptative meaning, RS science is more interested or limited to properties that significantly control light-vegetation interaction. This conceptual difference is not trivial. Hauser et al. (2021a; 2021b) showed that accounting for the variability of structural traits such as *LAI*, which are not considered functional traits, is necessary to explain spectral diversity. In our case, from the FunDivEUROPE traits used to compute FDMs, only *SLA* (inversely related to leaf dry matter content, C_{dm}), canopy height, and leaf area (related to leaf width) could be considered inputs of the most common vegetation RTMs. This fact does not entirely prevent connecting RS signals with vegetation functional diversity since some traits are shared or correlated (Kattenborn and Schmidtlein 2019). For example, C_{dm} can relate inversely with *SLA*, C_{ab} with nitrogen and maximum carboxylation rate (Evans and Clarke 2019), or *LAI* and canopy height with *DBH* in some cases (Fischer et al. 2019; Turner et al. 2000). However, although global relationships between plant traits have been reported (Reich 2014; Wright et al. 2004), these relationships can vary between species (Evans and Clarke 2019; Zhao et al. 2021). This variability in the indirect connections between traits governing spectral diversity and the traits used by ecologists to quantify functional diversity on the ground might obscure or prevent evaluating RS estimates of plant functional diversity using ecological field data. This challenge was present when assessing RS estimates of functional diversity in FunDivEUROPE since the field sampling was not designed for RS validation. We are aware that part of the uncertainty found in the relationships evaluated might arise from this discrepancy, even though we expect most field traits to correlate with RTM inputs. The remote sensing and ecology communities should work together to design diversity experiments stretching gradients of traits that can be remotely sensed, enabling the study of their relationship with function and development of remote sensing maps of plant functional diversity.

5. CONCLUSIONS

In this work, we have systematically evaluated the links between spectral and functional diversity and characterized the capability of remote sensing to provide accurate estimates of plant functional diversity. Our modeling framework circumvented a lack of comprehensive data, allowing us to 1) identify three functional diversity metrics (dispersion, richness, and Rao's *Q*) able to infer functional diversity robustly from spectral diversity, 2) validate the use of both reflectance factors and optical traits estimated via radiative transfer model inversion for these metrics, 3) determine that these metrics can deliver summaries in different ecosystems and times and are therefore suitable for the generation of global remote sensing products from the analysis of individual images, and 4) understand the effect of different remote sensing features on the methods and metrics analyzed, learning that high spatial resolution imagers can rely on reflectance factors despite the limited spectral information they provide, whereas hyperspectral imagers with lower spatial resolution should infer plant diversity from optical traits. The case study results using DESIS and Sentinel-2 imagery over FunDivEUROPE forest plots are coherent with the simulations.

Our approach clarifies some key issues, but further efforts are needed to generate field datasets suitable for validating remote sensing estimates of plant functional diversity. Also, the gap between the variables measured by biodiversity ecologists and those that can be remotely estimated (and therefore, controlling the spectroradiometric signals) should be reduced to promote the development, evaluation, and exploitation of such remote sensing products. The combination of new satellite missions overlapping complementary resolutions and spectral information (e.g., hyperspectral, radar, lidar, high spatial resolution imagery, etc.) could overcome some of the challenges found or not yet explored in this work.

ACKNOWLEDGEMENTS

JPL, MMi, and MMa acknowledge the German Aerospace Center (DLR) project OBEF-Accross2 "The Potential of Earth Observations to Capture Patterns of Biodiversity” (Contract No. 50EE1912, German Aerospace Center). JPL, MMi, AH, CW, MMa, GK, FJB, and UW acknowledge the German Aerospace Center (DLR) for providing DESIS imagery through the Announcement of Opportunity “EBioIDEA: Enhancing Biodiversity Inventories with DESIS Imagery Analysis”. FunDivEUROPE data collection was supported by the European Union Seventh Framework Programme (FP7/2007-2013) (grant agreement number: 265171) and the EU H2020 project Soil4Europe (Bioidversa 2017-2019). The in-situ plant traits data collected over Romanian and Spanish sites were supported by a Marie-Curie Fellowship (DIVERFOR, FP7-PEOPLE-2011-IEF. No. 302445) to R. Benavides. OB acknowledges funding from project 10PFE/2021 Ministry of Research, Innovation and Digitalization within Program 1 - Development of national research and development system, Subprogram 1.2 - Institutional Performance - RDI excellence funding projects. XM was supported by the National Natural Science Foundation of China (42171305), the Director Fund of the International Research Center of Big Data for Sustainable Development Goals (CBAS2022DF006), and the Open Fund of State Key Laboratory of Remote Sensing Science (OFSLRSS202229). We thank Prof. Dr. Michael Scherer-Lorenzen for coordinating the interaction with the FunDivEUROPE network and Dr. Fernando Valladares for coordinating data production in FunDivEUROPE sites in Spain. We thank Yuhan Li for helping collect and process Sentinel-2 data in 2020 for the verification task. ESA’s Copernicus Open Access Hub enabled the free use of Sentinel-2 data.

APPENDIX A. VEGETATION TRAITS SIMULATION

We avoided unplausible combinations of field plant traits (i.e., T_{RTM}) and other inputs of the SCOPE emulator during the definition of synthetic species combining three different approaches. First, we limited the random sampling of these traits within realistic ranges (Table S1) commonly reported in the literature (Bayat et al. 2018; Celesti et al. 2018; Feret et al. 2008; Houborg and Anderson 2009). Second, we avoided unrealistic combinations of the leaf traits constraining N, C_{ab}, C_{ca}, C_{dm}, and C_{w} covariance with a Gaussian Mixture Model (GMM). The GMM model was fit to the LOPEX (Hosgood et al. 1994) and ANGERS (Feret et al. 2008) datasets using the expectation-maximization (EM) algorithm (Dempster et al. 1977) implemented in the Python package *scikit-learn* (Pedregosa et al. 2011). We selected these databases since they were produced to calibrate the coefficients of leaf RTMs and therefore present most of the traits needed, including N. Notice that values of N are exclusively available in spectral libraries since this is a non-measurable model parameter that can only be inferred via inversion of the leaf radiative transfer model. Since N relates to the cellular arrangement inside the leaf, it can correlate with dry matter content, and it has been shown to correlate with the specific leaf area (Jacquemoud and Baret 1990; Pacheco-Labrador et al. 2021; Peters and Noble 2020). Third, we prevented the unrealistic co-existence of high chlorophyll (C_{ab}) with anthocyanins (C_{ant}) (Hughes et al. 2007) or senescent pigments (C_{s}) contents (Mattila et al. 2018) by scaling the randomly sampled C_{ant} and C_{s} values by a factor ($f_{\mathrm{C,max}}$) exponentially decreasing as a function of C_{ab} as described in Eq. A.1:

$$f_{C,\max} = \mathrm{e}^{z\cdot\left(\frac{100-C_{\mathrm{ab}}}{100}-1\right)} \tag{A.1}$$

$f_{\mathrm{C,max}}$ ranges between 0 and 1, and z controls its decrease with C_{ab}. High C_{s} was strongly limited to leaves featuring low C_{ab} ($z = 40$) since senescent pigments result from the degradation of chlorophylls and other leaf constituents (Mattila et al. 2018; Pourcel et al. 2007). Anthocyanins were less strongly limited ($z = 7$) since their functional role makes possible a positive correlation with C_{ab} in some cases (Gould 2004; Hughes et al. 2007; Manetas 2006).

APPENDIX B. SIMULATION OF SPECIES COMMUNITIES

We produced 81 synthetic communities from each regional pool by sampling the species with varying relative abundances (A). Each pool contained a randomized number of species ($n_T \in [5, 30]$), of which n_s were similar and n_{ds} were dissimilar ($n_T = n_s + n_{ds}$). We labeled the species with an integer (n_{sp}) ranging from 1 to n_T; first the similar species ($n_{sp} \in [1, n_s]$) and then the dissimilar ones ($n_{sp} \in [n_s + 1, n_T]$) (Fig. B.1a). Then we produced relative species abundances for each community with a Gaussian distribution function whose mean (μ_{sp}) and standard deviation (σ_{sp}) were relative to species index space n_{sp} (Fig. B.1c). For each pool, we produced 81 communities from μ_{sp} and σ_{sp} gradients crossed in a 9 x 9 grid (Fig. B.1b). σ_{sp} ranged between 0.4 and 5.0 species, whereas μ_{sp} ranged between 0.2 and n_μ, where $n_\mu = n_s + f_{ds} \cdot n_{ds}$ and f_{ds} was a random value within the range [0.2, 1.0]. f_{ds} reduced the dominance of some of the dissimilar species in the regional communities, increasing their exoticism. Finally, the abundances of each community were normalized to add up to one. These synthetic communities presented different degrees of richness, evenness, and divergence (Villéger et al. 2008) and dominant species.

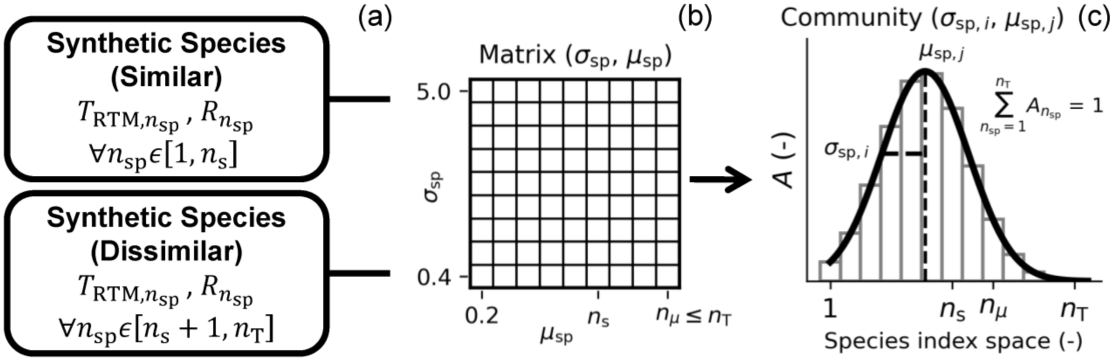

Figure B.1. Generation of several (81) synthetic communities from the same species pool. (a) Pool of n_s similar and n_{ds} dissimilar species adding up to n_T; each species is labeled with an integer n_{sp} and characterized by a specific set of field plant traits (T_{RTM}) and the corresponding reflectance factor (R). (b) Communities matrix presenting the 81 combinations of the median (μ_{sp}) and the standard deviation (σ_{sp}) of the Gaussian distribution used to define the relative species abundance (A) of each community. i and j are row and column indices of the matrix; only a fraction of the dissimilar species is allowed to dominate communities so that μ_{sp} ranges up to $n_{\mu} \leq n_{T}$. (c) Relative species abundance distribution of one of the communities.

APPENDIX C. DEGRADATION OF SPATIAL RESOLUTION

We simulated remote sensor spatial resolution degradation by mixing a fraction of the species within the community with each other (50 % or 100 % of the species). These mixtures represented the species observed by the remote sensor with a sub-optimal resolution, therefore, as a mixture. To do so, we generated a squared matrix (M) mapping the contribution of the original species (j columns) and to the species to be spatially degraded (i rows). The coefficients of the linear combination ($c_{i,j}$) were ($\sum_j \mathrm{c}_{i,j} = 1, \forall i$). For the species that were not mixed, $\mathrm{c}_{i,j} = 0\ \forall i \neq j; \mathrm{c}_{i,j} = 1\ \forall i = j$. Fig. C.1 shows an example of this matrix for a community of 4 species where only species 1 and 2 are mixed.

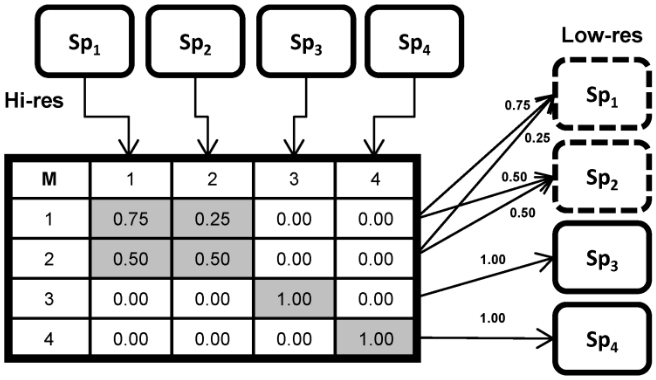

M	1	2	3	4
1	0.75	0.25	0.00	0.00
2	0.50	0.50	0.00	0.00
3	0.00	0.00	1.00	0.00
4	0.00	0.00	0.00	1.00

Figure C.1. Example of species mixture during spatial resolution degradation. Four species at high spatial resolution are observed from a sensor only able to distinguish two (solid lines); the rest are observed as a mixture (dashed lines). The table shows the coefficients of the mixture matrix M where columns represent the contribution of the original species to the degraded ones (rows). The procedure described is used to degrade the spatial resolution of reflectance factors, vegetation parameters, and relative abundances of the species of a regional pool.

Then, the reflectance factors, vegetation parameters, and abundances were mixed linearly, combining the respective variables with the row coefficients of the matrix M:

$$X_{\mathrm{low-Sres},i} = \sum_j \left(c_{i,j} X_{\mathrm{hi-Sres},j} \right) \tag{C.1}$$

where X represents any of the abovementioned variables, the subscripts "hi-Sres" and "low-Sres" stand for high and low spatial resolution. The example of Fig. C.1 (first row) shows that what the remote sensor would identify species 1 ($\mathrm{Sp}_{1,\mathrm{deg}}$) would be, in fact, a mixture 75% and 25% of the species 1 ($\mathrm{Sp}_{1,\mathrm{ori}}$) and 2 ($\mathrm{Sp}_{2,\mathrm{ori}}$), respectively. Relative abundances still had to be normalized after the combination to provide an accumulated probability of 1 in each community. The mixture enabled the apparition of new species within a community, which might happen when larger pixels sample a larger area outside the field plot used as a reference (e.g., for field measurements or from a remote sensor with higher spatial resolution).

REFERENCES

Adhikari, H., Valbuena, R., Pellikka, P.K.E., & Heiskanen, J. (2020). Mapping forest structural heterogeneity of tropical montane forest remnants from airborne laser scanning and Landsat time series. Ecological Indicators, 108, 105739

Almeida, D.R.A.d., Broadbent, E.N., Ferreira, M.P., Meli, P., Zambrano, A.M.A., Gorgens, E.B., Resende, A.F., de Almeida, C.T., do Amaral, C.H., Corte, A.P.D., Silva, C.A., Romanelli, J.P., Prata, G.A., de Almeida Papa, D., Stark, S.C., Valbuena, R., Nelson, B.W., Guillemot, J., Féret, J.-B., Chazdon, R., & Brancalion, P.H.S. (2021). Monitoring restored tropical forest diversity and structure through UAV-borne hyperspectral and lidar fusion. Remote Sensing of Environment, 264, 112582

Alonso, K., Bachmann, M., Burch, K., Carmona, E., Cerra, D., de los Reyes, R., Dietrich, D., Heiden, U., Hölderlin, A., Ickes, J., Knodt, U., Krutz, D., Lester, H., Müller, R., Pagnutti, M., Reinartz, P., Richter, R., Ryan, R., Sebastian, I., & Tegler, M. (2019). Data Products, Quality and Validation of the DLR Earth Sensing Imaging Spectrometer (DESIS). Sensors, 19, 4471

Anderson, M.J. (2006). Distance-Based Tests for Homogeneity of Multivariate Dispersions. Biometrics, 62, 245-253

Asner, G.P., Martin, R.E., Anderson, C.B., & Knapp, D.E. (2015). Quantifying forest canopy traits: Imaging spectroscopy versus field survey. Remote Sensing of Environment, 158, 15-27

Asner, G.P., Martin, R.E., Knapp, D.E., Tupayachi, R., Anderson, C.B., Sinca, F., Vaughn, N.R., & Llactayo, W. (2017). Airborne laser-guided imaging spectroscopy to map forest trait diversity and guide conservation. Science, 355, 385

Bae, S., Levick, S.R., Heidrich, L., Magdon, P., Leutner, B.F., Wöllauer, S., Serebryanyk, A., Nauss, T., Krzystek, P., Gossner, M.M., Schall, P., Heibl, C., Bässler, C., Doerfler, I., Schulze, E.-D., Krah, F.-S., Culmsee, H., Jung, K., Heurich, M., Fischer, M., Seibold, S., Thorn, S., Gerlach, T., Hothorn, T., Weisser, W.W., & Müller, J. (2019). Radar vision in the mapping of forest biodiversity from space. Nature Communications, 10, 4757

Baeten, L., Verheyen, K., Wirth, C., Bruelheide, H., Bussotti, F., Finér, L., Jaroszewicz, B., Selvi, F., Valladares, F., Allan, E., Ampoorter, E., Auge, H., Avăcăriei, D., Barbaro, L., Bărnoaiea, I., Bastias, C.C., Bauhus, J., Beinhoff, C., Benavides, R., Benneter, A., Berger, S., Berthold, F., Boberg, J., Bonal, D., Brüggemann, W., Carnol, M., Castagneyrol, B., Charbonnier, Y., Chećko, E., Coomes, D., Coppi, A., Dalmaris, E., Dănilă, G., Dawud, S.M., de Vries, W., De Wandeler, H., Deconchat, M., Domisch, T., Duduman, G., Fischer, M., Fotelli, M., Gessler, A., Gimeno, T.E., Granier, A., Grossiord, C., Guyot, V., Hantsch, L., Hättenschwiler, S., Hector, A., Hermy, M., Holland, V., Jactel, H., Joly, F.-X., Jucker, T., Kolb, S., Koricheva, J., Lexer, M.J., Liebergesell, M., Milligan, H., Müller, S., Muys, B., Nguyen, D., Nichiforel, L., Pollastrini, M., Proulx, R., Rabasa, S., Radoglou, K., Ratcliffe, S., Raulund-Rasmussen, K., Seiferling, I., Stenlid, J., Vesterdal, L., von Wilpert, K., Zavala, M.A., Zielinski, D., & Scherer-Lorenzen, M. (2013). A novel comparative research platform designed to determine the functional significance of tree species diversity in European forests. Perspectives in Plant Ecology, Evolution and Systematics, 15, 281-291

Barnosky, A.D., Matzke, N., Tomiya, S., Wogan, G.O.U., Swartz, B., Quental, T.B., Marshall, C., McGuire, J.L., Lindsey, E.L., Maguire, K.C., Mersey, B., & Ferrer, E.A. (2011). Has the Earth's sixth mass extinction already arrived? Nature, 471, 51-57

Bayat, B., van der Tol, C., & Verhoef, W. (2018). Integrating satellite optical and thermal infrared observations for improving daily ecosystem functioning estimations during a drought episode. Remote Sensing of Environment, 209, 375-394

Benavides, R., Scherer-Lorenzen, M., & Valladares, F. (2019a). The functional trait space of tree species is influenced by the species richness of the canopy and the type of forest. Oikos, 128, 1435-1445

Benavides, R., Valladares, F., Wirth, C., Müller, S., & Scherer-Lorenzen, M. (2019b). Intraspecific trait variability of trees is related to canopy species richness in European forests. Perspectives in Plant Ecology, Evolution and Systematics, 36, 24-32

Botta-Dukát, Z. (2005). Rao's quadratic entropy as a measure of functional diversity based on multiple traits. Journal of Vegetation Science, 16, 533-540

Brodu, N. (2017). Super-Resolving Multiresolution Images With Band-Independent Geometry of Multispectral Pixels. IEEE Transactions on Geoscience and Remote Sensing, 55, 4610-4617

Cavender-Bares, J., Gamon, J.A., & Townsend, P.A. (2020). The Use of Remote Sensing to Enhance Biodiversity Monitoring and Detection: A Critical Challenge for the Twenty-First Century. In J. Cavender-Bares, J.A. Gamon, & P.A. Townsend (Eds.), Remote Sensing of Plant Biodiversity (pp. 1-12). Cham: Springer International Publishing

Ceballos, G., Ehrlich, P.R., Barnosky, A.D., García, A., Pringle, R.M., & Palmer, T.M. (2015). Accelerated modern human–induced species losses: Entering the sixth mass extinction. Science Advances, 1, e1400253

Celesti, M., van der Tol, C., Cogliati, S., Panigada, C., Yang, P., Pinto, F., Rascher, U., Miglietta, F., Colombo, R., & Rossini, M. (2018). Exploring the physiological information of Sun-induced chlorophyll fluorescence through radiative transfer model inversion. Remote Sensing of Environment, 215, 97-108

Coyle, D., Stysley, P., Poulios, D., Clarke, G., & Kay, R. (2015). Laser transmitter development for NASA's Global Ecosystem Dynamics Investigation (GEDI) lidar. SPIE

Dalponte, M., Bruzzone, L., Vescovo, L., & Gianelle, D. (2009). The role of spectral resolution and classifier complexity in the analysis of hyperspectral images of forest areas. Remote Sensing of Environment, 113, 2345-2355

Darvishzadeh, R., Skidmore, A., Schlerf, M., & Atzberger, C. (2008). Inversion of a radiative transfer model for estimating vegetation LAI and chlorophyll in a heterogeneous grassland. Remote Sensing of Environment, 112, 2592-2604

Dempster, A.P., Laird, N.M., & Rubin, D.B. (1977). Maximum Likelihood from Incomplete Data via the EM Algorithm. Journal of the Royal Statistical Society. Series B (Methodological), 39, 1-38

Díaz, S., & Cabido, M. (2001). Vive la différence: plant functional diversity matters to ecosystem processes. Trends in Ecology & Evolution, 16, 646-655

Drusch, M., Del Bello, U., Carlier, S., Colin, O., Fernandez, V., Gascon, F., Hoersch, B., Isola, C., Laberinti, P., Martimort, P., Meygret, A., Spoto, F., Sy, O., Marchese, F., & Bargellini, P. (2012). Sentinel-2: ESA's Optical High-Resolution Mission for GMES Operational Services. Remote Sensing of Environment, 120, 25-36

ESA, 2017. Sentinel-2 Spectral Response Functions (S2-SRF). https://sentinels.copernicus.eu/web/sentinel/user-guides/sentinel-2-msi/document-library/-/asset_publisher/Wk0TKajiISaR/content/sentinel-2a-spectral-responses (accessed 7 December 2021)

Evans, J.R., & Clarke, V.C. (2019). The nitrogen cost of photosynthesis. Journal of Experimental Botany, 70, 7-15

Fassnacht, F.E., Müllerová, J., Conti, L., Malavasi, M., & Schmidtlein, S. (2022). About the link between biodiversity and spectral variation. Applied Vegetation Science, 25, e12643

Fauvel, M., Lopes, M., Dubo, T., Rivers-Moore, J., Frison, P.-L., Gross, N., & Ouin, A. (2020). Prediction of plant diversity in grasslands using Sentinel-1 and -2 satellite image time series. Remote Sensing of Environment, 237, 111536

Feilhauer, H., Zlinszky, A., Kania, A., Foody, G.M., Doktor, D., Lausch, A., & Schmidtlein, S. (2021). Let your maps be fuzzy!—Class probabilities and floristic gradients as alternatives to crisp mapping for remote sensing of vegetation. Remote Sensing in Ecology and Conservation, 7, 292-305

Féret, J.-B., & Asner, G.P. (2014). Mapping tropical forest canopy diversity using high-fidelity imaging spectroscopy. Ecological Applications, 24, 1289-1296

Feret, J.-B., François, C., Asner, G.P., Gitelson, A.A., Martin, R.E., Bidel, L.P.R., Ustin, S.L., le Maire, G., & Jacquemoud, S. (2008). PROSPECT-4 and 5: Advances in the leaf optical properties model separating photosynthetic pigments. Remote Sensing of Environment, 112, 3030-3043

Féret, J.B., Gitelson, A.A., Noble, S.D., & Jacquemoud, S. (2017). PROSPECT-D: Towards modeling leaf optical properties through a complete lifecycle. Remote Sensing of Environment, 193, 204-215

Fischer, F.J., Maréchaux, I., & Chave, J. (2019). Improving plant allometry by fusing forest models and remote sensing. New Phytologist, 223, 1159-1165

Gamon, J.A., Wang, R., Gholizadeh, H., Zutta, B., Townsend, P.A., & Cavender-Bares, J. (2020). Consideration of Scale in Remote Sensing of Biodiversity. In J. Cavender-Bares, J.A. Gamon, & P.A. Townsend (Eds.), Remote Sensing of Plant Biodiversity (pp. 425-447). Cham: Springer International Publishing

GCOS (2003). The second report on the adequacy of the global observing systems for climate in support of the UNFCCC. In, GCOS Report (p. 73). Geneva, Switzerland: World Meteorological Organization

Gholizadeh, H., Gamon, J.A., Townsend, P.A., Zygielbaum, A.I., Helzer, C.J., Hmimina, G.Y., Yu, R., Moore, R.M., Schweiger, A.K., & Cavender-Bares, J. (2019). Detecting prairie biodiversity with airborne remote sensing. Remote Sensing of Environment, 221, 38-49

Gholizadeh, H., Gamon, J.A., Zygielbaum, A.I., Wang, R., Schweiger, A.K., & Cavender-Bares, J. (2018). Remote sensing of biodiversity: Soil correction and data dimension reduction methods improve assessment of α-diversity (species richness) in prairie ecosystems. Remote Sensing of Environment, 206, 240-253

Goetz, A.F.H. (2009). Three decades of hyperspectral remote sensing of the Earth: A personal view. Remote Sensing of Environment, 113, S5-S16

Gómez-Dans, J.L., Lewis, P.E., & Disney, M. (2016). Efficient Emulation of Radiative Transfer Codes Using Gaussian Processes and Application to Land Surface Parameter Inferences. Remote Sensing, 8, 119

Gould, K.S. (2004). Nature's Swiss Army Knife: The Diverse Protective Roles of Anthocyanins in Leaves. Journal of biomedicine & biotechnology, 2004, 314-320

Grossiord, C., Granier, A., Ratcliffe, S., Bouriaud, O., Bruelheide, H., Chećko, E., Forrester, D.I., Dawud, S.M., Finér, L., Pollastrini, M., Scherer-Lorenzen, M., Valladares, F., Bonal, D., & Gessler, A. (2014). Tree diversity does not always improve resistance of forest ecosystems to drought. Proceedings of the National Academy of Sciences, 111, 14812

Hardisty, A.R., Michener, W.K., Agosti, D., Alonso García, E., Bastin, L., Belbin, L., Bowser, A., Buttigieg, P.L., Canhos, D.A.L., Egloff, W., De Giovanni, R., Figueira, R., Groom, Q., Guralnick, R.P., Hobern, D., Hugo, W., Koureas, D., Ji, L., Los, W., Manuel, J., Manset, D., Poelen, J., Saarenmaa, H., Schigel, D., Uhlir, P.F., & Kissling, W.D. (2019). The Bari Manifesto: An interoperability framework for essential biodiversity variables. Ecological Informatics, 49, 22-31

Hauser, L.T., Féret, J.-B., An Binh, N., van der Windt, N., Sil, Â.F., Timmermans, J., Soudzilovskaia, N.A., & van Bodegom, P.M. (2021a). Towards scalable estimation of plant functional diversity from Sentinel-2: In-situ validation in a heterogeneous (semi-)natural landscape. Remote Sensing of Environment, 262, 112505

Hauser, L.T., Timmermans, J., van der Windt, N., Sil, Â.F., César de Sá, N., Soudzilovskaia, N.A., & van Bodegom, P.M. (2021b). Explaining discrepancies between spectral and in-situ plant diversity in multispectral satellite earth observation. Remote Sensing of Environment, 265, 112684

Heumann, B.W., Hackett, R.A., & Monfils, A.K. (2015). Testing the spectral diversity hypothesis using spectroscopy data in a simulated wetland community. Ecological Informatics, 25, 29-34

Hosgood, B., Jacquemoud, S., Andreoli, G., Verdebout, J., Pedrini, G., & Schmuck, G. (1994). Leaf Optical Properties EXperiment 93 (LOPEX93). In E.C.J.R. Centre (Ed.). Ispra (Italy). Available online: [http://opticleaf.ipgp.fr/databases/LDB_lopex1993.xls], last accessed 11-Nov-2020

Houborg, R., & Anderson, M. (2009). Utility of an image-based canopy reflectance modeling tool for remote estimation of LAI and leaf chlorophyll content at regional scales. In (p. 29): SPIE

Hughes, N.M., Morley, C.B., & Smith, W.K. (2007). Coordination of anthocyanin decline and photosynthetic maturation in juvenile leaves of three deciduous tree species. New Phytologist, 175, 675-685

Ibarrola-Ulzurrun, E., Drumetz, L., Marcello, J., Gonzalo-Martín, C., & Chanussot, J. (2019). Hyperspectral Classification Through Unmixing Abundance Maps Addressing Spectral Variability. IEEE Transactions on Geoscience and Remote Sensing, 57, 4775-4788

Jacquemoud, S., & Baret, F. (1990). PROSPECT: A model of leaf optical properties spectra. Remote Sensing of Environment, 34, 75-91

Jacquemoud, S., Verhoef, W., Baret, F., Bacour, C., Zarco-Tejada, P.J., Asner, G.P., François, C., & Ustin, S.L. (2009). PROSPECT+SAIL models: A review of use for vegetation characterization. Remote Sensing of Environment, 113, S56-S66

Jetz, W., Cavender-Bares, J., Pavlick, R., Schimel, D., Davis, F.W., Asner, G.P., Guralnick, R., Kattge, J., Latimer, A.M., Moorcroft, P., Schaepman, M.E., Schildhauer, M.P., Schneider, F.D., Schrodt, F., Stahl, U., & Ustin, S.L. (2016). Monitoring plant functional diversity from space. Nature Plants, 2, 16024

Jetz, W., McGeoch, M.A., Guralnick, R., Ferrier, S., Beck, J., Costello, M.J., Fernandez, M., Geller, G.N., Keil, P., Merow, C., Meyer, C., Muller-Karger, F.E., Pereira, H.M., Regan, E.C., Schmeller, D.S., & Turak, E. (2019). Essential biodiversity variables for mapping and monitoring species populations. Nature Ecology & Evolution, 3, 539-551

Jucker, T., Bongalov, B., Burslem, D.F.R.P., Nilus, R., Dalponte, M., Lewis, S.L., Phillips, O.L., Qie, L., & Coomes, D.A. (2018). Topography shapes the structure, composition and function of tropical forest landscapes. Ecology Letters, 21, 989-1000

Kattenborn, T., & Schmidtlein, S. (2019). Radiative transfer modelling reveals why canopy reflectance follows function. Scientific Reports, 9, 6541

Kerr, G., Avbelj, J., Carmona, E., Eckardt, A., Gerasch, B., Graham, L., Günther, B., Heiden, U., Krutz, D., Krawczyk, H., Makarau, A., Miller, R., Müller, R., Perkins, R., & Walter, I. (2016). The hyperspectral sensor DESIS on MUSES: Processing and applications. In, 2016 IEEE International Geoscience and Remote Sensing Symposium (IGARSS) (pp. 268-271)

Kerr, J.T., & Ostrovsky, M. (2003). From space to species: ecological applications for remote sensing. Trends in Ecology & Evolution, 18, 299-305

Laliberté, E., & Legendre, P. (2010). A distance-based framework for measuring functional diversity from multiple traits. Ecology, 91, 299-305

Laliberté, E., Schweiger, A.K., & Legendre, P. (2020). Partitioning plant spectral diversity into alpha and beta components. Ecology Letters, 23, 370-380

Lee, K.-S., Cohen, W.B., Kennedy, R.E., Maiersperger, T.K., & Gower, S.T. (2004). Hyperspectral versus multispectral data for estimating leaf area index in four different biomes. Remote Sensing of Environment, 91, 508-520

Lu, B., He, Y., & Dao, P.D. (2019). Comparing the Performance of Multispectral and Hyperspectral Images for Estimating Vegetation Properties. IEEE Journal of Selected Topics in Applied Earth Observations and Remote Sensing, 12, 1784-1797

Ma, X., Mahecha, M.D., Migliavacca, M., van der Plas, F., Benavides, R., Ratcliffe, S., Kattge, J., Richter, R., Musavi, T., Baeten, L., Barnoaiea, I., Bohn, F.J., Bouriaud, O., Bussotti, F., Coppi, A., Domisch, T., Huth, A., Jaroszewicz, B., Joswig, J., Pabon-Moreno, D.E., Papale, D., Selvi, F., Laurin, G.V., Valladares, F., Reichstein, M., & Wirth, C. (2019). Inferring plant functional diversity from space: the potential of Sentinel-2. Remote Sensing of Environment, 233, 111368

Ma, X., Migliavacca, M., Wirth, C., Bohn, J.F., Huth, A., Richter, R., & Mahecha, D.M. (2020). Monitoring Plant Functional Diversity Using the Reflectance and Echo from Space. Remote Sensing, 12

Manetas, Y. (2006). Why some leaves are anthocyanic and why most anthocyanic leaves are red? Flora - Morphology, Distribution, Functional Ecology of Plants, 201, 163-177

Mason, N.W.H., Mouillot, D., Lee, W.G., & Wilson, J.B. (2005). Functional richness, functional evenness and functional divergence: the primary components of functional diversity. Oikos, 111, 112-118

Mattila, H., Valev, D., Havurinne, V., Khorobrykh, S., Virtanen, O., Antinluoma, M., Mishra, K.B., & Tyystjärvi, E. (2018). Degradation of chlorophyll and synthesis of flavonols during autumn senescence—the story told by individual leaves. AoB PLANTS, 10

Melville, B., Lucieer, A., & Aryal, J. (2019). Classification of Lowland Native Grassland Communities Using Hyperspectral Unmanned Aircraft System (UAS) Imagery in the Tasmanian Midlands. Drones, 3

Mouchet, M.A., Villéger, S., Mason, N.W.H., & Mouillot, D. (2010). Functional diversity measures: an overview of their redundancy and their ability to discriminate community assembly rules. Functional Ecology, 24, 867-876

Nagendra, H. (2001). Using remote sensing to assess biodiversity. International Journal of Remote Sensing, 22, 2377-2400

Nagendra, H., & Rocchini, D. (2008). High resolution satellite imagery for tropical biodiversity studies: the devil is in the detail. Biodiversity and Conservation, 17, 3431

North, P.R.J. (1996). Three-dimensional forest light interaction model using a Monte Carlo method. IEEE Transactions on Geoscience and Remote Sensing, 34, 946-956

Pacheco-Labrador, J., El-Madany, T.S., van der Tol, C., Martin, M.P., Gonzalez-Cascon, R., Perez-Priego, O., Guan, J., Moreno, G., Carrara, A., Reichstein, M., & Migliavacca, M. (2021). senSCOPE: Modeling mixed canopies combining green and brown senesced leaves. Evaluation in a Mediterranean Grassland. Remote Sensing of Environment, 257, 112352

Palmer, M.W., Earls, P.G., Hoagland, B.W., White, P.S., & Wohlgemuth, T. (2002). Quantitative tools for perfecting species lists. Environmetrics, 13, 121-137

Pearson, K. (1901). LIII. On lines and planes of closest fit to systems of points in space. The London, Edinburgh, and Dublin Philosophical Magazine and Journal of Science, 2, 559-572

Pedregosa, F., Varoquaux, G., Gramfort, A., Michel, V., Thirion, B., Grisel, O., Blondel, M., Prettenhofer, P., Weiss, R., Dubourg, V., Vanderplas, J., Passos, A., Cournapeau, D., Brucher, M., Perrot, M., & Duchesnay, É. (2011). Scikit-learn: Machine Learning in Python. Journal of Machine Learning Research, 12, 2825-2830

Pereira, H.M., Ferrier, S., Walters, M., Geller, G.N., Jongman, R.H.G., Scholes, R.J., Bruford, M.W., Brummitt, N., Butchart, S.H.M., Cardoso, A.C., Coops, N.C., Dulloo, E., Faith, D.P., Freyhof, J., Gregory, R.D., Heip, C., Höft, R., Hurtt, G., Jetz, W., Karp, D.S., McGeoch, M.A., Obura, D., Onoda, Y., Pettorelli, N., Reyers, B., Sayre, R., Scharlemann, J.P.W., Stuart, S.N., Turak, E., Walpole, M., & Wegmann, M. (2013). Essential Biodiversity Variables. Science, 339, 277

Pereira, H.M., Navarro, L.M., & Martins, I.S. (2012). Global Biodiversity Change: The Bad, the Good, and the Unknown. Annual Review of Environment and Resources, 37, 25-50

Peters, R.D., & Noble, S.D. (2020). Sensitivity and Correlation Analysis of PROSPECT-D and ABM-B Leaf Models. IEEE Transactions on Geoscience and Remote Sensing, 1-10

Pourcel, L., Routaboul, J.-M., Cheynier, V., Lepiniec, L., & Debeaujon, I. (2007). Flavonoid oxidation in plants: from biochemical properties to physiological functions. Trends in Plant Science, 12, 29-36

Reich, P.B. (2014). The world-wide ‘fast–slow’ plant economics spectrum: a traits manifesto. Journal of Ecology, 102, 275-301

Rocchini, D., Balkenhol, N., Carter, G.A., Foody, G.M., Gillespie, T.W., He, K.S., Kark, S., Levin, N., Lucas, K., Luoto, M., Nagendra, H., Oldeland, J., Ricotta, C., Southworth, J., & Neteler, M. (2010). Remotely sensed spectral heterogeneity as a proxy of species diversity: Recent advances and open challenges. Ecological Informatics, 5, 318-329

Rocchini, D., Marcantonio, M., Da Re, D., Bacaro, G., Feoli, E., Foody, G.M., Furrer, R., Harrigan, R.J., Kleijn, D., Iannacito, M., Lenoir, J., Lin, M., Malavasi, M., Marchetto, E., Meyer, R.S., Moudry, V., Schneider, F.D., Šímová, P., Thornhill, A.H., Thouverai, E., Vicario, S., Wayne, R.K., & Ricotta, C. (2021). From zero to infinity: Minimum to maximum diversity of the planet by spatio-parametric Rao's quadratic entropy. Global Ecology and Biogeography, 30, 1153-1162

Rossi, C., Kneubühler, M., Schütz, M., Schaepman, M.E., Haller, R.M., & Risch, A.C. (2020). From local to regional: Functional diversity in differently managed alpine grasslands. Remote Sensing of Environment, 236, 111415

Schneider, F.D., Morsdorf, F., Schmid, B., Petchey, O.L., Hueni, A., Schimel, D.S., & Schaepman, M.E. (2017). Mapping functional diversity from remotely sensed morphological and physiological forest traits. Nature Communications, 8, 1441

Scholes, R.J., Walters, M., Turak, E., Saarenmaa, H., Heip, C.H.R., Tuama, É.Ó., Faith, D.P., Mooney, H.A., Ferrier, S., Jongman, R.H.G., Harrison, I.J., Yahara, T., Pereira, H.M., Larigauderie, A., & Geller, G. (2012). Building a global observing system for biodiversity. Current Opinion in Environmental Sustainability, 4, 139-146

Schweiger, A.K., Cavender-Bares, J., Townsend, P.A., Hobbie, S.E., Madritch, M.D., Wang, R., Tilman, D., & Gamon, J.A. (2018). Plant spectral diversity integrates functional and phylogenetic components of biodiversity and predicts ecosystem function. Nature Ecology & Evolution, 2, 976-982

Shannon, C.E. (1948). A Mathematical Theory of Communication. Bell System Technical Journal, 27, 379-423

Simonson, W.D., Allen, H.D., & Coomes, D.A. (2014). Applications of airborne lidar for the assessment of animal species diversity. Methods in Ecology and Evolution, 5, 719-729

Skidmore, A.K., Coops, N.C., Neinavaz, E., Ali, A., Schaepman, M.E., Paganini, M., Kissling, W.D., Vihervaara, P., Darvishzadeh, R., Feilhauer, H., Fernandez, M., Fernández, N., Gorelick, N., Geijzendorffer, I., Heiden, U., Heurich, M., Hobern, D., Holzwarth, S., Muller-Karger, F.E., Van De Kerchove, R., Lausch, A., Leitão, P.J., Lock, M.C., Mücher, C.A., O'Connor, B., Rocchini, D., Roeoesli, C., Turner, W., Vis, J.K., Wang, T., Wegmann, M., & Wingate, V. (2021). Priority list of biodiversity metrics to observe from space. Nature Ecology & Evolution, 5, 896-906

Sluiter, R., & Pebesma, E.J. (2010). Comparing techniques for vegetation classification using multi- and hyperspectral images and ancillary environmental data. International Journal of Remote Sensing, 31, 6143-6161

Small, C., & Sousa, D. (2016). Humans on Earth: Global extents of anthropogenic land cover from remote sensing. Anthropocene, 14, 1-33

Sohl, T., & Sleeter, B. (2012). Role of Remote Sensing for Land-Use and Land-Cover Change Modeling. In C.P. Giri (Ed.), Remote sensing of land use and land cover: principles and applications (pp. 225-239). Boca Raton, FL: CRC Press

Stagakis, S., Vanikiotis, T., & Sykioti, O. (2016). Estimating forest species abundance through linear unmixing of CHRIS/PROBA imagery. ISPRS Journal of Photogrammetry and Remote Sensing, 119, 79-89

Stein, A., Gerstner, K., & Kreft, H. (2014). Environmental heterogeneity as a universal driver of species richness across taxa, biomes and spatial scales. Ecology Letters, 17, 866-880

Sun, Y., Huang, J., Ao, Z., Lao, D., & Xin, Q. (2019). Deep Learning Approaches for the Mapping of Tree Species Diversity in a Tropical Wetland Using Airborne LiDAR and High-Spatial-Resolution Remote Sensing Images. Forests, 10, 1047

Tagliabue, G., Panigada, C., Celesti, M., Cogliati, S., Colombo, R., Migliavacca, M., Rascher, U., Rocchini, D., Schüttemeyer, D., & Rossini, M. (2020). Sun–induced fluorescence heterogeneity as a measure of functional diversity. Remote Sensing of Environment, 247, 111934

Torres, R., Snoeij, P., Geudtner, D., Bibby, D., Davidson, M., Attema, E., Potin, P., Rommen, B., Floury, N., Brown, M., Traver, I.N., Deghaye, P., Duesmann, B., Rosich, B., Miranda, N., Bruno, C., L'Abbate, M., Croci, R., Pietropaolo, A., Huchler, M., & Rostan, F. (2012). GMES Sentinel-1 mission. Remote Sensing of Environment, 120, 9-24

Torresani, M., Feilhauer, H., Rocchini, D., Féret, J.-B., Zebisch, M., & Tonon, G. (2021). Which optical traits enable an estimation of tree species diversity based on the Spectral Variation Hypothesis? Applied Vegetation Science, 24, e12586

Torresani, M., Rocchini, D., Sonnenschein, R., Zebisch, M., Marcantonio, M., Ricotta, C., & Tonon, G. (2019). Estimating tree species diversity from space in an alpine conifer forest: The Rao's Q diversity index meets the spectral variation hypothesis. Ecological Informatics, 52, 26-34

Turner, D.P., Acker, S.A., Means, J.E., & Garman, S.L. (2000). Assessing alternative allometric algorithms for estimating leaf area of Douglas-fir trees and stands. Forest Ecology and Management, 126, 61-76

Turner, W., Spector, S., Gardiner, N., Fladeland, M., Sterling, E., & Steininger, M. (2003). Remote sensing for biodiversity science and conservation. Trends in Ecology & Evolution, 18, 306-314

Ustin, S.L., & Gamon, J.A. (2010). Remote sensing of plant functional types. New Phytologist, 186, 795-816

Valbuena, R., O'Connor, B., Zellweger, F., Simonson, W., Vihervaara, P., Maltamo, M., Silva, C.A., Almeida, D.R.A., Danks, F., Morsdorf, F., Chirici, G., Lucas, R., Coomes, D.A., & Coops, N.C. (2020). Standardizing Ecosystem Morphological Traits from 3D Information Sources. Trends in Ecology & Evolution, 35, 656-667

Van Cleemput, E., Helsen, K., Feilhauer, H., Honnay, O., & Somers, B. (2021). Spectrally defined plant functional types adequately capture multidimensional trait variation in herbaceous communities. Ecological Indicators, 120, 106970

van den Berg, R.A., Hoefsloot, H.C.J., Westerhuis, J.A., Smilde, A.K., & van der Werf, M.J. (2006). Centering, scaling, and transformations: improving the biological information content of metabolomics data. In, BMC genomics (p. 142)

van der Tol, C., Verhoef, W., Timmermans, J., Verhoef, A., & Su, Z. (2009). An integrated model of soil-canopy spectral radiances, photosynthesis, fluorescence, temperature and energy balance. Biogeosciences, 6, 3109-3129

Verhoef, W. (1985). Earth observation modeling based on layer scattering matrices. Remote Sensing of Environment, 17, 165-178

Vilfan, N., Van der Tol, C., Yang, P., Wyber, R., Malenovský, Z., Robinson, S.A., & Verhoef, W. (2018). Extending Fluspect to simulate xanthophyll driven leaf reflectance dynamics. Remote Sensing of Environment, 211, 345-356

Villéger, S., Mason, N.W.H., & Mouillot, D. (2008). New multidimensional functional diversity indices for a multifaceted framework in functional ecology. Ecology, 89, 2290-2301

Wang, R., & Gamon, J.A. (2019). Remote sensing of terrestrial plant biodiversity. Remote Sensing of Environment, 231, 111218

Wang, R., Gamon, J.A., Cavender-Bares, J., Townsend, P.A., & Zygielbaum, A.I. (2018a). The spatial sensitivity of the spectral diversity–biodiversity relationship: an experimental test in a prairie grassland. Ecological Applications, 28, 541-556

Wang, R., Gamon, J.A., Schweiger, A.K., Cavender-Bares, J., Townsend, P.A., Zygielbaum, A.I., & Kothari, S. (2018b). Influence of species richness, evenness, and composition on optical diversity: A simulation study. Remote Sensing of Environment, 211, 218-228

Warren, S.D., Alt, M., Olson, K.D., Irl, S.D.H., Steinbauer, M.J., & Jentsch, A. (2014). The relationship between the spectral diversity of satellite imagery, habitat heterogeneity, and plant species richness. Ecological Informatics, 24, 160-168

Wright, I.J., Reich, P.B., Westoby, M., Ackerly, D.D., Baruch, Z., Bongers, F., Cavender-Bares, J., Chapin, T., Cornelissen, J.H.C., Diemer, M., Flexas, J., Garnier, E., Groom, P.K., Gulias, J., Hikosaka, K., Lamont, B.B., Lee, T., Lee, W., Lusk, C., Midgley, J.J., Navas, M.-L., Niinemets, Ü., Oleksyn, J., Osada, N., Poorter, H., Poot, P., Prior, L., Pyankov, V.I., Roumet, C., Thomas, S.C., Tjoelker, M.G., Veneklaas, E.J., & Villar, R. (2004). The worldwide leaf economics spectrum. Nature, 428, 821

Yang, J., Gong, P., Fu, R., Zhang, M., Chen, J., Liang, S., Xu, B., Shi, J., & Dickinson, R. (2013). The role of satellite remote sensing in climate change studies. Nature Climate Change, 3, 875-883

Zhao, M., Tian, S., Zhu, Y., Li, Z., Zeng, S., & Liu, S. (2021). Allometric relationships, functional differentiations, and scaling of growth rates across 151 tree species in China. Ecosphere, 12, e03522

Zhao, Y., Zeng, Y., Zheng, Z., Dong, W., Zhao, D., Wu, B., & Zhao, Q. (2018). Forest species diversity mapping using airborne LiDAR and hyperspectral data in a subtropical forest in China. Remote Sensing of Environment, 213, 104-114

Zhu, C., Byrd, R.H., Lu, P., & Nocedal, J. (1997). Algorithm 778: L-BFGS-B: Fortran subroutines for large-scale bound-constrained optimization. ACM Trans. Math. Softw., 23, 550–560

SUPPLEMENTARY MATERIAL

SUPPLEMENTARY METHODS

SM1. Training and evaluation of SCOPE emulators

We trained two shallow neural networks (one layer) to enable fast computation of large datasets of reflectance factors with SCOPE. To do so, we built look-up tables (LUT) of 6,000 samples for training and 1,000 samples for validation of the models. These LUTs included plant traits (T_{RTM}) and other parameters of the model (illumination and soil) and the corresponding reflectance factors simulated with SCOPE (Table S1). Both neural networks predicted reflectance factors from these inputs. The neural networks featuring one hidden layer were fitted to the training dataset using the Python package *scikit-learn* (Pedregosa et al. 2011). Following Rivera et al. (2015), we added random noise of standard deviation equivalent to 0.5 % of the dataset's range of variability in each band and zero mean and then applied dimensionality reduction with principal component analysis (PCA). We trained two models from two different sets of LUTs: the first for simulation (section 2.3.3 of the manuscript) and the second to retrieve optical traits via radiative transfer model inversion (section 2.3.6 of the manuscript).Using two models that provided slightly different reflectance factor predictions for the same set of inputs allowed us to force a model error in the retrieval. Table S2 presents the emulators' training and comparison statistics.

SM2. Details of the inversion of the SCOPE emulator on simulated spectra

We estimated the optical traits in two steps. In the first step, we calculated an initial solution (ξ_0) from a look-up table of 10,000 samples generated with the emulator; assuming constant diffuse-to-global radiation ratio and sun zenith angle (δ_{DG} = 0.20, θ_{sun} = 30°, respectively), and nadiral observation. ξ_0 was the averaged value of the 10 samples (ξ_i) with the lowest sum of squares (χ^2) between the predicted (R_{pred}) and the "observed" (simulated) reflectance factors (R_{obs}) (Eq. SM2.1), weighted by χ^2 (Eq. SM2.2). In the case of DESIS and Sentinel-2 simulations, we convolved R_{pred} with the corresponding spectral response functions.

$$\chi^2 = \sum_{\lambda} \left(R_{\lambda,\mathrm{pred}} - R_{\lambda,\mathrm{obs}}\right)^2 \tag{SM2.1}$$

where λ stands for each spectral band

$$\xi_0 = \frac{\sum_{i=1}^{10} \frac{\xi_i^{\mathrm{sorted}}}{\chi_i^2}}{\sum_{i=1}^{10} \chi_i^2} \tag{SM2.2}$$

In the second step, we averaged soil parameters for all the species (pixels) of each community and canopy height (h_{c}) and leaf width (l_{w}), two traits with low influence on canopy reflectance and thus the most prone to equifinality. Then, we retrieved only the optical traits with the strongest effect on R (N, C_{ab}, C_{ca}, C_{ant}, C_{s}, C_{dm}, C_{w}, $LIDF_a$, $LIDF_b$, and LAI) by minimizing Eq. SM2.1 with the L-BFGS-B algorithm

(Zhu et al. 1997). In this step, we bound the optimization using the limits applied to the look-up tables to train the emulators (Table S1).

SM3. Evaluation of the temporal stability and filtering of FunDivEUROPE plots

The closest-to-DESIS (summer 2020) and cloud-free Sentinel-2 imagery was downloaded and processed as described in Ma et al. (2019) and section 2.4.2 of the manuscript. However, visual inspection made clear that the geometric correction presented some biases leading to the inclusion of nearby roads in the FunDivEUROPE plots. Sentinel-2 2020 imagery was further corrected by optimizing affine transformation parameters that maximized Pearson correlation between the average of all the spectral bands of the images of 2015 and 2020. Pixels classified as clouds or shadows in the L2A scene classification layer were excluded from the optimization. Notice that the full images, not the FunDivEUROPE plots, were used for the correction. Pearson correlation coefficient increased from 0.8485 to 0.8858 in Spain and 0.7622 to 0.8095 in Romania. The correction produced average shifts of 1.23 and 1.42 pixels in Spain and Romania, respectively. Pixels were resampled using the nearest neighbor approach.

Once corrected, we compared the normalized difference vegetation index (*NDVI*) of 2015 and 2020 imagery in the FunDivEUROPE plots. A linear model was fit using weighted least squares, resulting $NDVI_{2020} = 0.821 \cdot NDVI_{2015} + 0.164$. We considered that any plot whose *NDVI*-distance to the model was larger than 0.1 had significantly changed and was not comparable between 2015 and 2020. This way, we excluded ten sites in Romania and two in Spain for the analyses with DESIS and Sentinel-2 in 2020.

SM4. Estimation of optical traits in FunDivEUROPE plots

We retrieved optical traits in the FunDivEUROPE plots from DESIS and Sentinel-2 imagery. First, we estimated δ_{DG} (the fraction of diffuse radiation) per wavelength from the atmospheric optical thickness (*AOT*) and solar zenith angle using the model implemented in FLIGHT (North 1996) as described in Melendo-Vega et al. (2018). Then δ_{DG} was averaged within the optical domain and used as input of the emulator.

Then we produced an initial estimate of the unknown soil parameters and vegetation optical traits (Table S1) with a look-up table (LUT) inversion approach. We generated a LUT of 10,000 samples for each scene with the SCOPE RTM emulator. Averaged sun-view geometry and δ_{DG} were used for all the pixels, assuming little variability within the reduced area. Also, we forced a nadiral view zenith angle. The initial solution was the weighted average (Eq. SM2.2) of the 50 LUT samples providing the lowest χ^2 (Eq. SM2.2).

Since the emulator was trained for nadiral observations only, the SCOPE model (not the emulator) was inverted in a second step, accounting for the actual observation angles of each plot. As in the supplementary SM2, we retrieved only the optical traits with the strongest effect on R (N, C_{ab}, C_{ca}, C_{ant}, C_{s}, C_{dm}, C_{w}, $LIDF_a$, $LIDF_b$, and LAI). In this case, we set these optical traits at 25 % or 75 % of their bounded range whenever the initial solution was at the lower or the upper bound, respectively. The rest of the optical traits and soil parameters were averaged per plot. In the second step, we minimized a regularized cost function (Eq. SM4.1) using the trust-region-reflective algorithm (Coleman and Li 1996) implemented in the Matlab™ function *lsqnonlin* (MathWorks, Natick, MA, USA). The function penalized the carotenoids to chlorophyll ratio deviating from 0.20, a value close to the median calculated in the LOPEX and ANGERS databases, as well as the magnitude of anthocyanins content since high values were not expected. To improve the performance of the inversion, we also regularized LAI (LAI^{reg}) with prior information (Combal et al. 2003). For the plots in Spain, we added a penalty on the magnitude of *LAI* since it tended to take very high values ($LAI^{\text{reg}} = LAI$); in Romania, we regularized deviations from 6.0, a value close to field *LAI* ($LAI^{\text{reg}} = LAI - 6.0$).

$$\chi^2 = \sum_{\lambda} \left(R_{\lambda,\text{pred}} - R_{\lambda,\text{obs}}\right)^2 + \left(\gamma_1 \left(\frac{C_{\text{ca}}}{C_{\text{ab}}} - 0.20\right)\right)^2 + (\gamma_2 C_{\text{ant}})^2 + (\gamma_3 LAI^{\text{reg}})^2 \tag{SM4.1}$$

where γ_1, γ_2, and γ_3 are the regularization factors. $\gamma_1 = 10^{-1}$, $\gamma_2 = 10^{-2}$ and γ_3 equal $5 \cdot 10^{-3}$ or $4 \cdot 10^{-3}$ in Spain or Romania, respectively.

SUPPLEMENTARY TABLES AND FIGURES

Table S1

Table S1. SCOPE inputs, symbols, and bounds used in simulation and the inversion. In addition to plant traits described in the manuscript, SCOPE requires additional inputs. For example, the BSM module of SCOPE simulates soil reflectance factors as a function of soil brightness (*B*, unitless), spectral shape "latitude" and "longitude" color coordinates (*Lat* and *Lon*, degrees), soil moisture capacity (*SMC*, %) and content (SM_p, %). Illumination conditions were described by sun zenith angle (θ_{sun}, degrees) and the diffuse-to-global radiation ratio (δ_{DG}, -). Simulations assumed nadiral observation (view zenith angle, $\theta_{view} = 0°$).

Parameter	**Symbol**	**Units**	**Bounds**
Vegetation Parameters (P_{RTM})			
Leaf chlorophyll content	C_{ab}	µg cm^{-2}	[0, 100]
Leaf carotenoids content	C_{ca}	µg cm^{-2}	[0, 25]
Leaf anthocyanins content	C_{ant}	µg cm^{-2}	[0, 10]
Leaf senescent pigments content	C_s	a.u.	[0, 1]
Leaf water content	C_w	g cm^{-2}	[0.004, 0.045]
Leaf dry matter content	C_{dm}	g cm^{-2}	[0.00190, 0.01570]
Leaf structural parameter	N	layers	[1, 3]
Leaf area index	LAI	m^2 m^{-2}	[0, 8]
Leaf inclination distribution function	$LIDF_a$	-	[-1, 1]; $\lvert LIDF_a + LIDF_b \rvert \leq 1$
Bimodality of the leaf inclination	$LIDF_b$	-	
Canopy height	h_c	m	[0.1, 10.0]
Leaf width	l_{qw}	m	[0.01, 0.1]
Soil Parameters (BMS model)			
Soil brightness	B	-	[0.5, 1.0]
Spectral shape "latitude"	Lat	deg	[20, 40]
Spectral shape "longitude"	Lon	deg	[45, 65]
Soil moisture capacity	SMC	%	[5, 55]
Soil moisture content	SMp	-	[0, 1]
Sun view and atmosphere			
Sun zenith angle	θ_{sun}	deg	[0, 80]
Diffuse-to-global radiation ratio	δ_{DG}	-	[0, 1]

Table S2

Table S2. Statistics summarizing SCOPE emulator's training, validation, and the difference between their predictions. Training statistics are computed from datasets of 6,000 spectra; validation statistics and the comparison between the emulators are computed from 1,000 spectra. The table presents the mean values of the Root Mean Squared Error (*RMSE*, in reflectance factor units), the relative RMSE (*RRMSE*, %), and the normalized RMSE (*NRMSE*) of all the bands (400-2400 nm with 1 nm step).

Evaluation	***RMSE* (-)**	***RRMSE* (%)**	***NRMSE* (%)**
Emulator 1 (simulation)			
Training	0.0050	5.92	0.95
Validation	0.0056	6.59	1.29
Emulator 2 (model inversion)			
Training	0.0051	5.85	0.94
Validation	0.0058	6.41	1.26
Emulator 1 vs. Emulator 2			
Comparison	0.0143	9.26	3.55

Figure S1

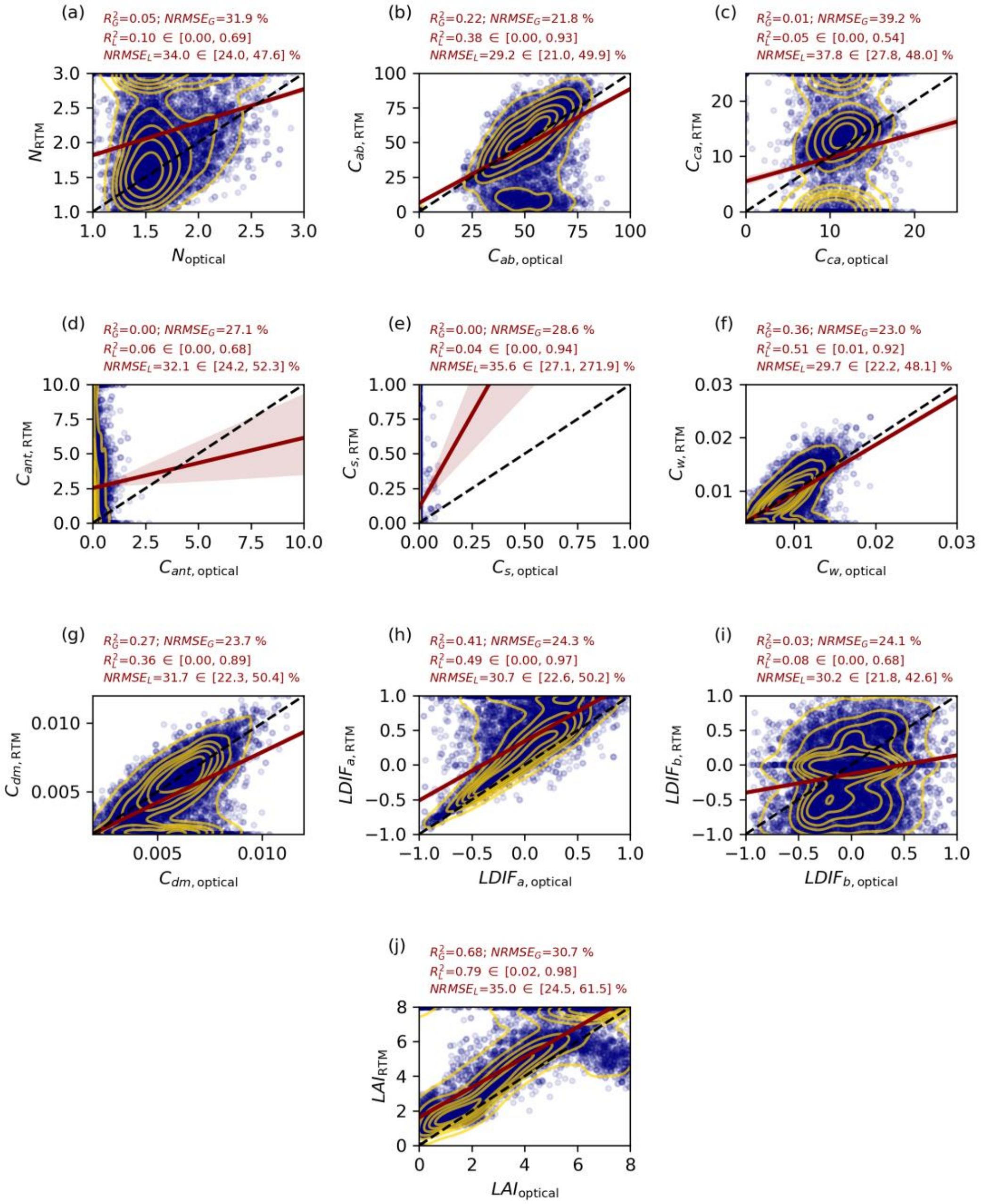

Figure S1. Evaluation of optical traits retrieval. Simulated field traits (subscript “RTM”) vs. optical traits estimated via inversion of the emulated radiative transfer model (subscript “optical”). Two different emulators simulated the reflectance factors and estimated the optical traits to induce model error. Regression lines summarize the comparison at the global scale; the shaded areas around the regression lines represent the 95 % confidence interval of the line. Each subplot includes the statistics of the relationship at the global scale (on top, subscript “G”) and the median and 95 % confidence interval of the statistics at the local scale (below, subscript “L”).

Figure S2

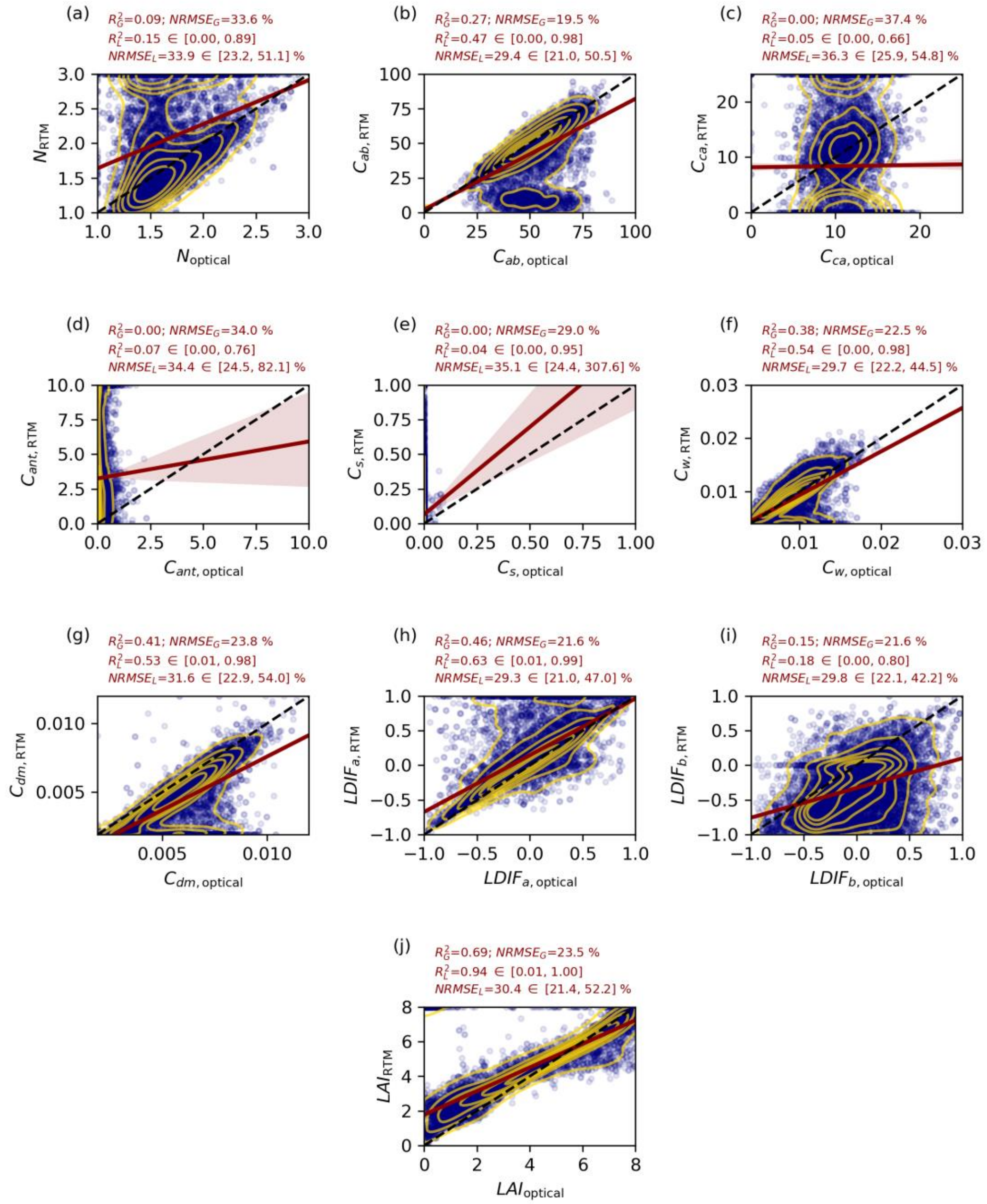

Figure S2. Evaluation of optical traits retrieval. Simulated field traits (subscript "RTM") vs. optical traits estimated via inversion of the emulated radiative transfer model (subscript "optical"). In this case, the same emulator was used to simulate the reflectance factors and estimate the optical traits, preventing model error. Regression lines summarize the comparison at the global scale; the shaded areas around the regression lines represent the 95 % confidence interval of the line. Each subplot includes the statistics of the relationship at the global scale (on top, subscript "G") and the median and 95 % confidence interval of the statistics at the local scale (below, subscript "L").

Figure S3

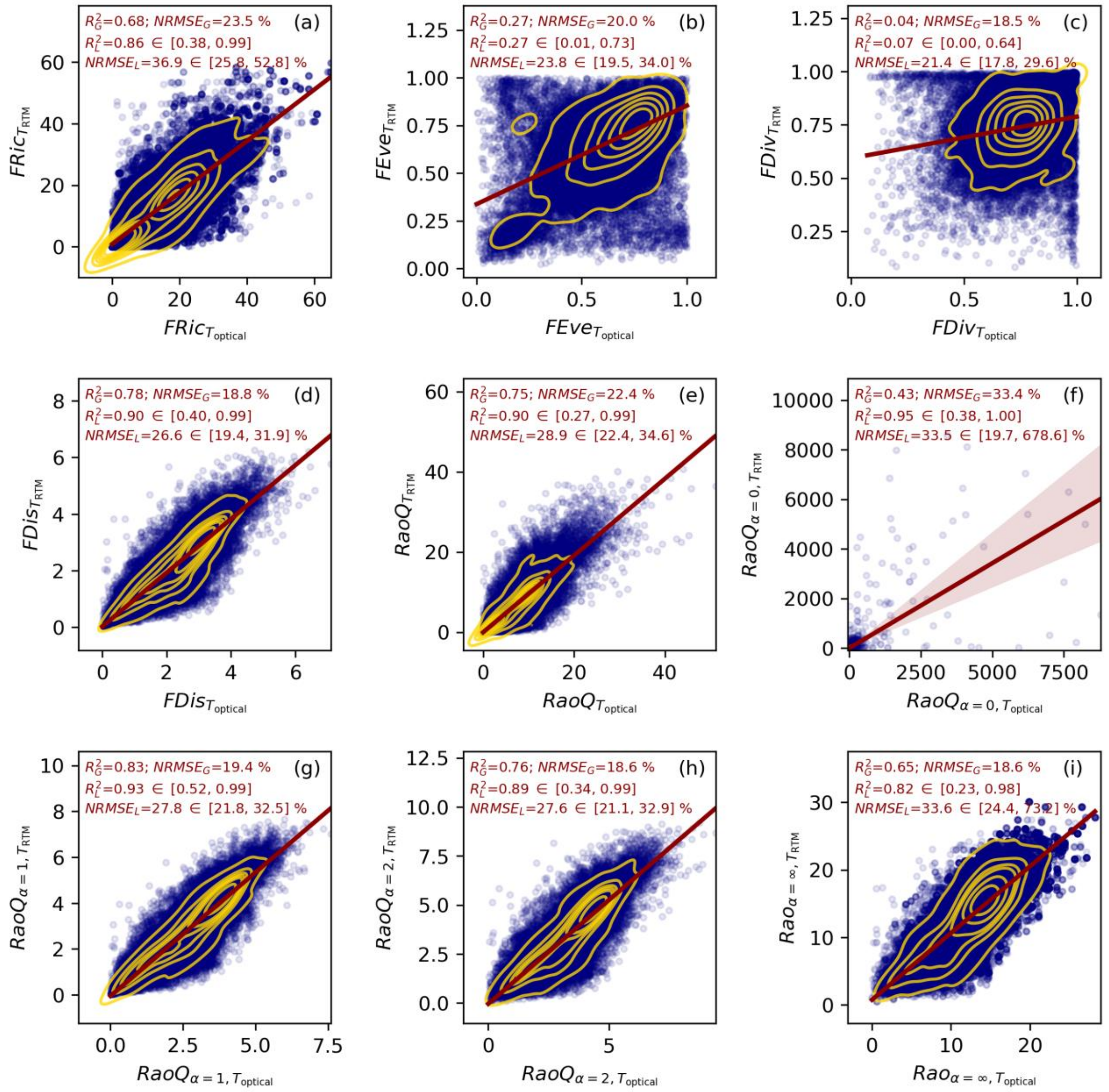

Figure S3. Relationship between the functional diversity metrics computed from optical traits estimated via radiative transfer model inversion (subscript "T_{optical}") and the simulated field plant traits (subscript "T_{RTM}") using the *dbFD* package (a-e), or the parametric Rao's Q formulation with different values of the parameter α (f-i). In this case, the same emulator was used to simulate the reflectance factors and estimate the optical traits, preventing model error. Regression lines summarize the comparison at the global scale; the shaded areas around the regression lines represent the 95 % confidence interval of the line. Each subplot includes the statistics of the relationship at the global scale (on top, subscript "G") and the median and 95 % confidence interval of the statistics at the local scale (below, subscript "L").

Table S3

Table S3. Median of the coefficient of determination ($\tilde{R}_{\mathrm{L}}^2$) of the relationships between field plant traits and optical traits estimated via radiative transfer model inversion compared both at the local scale for the different (27) simulation runs. Two different emulators were used to simulate the reflectance factors and estimate the optical traits, accounting for model error.

Spatial resolution		$S_{res,0}$			$S_{res,50}$			$S_{res,100}$		
Sensor		Hyper.	DESIS	S2	Hyper.	DESIS	S2	Hyper.	DESIS	S2
Trait	Noise (%)									
N	0	0.08	0.08	0.07	0.09	0.09	0.09	0.10	0.10	0.10
	5	0.07	0.05	0.05	0.08	0.06	0.06	0.09	0.06	0.05
	10	0.06	0.05	0.04	0.08	0.05	0.05	0.08	0.05	0.05
C_{ab}	0	0.26	0.26	0.21	0.34	0.33	0.33	0.38	0.33	0.37
	5	0.22	0.12	0.10	0.31	0.18	0.17	0.36	0.21	0.20
	10	0.16	0.09	0.07	0.27	0.12	0.12	0.33	0.15	0.15
C_{ca}	0	0.05	0.07	0.07	0.06	0.08	0.09	0.05	0.08	0.09
	5	0.06	0.05	0.04	0.05	0.06	0.06	0.05	0.06	0.06
	10	0.05	0.04	0.04	0.05	0.05	0.05	0.04	0.05	0.05
C_{ant}	0	0.09	0.05	0.06	0.06	0.06	0.06	0.06	0.06	0.06
	5	0.08	0.05	0.04	0.06	0.05	0.04	0.06	0.05	0.04
	10	0.06	0.04	0.03	0.06	0.04	0.04	0.06	0.04	0.04
C_s	0	0.06	0.05	0.05	0.04	0.04	0.04	0.04	0.03	0.04
	5	0.06	0.04	0.04	0.05	0.04	0.04	0.04	0.04	0.04
	10	0.05	0.04	0.04	0.05	0.04	0.04	0.04	0.04	0.04
C_w	0	0.31	0.10	0.20	0.49	0.13	0.38	0.51	0.17	0.46
	5	0.26	0.04	0.10	0.46	0.05	0.22	0.48	0.07	0.28
	10	0.19	0.04	0.07	0.39	0.04	0.12	0.45	0.05	0.15
C_{dm}	0	0.27	0.06	0.08	0.33	0.06	0.13	0.36	0.06	0.17
	5	0.24	0.04	0.04	0.32	0.04	0.06	0.36	0.04	0.07
	10	0.19	0.04	0.03	0.30	0.04	0.04	0.35	0.04	0.05
$LIDF_a$	0	0.28	0.14	0.16	0.43	0.34	0.41	0.49	0.41	0.50
	5	0.23	0.09	0.06	0.40	0.21	0.18	0.48	0.31	0.26
	10	0.19	0.07	0.05	0.36	0.17	0.11	0.44	0.24	0.15
$LIDF_b$	0	0.09	0.06	0.07	0.08	0.07	0.06	0.08	0.07	0.07
	5	0.07	0.05	0.04	0.07	0.05	0.04	0.07	0.05	0.04
	10	0.05	0.04	0.04	0.06	0.04	0.04	0.06	0.05	0.04
LAI	0	0.40	0.12	0.18	0.67	0.27	0.37	0.79	0.37	0.51
	5	0.35	0.06	0.07	0.62	0.13	0.16	0.75	0.19	0.21
	10	0.27	0.05	0.05	0.57	0.09	0.11	0.69	0.13	0.14

Table S4

Table S4. Coefficient of determination (R^2) of the relationships between functional diversity metrics computed from spectral reflectance and field plant traits, compared respectively at remote sensing and field spatial resolutions. Data are also presented in Fig. 8a,e. Each cell presents the R^2 of the relationship at the global scale, followed by the median and the 95 % confidence interval of R^2 at the local scale.

FDM	Noise	Hy			DESIS			Sentinel-2		
		100%	50%	0%	100%	50%	0%	100%	50%	0%
FRic	0%	0.61; 0.85 [0.36, 0.99]	0.03; 0.71 [0.10, 0.98]	0.00; 0.25 [0.01, 0.84]	0.58; 0.85 [0.36, 0.99]	0.19; 0.72 [0.09, 0.98]	0.00; 0.25 [0.00, 0.84]	0.62; 0.85 [0.37, 1.00]	0.18; 0.72 [0.10, 0.98]	0.00; 0.25 [0.01, 0.84]
	5%	0.59; 0.85 [0.37, 0.99]	0.00; 0.72 [0.09, 0.98]	0.00; 0.25 [0.01, 0.86]	0.57; 0.85 [0.37, 0.99]	0.12; 0.72 [0.10, 0.97]	0.01; 0.24 [0.01, 0.83]	0.60; 0.84 [0.33, 0.99]	0.26; 0.72 [0.06, 0.98]	0.01; 0.24 [0.01, 0.87]
	10%	0.57; 0.84 [0.35, 0.99]	0.01; 0.71 [0.09, 0.98]	0.00; 0.25 [0.01, 0.85]	0.56; 0.84 [0.34, 0.99]	0.09; 0.72 [0.08, 0.97]	0.01; 0.25 [0.01, 0.83]	0.58; 0.82 [0.33, 0.99]	0.27; 0.70 [0.05, 0.97]	0.01; 0.25 [0.01, 0.86]
FEve	0%	0.19; 0.21 [0.00, 0.64]	0.08; 0.10 [0.00, 0.50]	0.05; 0.09 [0.00, 0.54]	0.17; 0.19 [0.00, 0.62]	0.06; 0.09 [0.00, 0.52]	0.05; 0.09 [0.00, 0.52]	0.20; 0.23 [0.00, 0.64]	0.07; 0.10 [0.00, 0.55]	0.06; 0.09 [0.00, 0.58]
	5%	0.20; 0.21 [0.00, 0.69]	0.09; 0.11 [0.00, 0.53]	0.10; 0.13 [0.00, 0.61]	0.17; 0.20 [0.00, 0.63]	0.08; 0.11 [0.00, 0.55]	0.10; 0.13 [0.00, 0.60]	0.18; 0.19 [0.00, 0.63]	0.09; 0.11 [0.00, 0.55]	0.09; 0.12 [0.00, 0.60]
	10%	0.18; 0.19 [0.00, 0.64]	0.10; 0.11 [0.00, 0.57]	0.12; 0.15 [0.00, 0.63]	0.17; 0.18 [0.00, 0.66]	0.10; 0.11 [0.00, 0.62]	0.12; 0.16 [0.00, 0.63]	0.16; 0.17 [0.00, 0.62]	0.10; 0.11 [0.00, 0.59]	0.12; 0.15 [0.00, 0.60]
FDiv	0%	0.03; 0.07 [0.00, 0.62]	0.01; 0.05 [0.00, 0.57]	0.00; 0.05 [0.00, 0.56]	0.03; 0.06 [0.00, 0.59]	0.01; 0.05 [0.00, 0.54]	0.01; 0.05 [0.00, 0.51]	0.03; 0.06 [0.00, 0.62]	0.01; 0.05 [0.00, 0.56]	0.00; 0.05 [0.00, 0.54]
	5%	0.03; 0.06 [0.00, 0.66]	0.01; 0.05 [0.00, 0.56]	0.00; 0.05 [0.00, 0.56]	0.03; 0.06 [0.00, 0.60]	0.01; 0.05 [0.00, 0.60]	0.00; 0.05 [0.00, 0.55]	0.03; 0.06 [0.00, 0.59]	0.01; 0.05 [0.00, 0.55]	0.00; 0.05 [0.00, 0.52]
	10%	0.03; 0.07 [0.00, 0.58]	0.01; 0.05 [0.00, 0.55]	0.00; 0.05 [0.00, 0.53]	0.02; 0.06 [0.00, 0.57]	0.01; 0.05 [0.00, 0.55]	0.00; 0.05 [0.00, 0.50]	0.02; 0.05 [0.00, 0.55]	0.01; 0.05 [0.00, 0.53]	0.00; 0.05 [0.00, 0.54]
FDis	0%	0.70; 0.85 [0.31, 0.98]	0.50; 0.71 [0.04, 0.95]	0.13; 0.29 [0.00, 0.83]	0.70; 0.86 [0.29, 0.98]	0.52; 0.73 [0.06, 0.95]	0.15; 0.31 [0.00, 0.85]	0.73; 0.88 [0.32, 0.98]	0.54; 0.74 [0.07, 0.96]	0.15; 0.32 [0.00, 0.85]
	5%	0.68; 0.85 [0.29, 0.98]	0.49; 0.70 [0.06, 0.95]	0.11; 0.32 [0.00, 0.85]	0.69; 0.87 [0.27, 0.98]	0.50; 0.71 [0.08, 0.95]	0.12; 0.38 [0.00, 0.88]	0.71; 0.87 [0.29, 0.98]	0.52; 0.73 [0.07, 0.95]	0.12; 0.34 [0.00, 0.85]
	10%	0.67; 0.85 [0.27, 0.98]	0.47; 0.68 [0.08, 0.94]	0.11; 0.38 [0.00, 0.86]	0.68; 0.86 [0.24, 0.98]	0.48; 0.68 [0.09, 0.94]	0.12; 0.41 [0.00, 0.88]	0.67; 0.84 [0.23, 0.98]	0.48; 0.68 [0.07, 0.94]	0.11; 0.35 [0.00, 0.85]
RaoQ	0%	0.63; 0.84 [0.15, 0.98]	0.47; 0.73 [0.01, 0.97]	0.14; 0.31 [0.00, 0.89]	0.66; 0.86 [0.15, 0.98]	0.51; 0.75 [0.02, 0.97]	0.16; 0.35 [0.00, 0.89]	0.67; 0.86 [0.19, 0.98]	0.52; 0.77 [0.02, 0.97]	0.16; 0.35 [0.00, 0.89]
	5%	0.61; 0.83 [0.13, 0.98]	0.45; 0.71 [0.02, 0.97]	0.12; 0.32 [0.00, 0.88]	0.63; 0.86 [0.13, 0.98]	0.48; 0.75 [0.02, 0.97]	0.13; 0.36 [0.00, 0.90]	0.64; 0.85 [0.13, 0.98]	0.48; 0.75 [0.02, 0.97]	0.13; 0.34 [0.00, 0.88]

	10%	0.58; 0.82 [0.13, 0.98]	0.42; 0.70 [0.02, 0.96]	0.11; 0.34 [0.00, 0.88]	0.60; 0.84 [0.10, 0.98]	0.44; 0.72 [0.03, 0.96]	0.11; 0.38 [0.00, 0.90]	0.60; 0.82 [0.10, 0.98]	0.44; 0.71 [0.03, 0.96]	0.11; 0.33 [0.00, 0.88]
$RaoQ_{\alpha=0}$	0%	0.31; 0.67 [0.03, 0.98]	0.00; 0.04 [0.00, 0.83]	0.00; 0.09 [0.00, 0.67]	0.21; 0.89 [0.26, 1.00]	0.00; 0.05 [0.00, 0.85]	0.00; 0.06 [0.00, 0.63]	0.21; 0.92 [0.14, 1.00]	0.00; 0.08 [0.00, 0.86]	0.00; 0.07 [0.00, 0.63]
	5%	0.34; 0.65 [0.06, 0.98]	0.00; 0.03 [0.00, 0.83]	0.00; 0.07 [0.00, 0.68]	0.22; 0.88 [0.27, 1.00]	0.00; 0.04 [0.00, 0.87]	0.00; 0.06 [0.00, 0.59]	0.25; 0.93 [0.31, 1.00]	0.00; 0.06 [0.00, 0.87]	0.00; 0.05 [0.00, 0.63]
	10%	0.41; 0.64 [0.11, 0.97]	0.00; 0.03 [0.00, 0.83]	0.00; 0.07 [0.00, 0.69]	0.37; 0.86 [0.32, 1.00]	0.00; 0.03 [0.00, 0.86]	0.00; 0.05 [0.00, 0.59]	0.38; 0.93 [0.39, 1.00]	0.00; 0.04 [0.00, 0.88]	0.00; 0.05 [0.00, 0.63]
$RaoQ_{\alpha=1}$	0%	0.75; 0.89 [0.42, 0.99]	0.57; 0.78 [0.13, 0.96]	0.20; 0.40 [0.00, 0.88]	0.75; 0.90 [0.42, 0.98]	0.58; 0.79 [0.15, 0.96]	0.21; 0.43 [0.00, 0.89]	0.77; 0.91 [0.47, 0.99]	0.60; 0.80 [0.17, 0.97]	0.21; 0.43 [0.00, 0.90]
	5%	0.74; 0.90 [0.42, 0.99]	0.56; 0.78 [0.16, 0.97]	0.17; 0.45 [0.00, 0.89]	0.75; 0.91 [0.39, 0.99]	0.57; 0.78 [0.19, 0.96]	0.19; 0.50 [0.01, 0.91]	0.76; 0.91 [0.43, 0.99]	0.58; 0.79 [0.16, 0.97]	0.18; 0.47 [0.00, 0.90]
	10%	0.73; 0.89 [0.37, 0.99]	0.55; 0.74 [0.18, 0.96]	0.18; 0.51 [0.01, 0.89]	0.75; 0.90 [0.36, 0.99]	0.56; 0.75 [0.19, 0.96]	0.20; 0.53 [0.01, 0.92]	0.74; 0.89 [0.37, 0.99]	0.56; 0.75 [0.18, 0.97]	0.18; 0.48 [0.00, 0.90]
$RaoQ_{\alpha=2}$	0%	0.69; 0.85 [0.23, 0.98]	0.52; 0.73 [0.03, 0.96]	0.18; 0.32 [0.00, 0.86]	0.71; 0.87 [0.22, 0.98]	0.54; 0.75 [0.04, 0.96]	0.19; 0.35 [0.00, 0.89]	0.73; 0.88 [0.27, 0.98]	0.56; 0.76 [0.05, 0.96]	0.19; 0.36 [0.00, 0.88]
	5%	0.68; 0.86 [0.21, 0.98]	0.51; 0.72 [0.04, 0.96]	0.16; 0.34 [0.00, 0.87]	0.69; 0.87 [0.20, 0.98]	0.52; 0.75 [0.05, 0.96]	0.18; 0.38 [0.00, 0.89]	0.70; 0.87 [0.24, 0.98]	0.53; 0.75 [0.04, 0.96]	0.17; 0.36 [0.00, 0.88]
	10%	0.65; 0.84 [0.20, 0.98]	0.48; 0.70 [0.04, 0.95]	0.16; 0.37 [0.00, 0.87]	0.66; 0.86 [0.17, 0.98]	0.49; 0.71 [0.05, 0.95]	0.17; 0.40 [0.00, 0.89]	0.66; 0.84 [0.18, 0.98]	0.50; 0.70 [0.04, 0.95]	0.16; 0.36 [0.00, 0.87]
$RaoQ_{\alpha=\infty}$	0%	0.59; 0.78 [0.19, 0.98]	0.37; 0.60 [0.03, 0.95]	0.03; 0.16 [0.00, 0.84]	0.62; 0.80 [0.18, 0.98]	0.38; 0.62 [0.03, 0.96]	0.02; 0.16 [0.00, 0.83]	0.63; 0.80 [0.20, 0.98]	0.39; 0.63 [0.03, 0.96]	0.02; 0.16 [0.00, 0.83]
	5%	0.57; 0.77 [0.18, 0.98]	0.36; 0.59 [0.02, 0.96]	0.03; 0.15 [0.00, 0.83]	0.60; 0.80 [0.17, 0.98]	0.37; 0.62 [0.04, 0.96]	0.02; 0.16 [0.00, 0.83]	0.60; 0.79 [0.20, 0.98]	0.37; 0.63 [0.03, 0.97]	0.02; 0.16 [0.00, 0.84]
	10%	0.53; 0.75 [0.17, 0.97]	0.33; 0.59 [0.03, 0.96]	0.03; 0.16 [0.00, 0.82]	0.55; 0.77 [0.15, 0.97]	0.33; 0.60 [0.03, 0.96]	0.02; 0.16 [0.00, 0.84]	0.55; 0.77 [0.17, 0.97]	0.33; 0.60 [0.03, 0.96]	0.02; 0.17 [0.00, 0.83]

Table S5

Table S5. Coefficient of determination (R^2) of the relationships between functional diversity metrics computed from optical traits and field plant traits, compared respectively at remote sensing and field spatial resolutions. Data are also presented in Fig. 8c,g. Each cell presents the R^2 of the relationship at the global scale, followed by the median and the 95 % confidence interval of R^2 at the local scale.

FDM	Noise	Hy			DESIS			Sentinel-2		
		100%	50%	0%	100%	50%	0%	100%	50%	0%
FRic	0%	0.67; 0.85 [0.33, 0.99]	0.30; 0.71 [0.09, 0.98]	0.01; 0.23 [0.01, 0.86]	0.62; 0.82 [0.25, 0.99]	0.26; 0.70 [0.08, 0.98]	0.01; 0.24 [0.01, 0.86]	0.63; 0.83 [0.29, 0.99]	0.26; 0.70 [0.09, 0.97]	0.01; 0.25 [0.01, 0.84]
	5%	0.65; 0.84 [0.31, 0.99]	0.28; 0.72 [0.07, 0.98]	0.01; 0.23 [0.00, 0.87]	0.49; 0.76 [0.08, 0.97]	0.14; 0.64 [0.02, 0.97]	0.01; 0.23 [0.01, 0.81]	0.46; 0.72 [0.07, 0.98]	0.14; 0.62 [0.03, 0.96]	0.01; 0.23 [0.01, 0.84]
	10%	0.63; 0.83 [0.29, 0.99]	0.25; 0.71 [0.05, 0.98]	0.01; 0.23 [0.00, 0.85]	0.42; 0.71 [0.05, 0.97]	0.11; 0.60 [0.02, 0.96]	0.01; 0.23 [0.01, 0.82]	0.39; 0.68 [0.02, 0.97]	0.10; 0.59 [0.02, 0.95]	0.01; 0.24 [0.01, 0.85]
FEve	0%	0.22; 0.24 [0.00, 0.71]	0.10; 0.12 [0.00, 0.53]	0.07; 0.11 [0.00, 0.60]	0.19; 0.19 [0.00, 0.63]	0.10; 0.10 [0.00, 0.61]	0.05; 0.10 [0.00, 0.53]	0.20; 0.22 [0.00, 0.63]	0.10; 0.11 [0.00, 0.59]	0.07; 0.11 [0.00, 0.60]
	5%	0.19; 0.21 [0.00, 0.68]	0.10; 0.12 [0.00, 0.62]	0.07; 0.11 [0.00, 0.62]	0.14; 0.14 [0.00, 0.59]	0.09; 0.09 [0.00, 0.60]	0.08; 0.13 [0.00, 0.61]	0.12; 0.13 [0.00, 0.58]	0.08; 0.08 [0.00, 0.57]	0.09; 0.13 [0.00, 0.56]
	10%	0.18; 0.19 [0.00, 0.62]	0.10; 0.11 [0.00, 0.58]	0.07; 0.12 [0.00, 0.60]	0.13; 0.12 [0.00, 0.58]	0.09; 0.09 [0.00, 0.56]	0.09; 0.14 [0.00, 0.61]	0.11; 0.12 [0.00, 0.58]	0.09; 0.09 [0.00, 0.58]	0.10; 0.14 [0.00, 0.59]
FDiv	0%	0.03; 0.06 [0.00, 0.62]	0.01; 0.05 [0.00, 0.58]	0.01; 0.05 [0.00, 0.60]	0.02; 0.06 [0.00, 0.57]	0.01; 0.05 [0.00, 0.53]	0.00; 0.05 [0.00, 0.57]	0.02; 0.06 [0.00, 0.58]	0.01; 0.05 [0.00, 0.61]	0.01; 0.06 [0.00, 0.57]
	5%	0.02; 0.06 [0.00, 0.58]	0.01; 0.05 [0.00, 0.57]	0.01; 0.06 [0.00, 0.61]	0.00; 0.05 [0.00, 0.56]	0.00; 0.04 [0.00, 0.56]	0.00; 0.05 [0.00, 0.55]	0.00; 0.05 [0.00, 0.50]	0.00; 0.05 [0.00, 0.57]	0.00; 0.05 [0.00, 0.55]
	10%	0.02; 0.05 [0.00, 0.61]	0.01; 0.06 [0.00, 0.57]	0.00; 0.05 [0.00, 0.61]	0.00; 0.04 [0.00, 0.43]	0.00; 0.05 [0.00, 0.53]	0.00; 0.05 [0.00, 0.62]	0.00; 0.05 [0.00, 0.46]	0.00; 0.05 [0.00, 0.47]	0.00; 0.05 [0.00, 0.53]
FDis	0%	0.76; 0.88 [0.40, 0.98]	0.57; 0.72 [0.16, 0.96]	0.13; 0.28 [0.00, 0.84]	0.68; 0.84 [0.18, 0.98]	0.52; 0.65 [0.12, 0.94]	0.13; 0.32 [0.00, 0.83]	0.72; 0.85 [0.28, 0.99]	0.53; 0.67 [0.12, 0.94]	0.14; 0.32 [0.00, 0.85]
	5%	0.75; 0.87 [0.39, 0.98]	0.55; 0.70 [0.13, 0.95]	0.13; 0.30 [0.00, 0.86]	0.53; 0.70 [0.14, 0.97]	0.36; 0.48 [0.03, 0.92]	0.08; 0.25 [0.00, 0.83]	0.52; 0.66 [0.15, 0.97]	0.36; 0.47 [0.04, 0.92]	0.07; 0.23 [0.00, 0.85]
	10%	0.72; 0.85 [0.35, 0.98]	0.53; 0.68 [0.11, 0.94]	0.12; 0.27 [0.00, 0.84]	0.49; 0.62 [0.14, 0.97]	0.33; 0.45 [0.02, 0.91]	0.08; 0.22 [0.00, 0.83]	0.47; 0.62 [0.09, 0.97]	0.31; 0.42 [0.03, 0.91]	0.06; 0.20 [0.00, 0.81]
RaoQ	0%	0.73; 0.89 [0.24, 0.99]	0.56; 0.76 [0.03, 0.97]	0.12; 0.30 [0.00, 0.88]	0.64; 0.84 [0.07, 0.98]	0.52; 0.69 [0.03, 0.97]	0.12; 0.33 [0.00, 0.87]	0.68; 0.86 [0.15, 0.99]	0.52; 0.72 [0.03, 0.96]	0.13; 0.33 [0.00, 0.89]
	5%	0.71; 0.87 [0.21, 0.99]	0.54; 0.74 [0.04, 0.97]	0.12; 0.32 [0.00, 0.89]	0.45; 0.67 [0.03, 0.97]	0.32; 0.51 [0.00, 0.93]	0.06; 0.23 [0.00, 0.86]	0.44; 0.64 [0.04, 0.97]	0.32; 0.47 [0.01, 0.94]	0.05; 0.23 [0.00, 0.87]

	10%	0.67; 0.85 [0.21, 0.98]	0.51; 0.71 [0.04, 0.96]	0.10; 0.29 [0.00, 0.88]	0.38; 0.57 [0.01, 0.96]	0.26; 0.45 [0.01, 0.92]	0.05; 0.21 [0.00, 0.84]	0.34; 0.55 [0.01, 0.96]	0.23; 0.41 [0.00, 0.92]	0.03; 0.18 [0.00, 0.83]
$RaoQ_{\alpha=0}$	0%	0.29; 0.94 [0.35, 1.00]	0.00; 0.06 [0.00, 0.91]	0.00; 0.08 [0.00, 0.69]	0.42; 0.92 [0.30, 1.00]	0.00; 0.05 [0.00, 0.87]	0.00; 0.06 [0.00, 0.64]	0.23; 0.93 [0.33, 1.00]	0.00; 0.05 [0.00, 0.92]	0.00; 0.06 [0.00, 0.64]
	5%	0.35; 0.94 [0.32, 1.00]	0.00; 0.05 [0.00, 0.91]	0.00; 0.06 [0.00, 0.69]	0.17; 0.85 [0.21, 1.00]	0.00; 0.03 [0.00, 0.85]	0.00; 0.04 [0.00, 0.63]	0.18; 0.83 [0.22, 1.00]	0.00; 0.03 [0.00, 0.88]	0.00; 0.05 [0.00, 0.62]
	10%	0.29; 0.94 [0.40, 1.00]	0.00; 0.04 [0.00, 0.89]	0.00; 0.05 [0.00, 0.68]	0.16; 0.87 [0.27, 1.00]	0.00; 0.03 [0.00, 0.89]	0.00; 0.04 [0.00, 0.64]	0.15; 0.86 [0.28, 1.00]	0.00; 0.03 [0.00, 0.88]	0.00; 0.04 [0.00, 0.61]
$RaoQ_{\alpha=1}$	0%	0.81; 0.92 [0.51, 0.99]	0.63; 0.77 [0.28, 0.97]	0.19; 0.42 [0.00, 0.89]	0.75; 0.89 [0.31, 0.99]	0.59; 0.72 [0.22, 0.96]	0.18; 0.45 [0.00, 0.88]	0.77; 0.89 [0.41, 0.99]	0.59; 0.73 [0.20, 0.96]	0.21; 0.45 [0.00, 0.89]
	5%	0.80; 0.91 [0.51, 0.99]	0.62; 0.76 [0.25, 0.97]	0.19; 0.44 [0.00, 0.91]	0.62; 0.77 [0.23, 0.98]	0.44; 0.57 [0.10, 0.95]	0.14; 0.39 [0.00, 0.88]	0.60; 0.73 [0.26, 0.98]	0.44; 0.56 [0.10, 0.95]	0.13; 0.38 [0.00, 0.90]
	10%	0.78; 0.89 [0.48, 0.99]	0.60; 0.74 [0.25, 0.96]	0.18; 0.42 [0.00, 0.89]	0.60; 0.72 [0.25, 0.98]	0.42; 0.55 [0.08, 0.94]	0.15; 0.38 [0.00, 0.88]	0.57; 0.71 [0.19, 0.99]	0.40; 0.52 [0.08, 0.94]	0.13; 0.35 [0.00, 0.86]
$RaoQ_{\alpha=2}$	0%	0.75; 0.88 [0.32, 0.98]	0.57; 0.73 [0.10, 0.96]	0.15; 0.33 [0.00, 0.88]	0.67; 0.84 [0.13, 0.98]	0.52; 0.67 [0.08, 0.95]	0.16; 0.35 [0.00, 0.85]	0.70; 0.84 [0.23, 0.99]	0.53; 0.68 [0.06, 0.95]	0.17; 0.35 [0.00, 0.87]
	5%	0.73; 0.86 [0.30, 0.98]	0.56; 0.71 [0.09, 0.96]	0.15; 0.35 [0.00, 0.88]	0.51; 0.67 [0.06, 0.96]	0.36; 0.50 [0.02, 0.92]	0.10; 0.25 [0.00, 0.84]	0.49; 0.64 [0.09, 0.96]	0.36; 0.47 [0.02, 0.93]	0.10; 0.25 [0.00, 0.87]
	10%	0.70; 0.83 [0.28, 0.98]	0.53; 0.69 [0.09, 0.95]	0.13; 0.30 [0.00, 0.86]	0.45; 0.59 [0.06, 0.96]	0.31; 0.45 [0.01, 0.91]	0.10; 0.23 [0.00, 0.82]	0.42; 0.59 [0.03, 0.96]	0.29; 0.40 [0.01, 0.92]	0.08; 0.21 [0.00, 0.83]
$RaoQ_{\alpha=\infty}$	0%	0.63; 0.81 [0.19, 0.97]	0.33; 0.58 [0.03, 0.96]	0.00; 0.15 [0.00, 0.81]	0.56; 0.76 [0.09, 0.97]	0.27; 0.50 [0.02, 0.95]	0.00; 0.13 [0.00, 0.86]	0.58; 0.78 [0.14, 0.97]	0.29; 0.54 [0.02, 0.96]	0.00; 0.14 [0.00, 0.84]
	5%	0.59; 0.78 [0.15, 0.97]	0.30; 0.57 [0.03, 0.95]	0.00; 0.15 [0.00, 0.82]	0.40; 0.62 [0.04, 0.94]	0.15; 0.36 [0.00, 0.93]	0.00; 0.10 [0.00, 0.78]	0.39; 0.59 [0.07, 0.93]	0.17; 0.40 [0.01, 0.92]	0.00; 0.10 [0.00, 0.81]
	10%	0.55; 0.75 [0.15, 0.96]	0.27; 0.53 [0.03, 0.95]	0.00; 0.14 [0.00, 0.81]	0.34; 0.53 [0.03, 0.89]	0.12; 0.35 [0.01, 0.89]	0.00; 0.10 [0.00, 0.75]	0.32; 0.53 [0.03, 0.92]	0.13; 0.31 [0.00, 0.91]	0.00; 0.10 [0.00, 0.76]

Table S6

Table S6. Coefficient of determination (R^2) of the relationships between functional diversity metrics computed from spectral reflectance and field plant traits, compared both at remote sensing resolution. Data are also presented in Fig. 8b,f. Each cell presents the R^2 of the relationship at the global scale, followed by the median and the 95 % confidence interval of R^2 at the local scale.

FDM	Noise	Hy			DESIS			Sentinel-2		
		100%	50%	0%	100%	50%	0%	100%	50%	0%
FRic	0%	0.61; 0.85 [0.36, 0.99]	0.08; 0.90 [0.36, 1.00]	0.02; 0.99 [0.89, 1.00]	0.58; 0.85 [0.36, 0.99]	0.26; 0.91 [0.38, 1.00]	0.33; 0.99 [0.88, 1.00]	0.62; 0.85 [0.37, 1.00]	0.14; 0.90 [0.37, 1.00]	0.34; 0.99 [0.87, 1.00]
	5%	0.59; 0.85 [0.37, 0.99]	0.00; 0.89 [0.35, 1.00]	0.00; 0.97 [0.75, 1.00]	0.57; 0.85 [0.37, 0.99]	0.28; 0.87 [0.32, 0.99]	0.02; 0.97 [0.77, 1.00]	0.60; 0.84 [0.33, 0.99]	0.35; 0.86 [0.33, 0.99]	0.65; 0.96 [0.70, 1.00]
	10%	0.57; 0.84 [0.35, 0.99]	0.00; 0.87 [0.32, 1.00]	0.00; 0.95 [0.61, 1.00]	0.56; 0.84 [0.34, 0.99]	0.27; 0.85 [0.32, 0.99]	0.01; 0.97 [0.71, 1.00]	0.58; 0.82 [0.33, 0.99]	0.51; 0.84 [0.26, 0.99]	0.76; 0.95 [0.67, 1.00]
FEve	0%	0.19; 0.21 [0.00, 0.64]	0.27; 0.32 [0.01, 0.76]	0.38; 0.48 [0.04, 0.89]	0.17; 0.19 [0.00, 0.62]	0.25; 0.33 [0.00, 0.77]	0.35; 0.44 [0.02, 0.89]	0.20; 0.23 [0.00, 0.64]	0.28; 0.35 [0.01, 0.79]	0.40; 0.47 [0.05, 0.90]
	5%	0.20; 0.21 [0.00, 0.69]	0.35; 0.40 [0.02, 0.84]	0.50; 0.60 [0.16, 0.92]	0.17; 0.20 [0.00, 0.63]	0.33; 0.39 [0.01, 0.83]	0.47; 0.59 [0.13, 0.90]	0.18; 0.19 [0.00, 0.63]	0.33; 0.38 [0.01, 0.81]	0.44; 0.55 [0.14, 0.89]
	10%	0.18; 0.19 [0.00, 0.64]	0.41; 0.45 [0.04, 0.86]	0.55; 0.64 [0.19, 0.92]	0.17; 0.18 [0.00, 0.66]	0.38; 0.43 [0.05, 0.86]	0.52; 0.62 [0.15, 0.92]	0.16; 0.17 [0.00, 0.62]	0.36; 0.39 [0.02, 0.82]	0.48; 0.58 [0.15, 0.90]
FDiv	0%	0.03; 0.07 [0.00, 0.62]	0.13; 0.21 [0.00, 0.82]	0.34; 0.54 [0.01, 0.93]	0.03; 0.06 [0.00, 0.59]	0.13; 0.20 [0.00, 0.81]	0.31; 0.49 [0.01, 0.94]	0.03; 0.06 [0.00, 0.62]	0.15; 0.22 [0.00, 0.82]	0.34; 0.54 [0.01, 0.95]
	5%	0.03; 0.06 [0.00, 0.66]	0.13; 0.22 [0.00, 0.83]	0.28; 0.48 [0.01, 0.93]	0.03; 0.06 [0.00, 0.60]	0.13; 0.20 [0.00, 0.79]	0.19; 0.41 [0.00, 0.92]	0.03; 0.06 [0.00, 0.59]	0.11; 0.19 [0.00, 0.81]	0.18; 0.36 [0.00, 0.91]
	10%	0.03; 0.07 [0.00, 0.58]	0.11; 0.20 [0.00, 0.83]	0.21; 0.34 [0.00, 0.90]	0.02; 0.06 [0.00, 0.57]	0.12; 0.18 [0.00, 0.77]	0.16; 0.29 [0.00, 0.90]	0.02; 0.05 [0.00, 0.55]	0.08; 0.15 [0.00, 0.77]	0.09; 0.23 [0.00, 0.87]
FDis	0%	0.70; 0.85 [0.31, 0.98]	0.62; 0.80 [0.18, 0.97]	0.48; 0.60 [0.01, 0.96]	0.70; 0.86 [0.29, 0.98]	0.63; 0.80 [0.22, 0.97]	0.47; 0.59 [0.01, 0.96]	0.73; 0.88 [0.32, 0.98]	0.65; 0.83 [0.24, 0.98]	0.51; 0.63 [0.01, 0.97]
	5%	0.68; 0.85 [0.29, 0.98]	0.61; 0.81 [0.19, 0.97]	0.43; 0.57 [0.00, 0.96]	0.69; 0.87 [0.27, 0.98]	0.62; 0.82 [0.20, 0.98]	0.42; 0.57 [0.01, 0.97]	0.71; 0.87 [0.29, 0.98]	0.63; 0.82 [0.23, 0.98]	0.41; 0.55 [0.00, 0.95]
	10%	0.67; 0.85 [0.27, 0.98]	0.60; 0.81 [0.20, 0.97]	0.39; 0.53 [0.00, 0.95]	0.68; 0.86 [0.24, 0.98]	0.61; 0.81 [0.20, 0.97]	0.39; 0.50 [0.00, 0.96]	0.67; 0.84 [0.23, 0.98]	0.61; 0.79 [0.21, 0.97]	0.35; 0.45 [0.00, 0.94]
RaoQ	0%	0.63; 0.84 [0.15, 0.98]	0.57; 0.79 [0.08, 0.98]	0.49; 0.60 [0.01, 0.97]	0.66; 0.86 [0.15, 0.98]	0.60; 0.80 [0.11, 0.98]	0.49; 0.60 [0.01, 0.97]	0.67; 0.86 [0.19, 0.98]	0.62; 0.82 [0.12, 0.98]	0.52; 0.62 [0.01, 0.97]
	5%	0.61; 0.83 [0.13, 0.98]	0.55; 0.77 [0.07, 0.98]	0.44; 0.58 [0.00, 0.97]	0.63; 0.86 [0.13, 0.98]	0.57; 0.80 [0.08, 0.98]	0.44; 0.58 [0.00, 0.97]	0.64; 0.85 [0.13, 0.98]	0.58; 0.80 [0.09, 0.98]	0.45; 0.56 [0.00, 0.97]

	10%	0.58; 0.82 [0.13, 0.98]	0.51; 0.77 [0.06, 0.97]	0.40; 0.55 [0.00, 0.96]	0.60; 0.84 [0.10, 0.98]	0.53; 0.79 [0.06, 0.98]	0.39; 0.52 [0.00, 0.97]	0.60; 0.82 [0.10, 0.98]	0.53; 0.77 [0.07, 0.97]	0.38; 0.48 [0.00, 0.95]
$RaoQ_{\alpha=0}$	0%	0.31; 0.67 [0.03, 0.98]	0.34; 0.71 [0.06, 0.99]	0.22; 0.67 [0.01, 1.00]	0.21; 0.89 [0.26, 1.00]	0.06; 0.88 [0.13, 1.00]	0.31; 0.76 [0.03, 1.00]	0.21; 0.92 [0.14, 1.00]	0.29; 0.91 [0.19, 1.00]	0.33; 0.82 [0.03, 1.00]
	5%	0.34; 0.65 [0.06, 0.98]	0.33; 0.66 [0.04, 0.99]	0.13; 0.48 [0.00, 1.00]	0.22; 0.88 [0.27, 1.00]	0.47; 0.86 [0.10, 1.00]	0.26; 0.61 [0.00, 1.00]	0.25; 0.93 [0.31, 1.00]	0.19; 0.92 [0.14, 1.00]	0.27; 0.67 [0.01, 1.00]
	10%	0.41; 0.64 [0.11, 0.97]	0.40; 0.66 [0.04, 0.99]	0.18; 0.34 [0.00, 1.00]	0.37; 0.86 [0.32, 1.00]	0.54; 0.87 [0.05, 1.00]	0.34; 0.45 [0.00, 1.00]	0.38; 0.93 [0.39, 1.00]	0.39; 0.93 [0.18, 1.00]	0.28; 0.49 [0.00, 1.00]
$RaoQ_{\alpha=1}$	0%	0.75; 0.89 [0.42, 0.99]	0.67; 0.85 [0.31, 0.98]	0.54; 0.68 [0.04, 0.97]	0.75; 0.90 [0.42, 0.98]	0.68; 0.85 [0.35, 0.98]	0.53; 0.68 [0.02, 0.97]	0.77; 0.91 [0.47, 0.99]	0.70; 0.87 [0.37, 0.98]	0.56; 0.71 [0.04, 0.97]
	5%	0.74; 0.90 [0.42, 0.99]	0.67; 0.86 [0.34, 0.98]	0.51; 0.69 [0.03, 0.97]	0.75; 0.91 [0.39, 0.99]	0.68; 0.87 [0.35, 0.98]	0.50; 0.68 [0.03, 0.98]	0.76; 0.91 [0.43, 0.99]	0.69; 0.87 [0.36, 0.98]	0.50; 0.66 [0.02, 0.97]
	10%	0.73; 0.89 [0.37, 0.99]	0.67; 0.86 [0.33, 0.98]	0.50; 0.68 [0.03, 0.97]	0.75; 0.90 [0.36, 0.99]	0.69; 0.87 [0.34, 0.98]	0.50; 0.65 [0.02, 0.98]	0.74; 0.89 [0.37, 0.99]	0.68; 0.86 [0.33, 0.98]	0.47; 0.60 [0.01, 0.97]
$RaoQ_{\alpha=2}$	0%	0.69; 0.85 [0.23, 0.98]	0.62; 0.79 [0.14, 0.97]	0.51; 0.62 [0.01, 0.97]	0.71; 0.87 [0.22, 0.98]	0.63; 0.81 [0.18, 0.98]	0.51; 0.61 [0.01, 0.97]	0.73; 0.88 [0.27, 0.98]	0.65; 0.83 [0.18, 0.98]	0.54; 0.64 [0.01, 0.97]
	5%	0.68; 0.86 [0.21, 0.98]	0.60; 0.79 [0.13, 0.97]	0.45; 0.60 [0.01, 0.97]	0.69; 0.87 [0.20, 0.98]	0.61; 0.81 [0.14, 0.98]	0.44; 0.59 [0.01, 0.97]	0.70; 0.87 [0.24, 0.98]	0.63; 0.82 [0.17, 0.98]	0.45; 0.57 [0.01, 0.96]
	10%	0.65; 0.84 [0.20, 0.98]	0.57; 0.79 [0.14, 0.97]	0.39; 0.56 [0.00, 0.96]	0.66; 0.86 [0.17, 0.98]	0.59; 0.80 [0.12, 0.97]	0.38; 0.54 [0.00, 0.97]	0.66; 0.84 [0.18, 0.98]	0.59; 0.78 [0.12, 0.97]	0.37; 0.48 [0.00, 0.95]
$RaoQ_{\alpha=\infty}$	0%	0.59; 0.78 [0.19, 0.98]	0.47; 0.68 [0.09, 0.98]	0.39; 0.55 [0.00, 1.00]	0.62; 0.80 [0.18, 0.98]	0.50; 0.71 [0.12, 0.98]	0.41; 0.60 [0.00, 1.00]	0.63; 0.80 [0.20, 0.98]	0.50; 0.72 [0.11, 0.98]	0.41; 0.59 [0.00, 1.00]
	5%	0.57; 0.77 [0.18, 0.98]	0.43; 0.67 [0.06, 0.98]	0.27; 0.53 [0.00, 1.00]	0.60; 0.80 [0.17, 0.98]	0.45; 0.70 [0.08, 0.98]	0.27; 0.55 [0.00, 1.00]	0.60; 0.79 [0.20, 0.98]	0.46; 0.71 [0.11, 0.98]	0.28; 0.54 [0.00, 1.00]
	10%	0.53; 0.75 [0.17, 0.97]	0.38; 0.64 [0.07, 0.98]	0.18; 0.51 [0.00, 1.00]	0.55; 0.77 [0.15, 0.97]	0.39; 0.68 [0.08, 0.98]	0.18; 0.47 [0.00, 1.00]	0.55; 0.77 [0.17, 0.97]	0.40; 0.68 [0.07, 0.98]	0.20; 0.44 [0.00, 1.00]

Table S7

Table S7. Coefficient of determination (R^2) of the relationships between functional diversity metrics computed from optical traits and field plant traits, compared both at remote sensing resolution. Data are also presented in Fig. 8d,h. Each cell presents the R^2 of the relationship at the global scale, followed by the median and the 95 % confidence interval of R^2 at the local scale.

FDM	Noise	Hy			DESIS			Sentinel-2		
		100%	50%	0%	100%	50%	0%	100%	50%	0%
FRic	0%	0.67; 0.85 [0.33, 0.99]	0.67; 0.86 [0.30, 1.00]	0.66; 0.97 [0.63, 1.00]	0.62; 0.82 [0.25, 0.99]	0.60; 0.82 [0.29, 0.99]	0.76; 0.96 [0.58, 1.00]	0.63; 0.83 [0.29, 0.99]	0.62; 0.83 [0.28, 0.99]	0.77; 0.96 [0.63, 1.00]
	5%	0.65; 0.84 [0.31, 0.99]	0.65; 0.85 [0.29, 1.00]	0.68; 0.97 [0.66, 1.00]	0.49; 0.76 [0.08, 0.97]	0.47; 0.73 [0.14, 0.99]	0.77; 0.94 [0.58, 1.00]	0.46; 0.72 [0.07, 0.98]	0.46; 0.72 [0.13, 0.98]	0.76; 0.94 [0.58, 1.00]
	10%	0.63; 0.83 [0.29, 0.99]	0.63; 0.85 [0.26, 1.00]	0.64; 0.96 [0.62, 1.00]	0.42; 0.71 [0.05, 0.97]	0.45; 0.70 [0.08, 0.98]	0.81; 0.94 [0.63, 1.00]	0.39; 0.68 [0.02, 0.97]	0.42; 0.69 [0.10, 0.98]	0.75; 0.93 [0.55, 1.00]
FEve	0%	0.22; 0.24 [0.00, 0.71]	0.30; 0.36 [0.01, 0.83]	0.31; 0.48 [0.04, 0.87]	0.19; 0.19 [0.00, 0.63]	0.26; 0.31 [0.01, 0.81]	0.23; 0.41 [0.02, 0.81]	0.20; 0.22 [0.00, 0.63]	0.28; 0.32 [0.00, 0.82]	0.30; 0.44 [0.02, 0.87]
	5%	0.19; 0.21 [0.00, 0.68]	0.30; 0.35 [0.01, 0.84]	0.31; 0.48 [0.06, 0.88]	0.14; 0.14 [0.00, 0.59]	0.25; 0.29 [0.00, 0.81]	0.30; 0.48 [0.04, 0.87]	0.12; 0.13 [0.00, 0.58]	0.25; 0.29 [0.01, 0.78]	0.34; 0.50 [0.08, 0.88]
	10%	0.18; 0.19 [0.00, 0.62]	0.31; 0.38 [0.01, 0.84]	0.33; 0.51 [0.08, 0.88]	0.13; 0.12 [0.00, 0.58]	0.29; 0.34 [0.02, 0.80]	0.39; 0.53 [0.09, 0.86]	0.11; 0.12 [0.00, 0.58]	0.29; 0.33 [0.01, 0.79]	0.38; 0.52 [0.09, 0.86]
FDiv	0%	0.03; 0.06 [0.00, 0.62]	0.09; 0.17 [0.00, 0.82]	0.18; 0.40 [0.00, 0.95]	0.02; 0.06 [0.00, 0.57]	0.04; 0.11 [0.00, 0.74]	0.08; 0.25 [0.00, 0.88]	0.02; 0.06 [0.00, 0.58]	0.05; 0.11 [0.00, 0.79]	0.10; 0.24 [0.00, 0.88]
	5%	0.02; 0.06 [0.00, 0.58]	0.07; 0.15 [0.00, 0.77]	0.09; 0.29 [0.00, 0.90]	0.00; 0.05 [0.00, 0.56]	0.01; 0.09 [0.00, 0.71]	0.00; 0.16 [0.00, 0.81]	0.00; 0.05 [0.00, 0.50]	0.01; 0.08 [0.00, 0.73]	0.01; 0.14 [0.00, 0.83]
	10%	0.02; 0.05 [0.00, 0.61]	0.04; 0.11 [0.00, 0.73]	0.04; 0.22 [0.00, 0.90]	0.00; 0.04 [0.00, 0.43]	0.00; 0.08 [0.00, 0.67]	0.01; 0.13 [0.00, 0.83]	0.00; 0.05 [0.00, 0.46]	0.01; 0.09 [0.00, 0.64]	0.00; 0.12 [0.00, 0.82]
FDis	0%	0.76; 0.88 [0.40, 0.98]	0.68; 0.82 [0.28, 0.97]	0.39; 0.53 [0.01, 0.96]	0.68; 0.84 [0.18, 0.98]	0.59; 0.74 [0.18, 0.97]	0.26; 0.39 [0.00, 0.92]	0.72; 0.85 [0.28, 0.99]	0.62; 0.77 [0.18, 0.98]	0.28; 0.38 [0.00, 0.94]
	5%	0.75; 0.87 [0.39, 0.98]	0.66; 0.81 [0.26, 0.98]	0.35; 0.46 [0.00, 0.95]	0.53; 0.70 [0.14, 0.97]	0.45; 0.62 [0.06, 0.96]	0.15; 0.26 [0.00, 0.88]	0.52; 0.66 [0.15, 0.97]	0.43; 0.61 [0.05, 0.96]	0.15; 0.23 [0.00, 0.89]
	10%	0.72; 0.85 [0.35, 0.98]	0.65; 0.79 [0.25, 0.97]	0.31; 0.41 [0.00, 0.95]	0.49; 0.62 [0.14, 0.97]	0.43; 0.60 [0.04, 0.96]	0.18; 0.22 [0.00, 0.91]	0.47; 0.62 [0.09, 0.97]	0.40; 0.58 [0.05, 0.95]	0.12; 0.20 [0.00, 0.86]
RaoQ	0%	0.73; 0.89 [0.24, 0.99]	0.66; 0.83 [0.17, 0.98]	0.44; 0.54 [0.00, 0.97]	0.64; 0.84 [0.07, 0.98]	0.56; 0.75 [0.05, 0.97]	0.31; 0.42 [0.00, 0.95]	0.68; 0.86 [0.15, 0.99]	0.59; 0.77 [0.08, 0.98]	0.34; 0.41 [0.00, 0.96]
	5%	0.71; 0.87 [0.21, 0.99]	0.63; 0.81 [0.12, 0.98]	0.40; 0.50 [0.00, 0.96]	0.45; 0.67 [0.03, 0.97]	0.36; 0.58 [0.01, 0.96]	0.18; 0.26 [0.00, 0.91]	0.44; 0.64 [0.04, 0.97]	0.35; 0.56 [0.01, 0.95]	0.18; 0.25 [0.00, 0.91]

	10%	0.67; 0.85 [0.21, 0.98]	0.59; 0.78 [0.13, 0.97]	0.36; 0.43 [0.00, 0.95]	0.38; 0.57 [0.01, 0.96]	0.30; 0.52 [0.01, 0.95]	0.19; 0.23 [0.00, 0.91]	0.34; 0.55 [0.01, 0.96]	0.27; 0.49 [0.00, 0.94]	0.14; 0.20 [0.00, 0.88]
$RaoQ_{\alpha=0}$	0%	0.29; 0.94 [0.35, 1.00]	0.30; 0.92 [0.11, 1.00]	0.15; 0.75 [0.01, 1.00]	0.42; 0.92 [0.30, 1.00]	0.27; 0.88 [0.07, 1.00]	0.09; 0.57 [0.00, 1.00]	0.23; 0.93 [0.33, 1.00]	0.08; 0.89 [0.07, 1.00]	0.12; 0.57 [0.01, 1.00]
	5%	0.35; 0.94 [0.32, 1.00]	0.09; 0.92 [0.10, 1.00]	0.08; 0.64 [0.00, 1.00]	0.17; 0.85 [0.21, 1.00]	0.16; 0.84 [0.04, 1.00]	0.04; 0.32 [0.00, 1.00]	0.18; 0.83 [0.22, 1.00]	0.32; 0.84 [0.04, 1.00]	0.05; 0.31 [0.00, 1.00]
	10%	0.29; 0.94 [0.40, 1.00]	0.38; 0.93 [0.09, 1.00]	0.07; 0.55 [0.00, 1.00]	0.16; 0.87 [0.27, 1.00]	0.45; 0.88 [0.04, 1.00]	0.12; 0.25 [0.00, 1.00]	0.15; 0.86 [0.28, 1.00]	0.23; 0.87 [0.04, 1.00]	0.09; 0.23 [0.00, 1.00]
$RaoQ_{\alpha=1}$	0%	0.81; 0.92 [0.51, 0.99]	0.74; 0.88 [0.41, 0.99]	0.44; 0.65 [0.02, 0.98]	0.75; 0.89 [0.31, 0.99]	0.67; 0.82 [0.31, 0.98]	0.34; 0.54 [0.01, 0.95]	0.77; 0.89 [0.41, 0.99]	0.69; 0.84 [0.33, 0.99]	0.39; 0.55 [0.00, 0.96]
	5%	0.80; 0.91 [0.51, 0.99]	0.72; 0.87 [0.40, 0.98]	0.41; 0.62 [0.01, 0.97]	0.62; 0.77 [0.23, 0.98]	0.54; 0.72 [0.14, 0.98]	0.26; 0.42 [0.00, 0.94]	0.60; 0.73 [0.26, 0.98]	0.53; 0.71 [0.14, 0.98]	0.26; 0.39 [0.00, 0.93]
	10%	0.78; 0.89 [0.48, 0.99]	0.71; 0.85 [0.40, 0.98]	0.39; 0.57 [0.01, 0.97]	0.60; 0.72 [0.25, 0.98]	0.54; 0.72 [0.12, 0.97]	0.32; 0.41 [0.00, 0.95]	0.57; 0.71 [0.19, 0.99]	0.51; 0.69 [0.14, 0.97]	0.26; 0.36 [0.00, 0.93]
$RaoQ_{\alpha=2}$	0%	0.75; 0.88 [0.32, 0.98]	0.67; 0.82 [0.23, 0.98]	0.39; 0.55 [0.00, 0.97]	0.67; 0.84 [0.13, 0.98]	0.58; 0.74 [0.10, 0.97]	0.29; 0.42 [0.00, 0.95]	0.70; 0.84 [0.23, 0.99]	0.61; 0.76 [0.14, 0.98]	0.33; 0.41 [0.00, 0.95]
	5%	0.73; 0.86 [0.30, 0.98]	0.65; 0.80 [0.21, 0.97]	0.34; 0.50 [0.00, 0.96]	0.51; 0.67 [0.06, 0.96]	0.42; 0.59 [0.02, 0.96]	0.16; 0.27 [0.00, 0.90]	0.49; 0.64 [0.09, 0.96]	0.40; 0.58 [0.02, 0.96]	0.15; 0.25 [0.00, 0.90]
	10%	0.70; 0.83 [0.28, 0.98]	0.62; 0.77 [0.20, 0.97]	0.30; 0.43 [0.00, 0.95]	0.45; 0.59 [0.06, 0.96]	0.37; 0.56 [0.01, 0.95]	0.15; 0.23 [0.00, 0.91]	0.42; 0.59 [0.03, 0.96]	0.34; 0.52 [0.01, 0.94]	0.10; 0.20 [0.00, 0.88]
$RaoQ_{\alpha=\infty}$	0%	0.63; 0.81 [0.19, 0.97]	0.47; 0.70 [0.08, 0.98]	0.35; 0.58 [0.00, 1.00]	0.56; 0.76 [0.09, 0.97]	0.38; 0.62 [0.03, 0.98]	0.25; 0.37 [0.00, 1.00]	0.58; 0.78 [0.14, 0.97]	0.41; 0.67 [0.03, 0.98]	0.27; 0.39 [0.00, 1.00]
	5%	0.59; 0.78 [0.15, 0.97]	0.43; 0.69 [0.06, 0.98]	0.24; 0.47 [0.00, 1.00]	0.40; 0.62 [0.04, 0.94]	0.22; 0.46 [0.01, 0.96]	0.13; 0.23 [0.00, 1.00]	0.39; 0.59 [0.07, 0.93]	0.24; 0.50 [0.02, 0.95]	0.17; 0.25 [0.00, 1.00]
	10%	0.55; 0.75 [0.15, 0.96]	0.38; 0.62 [0.07, 0.97]	0.18; 0.39 [0.00, 1.00]	0.34; 0.53 [0.03, 0.89]	0.18; 0.42 [0.01, 0.95]	0.10; 0.20 [0.00, 1.00]	0.32; 0.53 [0.03, 0.92]	0.19; 0.43 [0.01, 0.95]	0.10; 0.25 [0.00, 1.00]

Figure S4

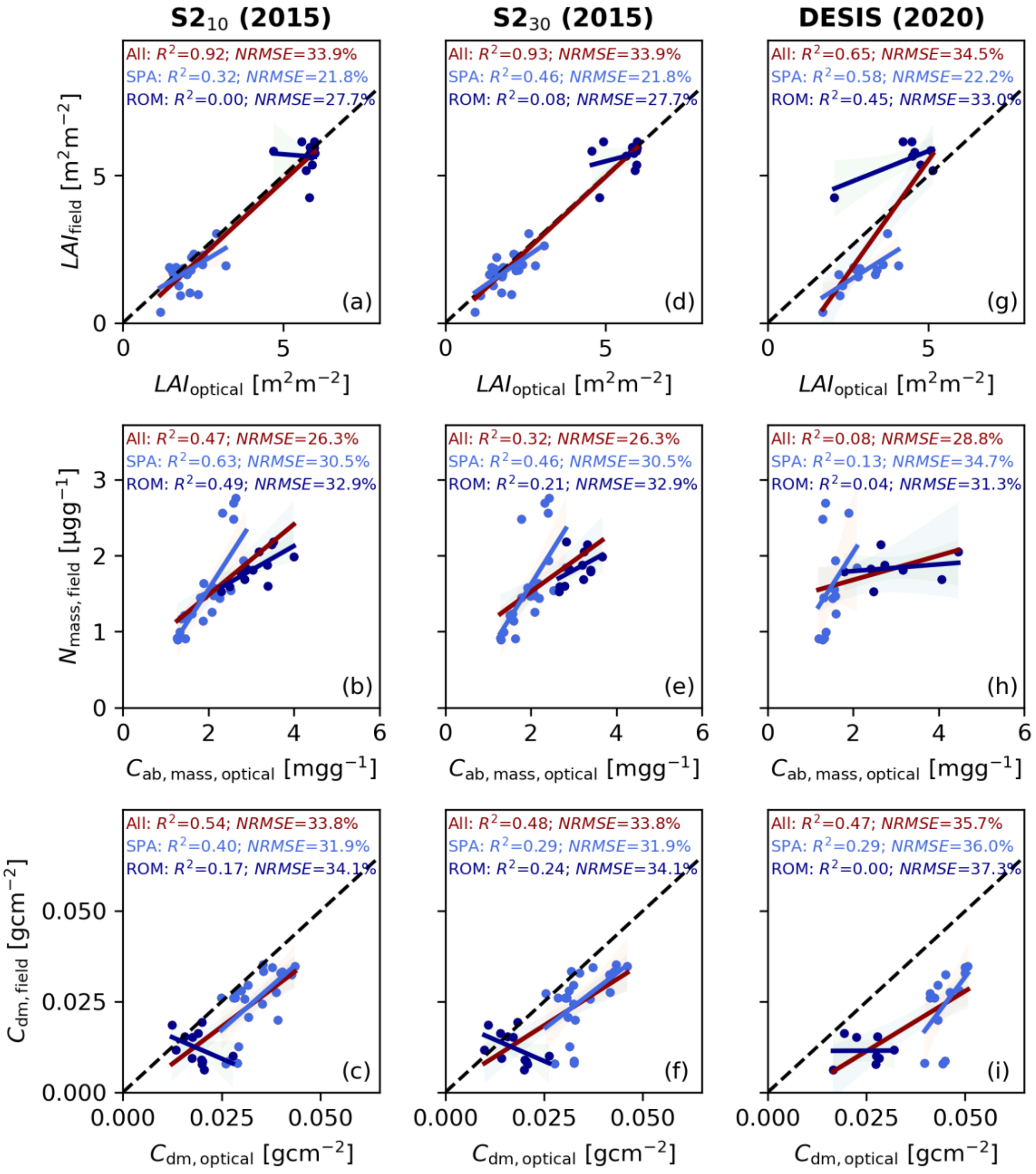

Figure S4. Evaluation of the optical traits retrieval via inversion of the radiative transfer model SCOPE in the FunDivEUROPE plots. The model was constrained with the reflectance factors of Sentinel-2 MSI at 10 m spatial resolution (first column), Sentinel-2 MSI at 30 m spatial resolution (second column), and DESIS at 30 m spatial resolution (third column). Sentinel-2 imagery was acquired in 2015. Median values of the 3 x 3 pixels window centered on the field plots are compared against the mean values of different traits measured on the ground. Leaf area index (first row) and dry matter content (third row) are directly compared with field measurements. In contrast, chlorophyll concentration computed from estimated chlorophyll and dry matter contents is compared with foliar Nitrogen concentration (mas per mass).

Figure S5

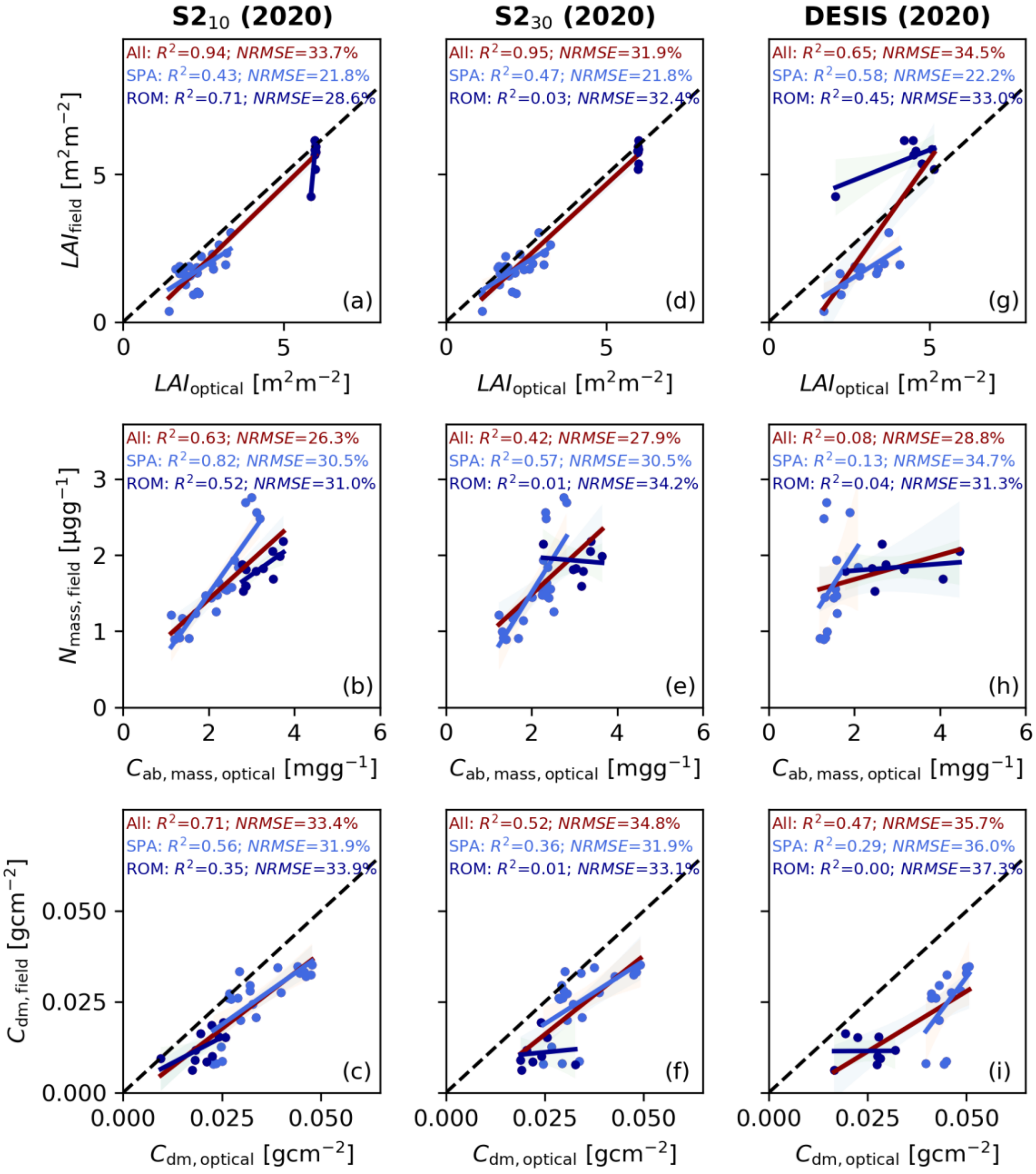

Figure S5. Evaluation of the optical traits retrieval via inversion of the radiative transfer model SCOPE in the FunDivEUROPE plots. The model was constrained with the reflectance factors of Sentinel-2 MSI at 10 m spatial resolution (first column), Sentinel-2 MSI at 30 m spatial resolution (second column), and DESIS at 30 m spatial resolution (third column). Sentinel-2 imagery was acquired in 2020. Median values of the 3 x 3 pixels window centered on the field plots are compared against the mean values of different traits measured on the ground. Leaf area index (first row) and dry matter content (third row) are directly compared with field measurements. In contrast, chlorophyll concentration computed from estimated chlorophyll and dry matter contents is compared with foliar Nitrogen concentration (mas per mass).

Figure S6

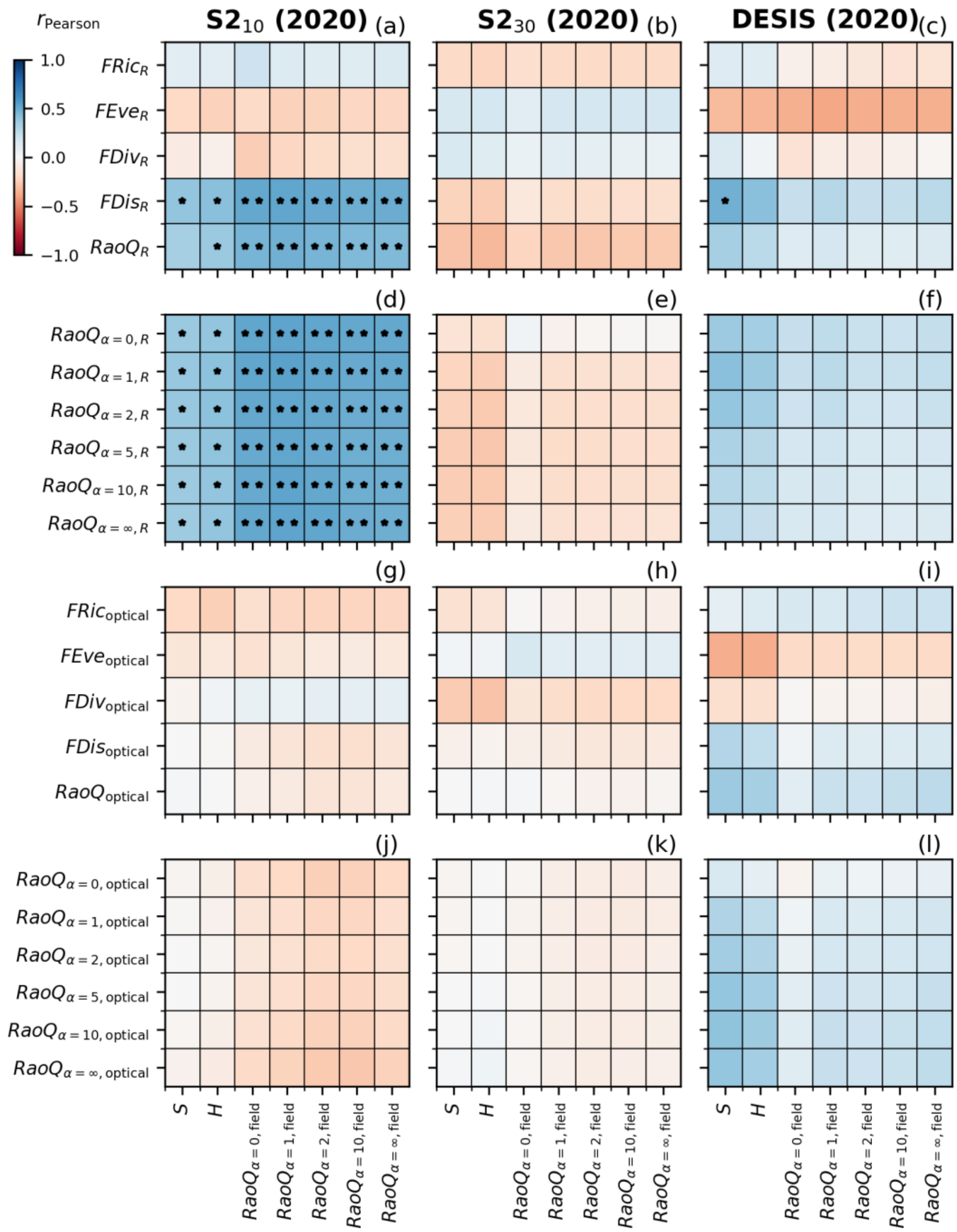

Figure S6. Pearson correlation coefficient between taxonomical and functional diversity metrics computed from field plant traits (subscript "field", *x*-axis) and functional diversity metrics computed from remote sensing information (*y*-axis): the reflectance factors (subscript "*R*", first two rows) or the optical traits (subscript "optical", last two rows). In each case, the *dbFD* package metrics are presented first, and the parametric Rao's *Q* afterward. The statistics correspond to Sentinel-2 MSI @ 10 m spatial resolution (S2$_{10}$, first column), Sentinel-2 MSI @ 30 m spatial resolution (S2$_{30}$, second column), and DESIS at 30 m spatial resolution (DESIS, third column). Sentinel-2 imagery was acquired in 2020. Asterisks indicate the significance of the correlation (two-tailed) according to its p-value (p): *** → $p < 0.001$, ** → $0.001 \leqslant p < 0.01$, and ** → $0.01 \leqslant p < 0.05$..

SUPPLEMENTARY REFERENCES

Coleman, T.F., & Li, Y. (1996). An Interior Trust Region Approach for Nonlinear Minimization Subject to Bounds. *SIAM Journal on Optimization, 6*, 418-445

Combal, B., Baret, F., Weiss, M., Trubuil, A., Macé, D., Pragnère, A., Myneni, R., Knyazikhin, Y., & Wang, L. (2003). Retrieval of canopy biophysical variables from bidirectional reflectance: Using prior information to solve the ill-posed inverse problem. *Remote Sensing of Environment, 84*, 1-15

Ma, X., Mahecha, M.D., Migliavacca, M., van der Plas, F., Benavides, R., Ratcliffe, S., Kattge, J., Richter, R., Musavi, T., Baeten, L., Barnoaiea, I., Bohn, F.J., Bouriaud, O., Bussotti, F., Coppi, A., Domisch, T., Huth, A., Jaroszewicz, B., Joswig, J., Pabon-Moreno, D.E., Papale, D., Selvi, F., Laurin, G.V., Valladares, F., Reichstein, M., & Wirth, C. (2019). Inferring plant functional diversity from space: the potential of Sentinel-2. *Remote Sensing of Environment, 233*, 111368

Melendo-Vega, J., Martín, M., Pacheco-Labrador, J., González-Cascón, R., Moreno, G., Pérez, F., Migliavacca, M., García, M., North, P., & Riaño, D. (2018). Improving the Performance of 3-D Radiative Transfer Model FLIGHT to Simulate Optical Properties of a Tree-Grass Ecosystem. *Remote Sensing, 10*, 2061

North, P.R.J. (1996). Three-dimensional forest light interaction model using a Monte Carlo method. *IEEE Transactions on Geoscience and Remote Sensing, 34*, 946-956

Pedregosa, F., Varoquaux, G., Gramfort, A., Michel, V., Thirion, B., Grisel, O., Blondel, M., Prettenhofer, P., Weiss, R., Dubourg, V., Vanderplas, J., Passos, A., Cournapeau, D., Brucher, M., Perrot, M., & Duchesnay, É. (2011). Scikit-learn: Machine Learning in Python. *Journal of Machine Learning Research, 12*, 2825-2830

Rivera, J.P., Verrelst, J., Gómez-Dans, J., Muñoz-Marí, J., Moreno, J., & Camps-Valls, G. (2015). An Emulator Toolbox to Approximate Radiative Transfer Models with Statistical Learning. *Remote Sensing, 7*

Zhu, C., Byrd, R.H., Lu, P., & Nocedal, J. (1997). Algorithm 778: L-BFGS-B: Fortran subroutines for large-scale bound-constrained optimization. *ACM Trans. Math. Softw., 23*, 550–560